The Pennsylvania State University

The Graduate School

Department of Geosciences

INSIGHTS FROM INSIDE THE VOLCANO: GENESIS AND ERUPTION OF THRÍHNÚKAGÍGUR VOLCANICS, REYKJANES PENINSULA, ICELAND

A Thesis in

Geosciences

by

Michael R. Hudak

Submitted in Partial Fulfillment
of the Requirements
for the Degree of

Master of Science

May 2016

The thesis of Michael R. Hudak was reviewed and approved* by the following:

Maureen D. Feineman
Assistant Professor of Geosciences
Thesis Co-Advisor

Peter C. LaFemina
Professor of Geosciences
Thesis Co-Advisor

Tanya Furman
Professor of Geosciences
Associate Vice President and Associate Dean for Undergraduate Education

Michael Arthur
Professor of Geosciences
Interim Head of Graduate Programs of the Geosciences Department

*Signatures are on file in the Graduate School

ABSTRACT

Thríhnúkagígur is the main cone of a small 3500 ka fissure eruption in the Brennisteinsfjöll fissure swarm on the Reykjanes Peninsula. Beneath the summit of the main cone is a 120 m deep cave exposing a large part of the uppermost magmatic plumbing system and a buried tephra cone. The exposure of this structure offers a unique view into a non-unique eruptive process. Basaltic fissure eruptions are common in many tectonic and volcanic settings. Direct observations in the cave in addition to major element, trace element and Sr-Nd-Pb isotope analyses allow a fissure eruption on the Reykjanes Peninsula to be investigated from melt generation in the mantle to eruption. Field relationships between the main dike that fed the eruption and the unconsolidated buried tephra suggest that the tephra was entrained by the erupting magma. Assuming the cave represents the volume of tephra entrained and removed from the system, estimates of the erupted volume of lava produce maximum estimates of ~29% tephra content in the lavas. Furthermore, the location of the buried tephra directly beneath the main cone of Thríhnúkagígur suggest that the buried tephra acted as a local asperity in the crust forming a preferential pathway for the magma to ascend to the surface. The main vents were developed here because flow was focused by the buried tephra. However, the vertical sheet-like structure of the dike indicates that the far field stresses dictate the orientation of fissure despite the contrast in competency between the buried tephra and overlying basaltic lava flow.

The Sr-Nd-Pb isotope systematics illustrate that Thríhnúkagígur lavas are consistent with other relatively enriched compositions observed on the Reykjanes Peninsula, with radiogenic Pb and Sr, and relatively unradiogenic Nd. These isotopes suggest that Thríhnúkagígur magmas are derived from two main components – an enriched plume source and a depleted mantle source – with possible minor contributions from an EM1-like mantle source. Anomalously high ratios of Nb/U at Thríhnúkagígur suggest that despite isotopic similarities between the Reykjanes Peninsula and the Eastern Volcanic Zone (EVZ), the enriched plume source at the Reykjanes is unique from the EVZ in its enriched Nb. Decoupling of the Sr isotopes from Pb and Nd isotopes suggests that the source of radiogenic Sr at Thríhnúkagígur may be assimilation of basaltic crust that has been hydrothermally altered by seawater. The tephra entrainment hypothesis is tested with immobile trace element mixing models. Models of La/Yb vs. Nb/Zr yield maximum estimate 28-35% of the tephra component in the lavas, consistent with results from the geophysical analysis. However, large uncertainty in the initial magma composition limits the precision of this model and some samples may not contain any entrained tephra. Finally, the variability in the major and trace element geochemistry and the Sr isotopes, particularly in the uppermost magmatic plumbing system, suggest that the small volume of erupted magma was not homogenized prior to eruption. In the absence of a central volcano at Brennisteinsfjöll, we invoke a network of dikes and sills that are quasi-isolated until the eruption, allowing for variable geochemical evolution. This model both preserves magma heterogeneity from the mantle and facilitates the evolution of magmas with variable compositions, consistent with the variation in geochemistry observed at multiple levels in this single eruption.

TABLE OF CONTENTS

LIST OF FIGURES

LIST OF TABLES

ACKNOWLEDGEMENTS

First of all, this thesis would not have been possible without generous funding from the Department of Geosciences. Thank you to Hiroshi and Koya Ohmoto, the family of Charles E. Knopf, and the Hess Corporation for graciously endowing the department thereby allowing students like myself to conduct research in the field. And thanks to the NSF for funding my isotopic analyses through an international collaboration grant.

I must also thank Björn Òlafsson and all of the folks at Inside the Volcano for granting me access to the cave below Thríhnúkagígur. The title of this thesis is in honor of your assistance.

Thanks also to Jim Normandeau at UNAVCO for providing me with such an excellent LiDAR data set.

To Halldór, your assistance in the field was invaluable. I also deeply appreciate your input throughout this project and your willingness to share your experience with me.

Samuele, thanks for teaching me ion chromatography and TIMS methodology. I learned a ton from you. Grazie mille also for being so hospitable. You were a fantastic host!

To my parents, Mark and Bonnie, you're the greatest. Thanks for all your emotional (and occasional financial) support of my endeavors. I cannot describe how much it means to me.

These last three years have been truly enjoyable largely because of the great people I have been able to call my friends. It was not always a smooth ride, but your incredible support helped me with the road bumps along the way. Thank you guys! Nick and Helen, I especially do not know what I would have done without you.

Tanya, I appreciate the tough love. I really believe it has forced me to address some of my weakness and helped me to become a better scientist. Thanks for being a skeptic and asking me tough questions.

Pete, thanks for forcing me to step outside of my comfort zone. You have helped me to become more comfortable incorporating geophysics into my research. Thanks also for allowing me to take on this project! It was a great opportunity and an exciting for me.

And to Maureen, thanks for being so accessible and helpful. I am certain that I have tried your patience during this process, so thanks for putting up with me! You've given me some great opportunities and connections, for which I cannot express my appreciation enough. Thank you.

Chapter 1

Geologic Overview

1.1 Introduction

The goal of this project is to better understand the origin, evolution, and ultimately the eruption of basalts on the Reykjanes Peninsula in Iceland in the absence of central volcanoes or any large homogenizing magma chambers. Direct observations of the shallow magmatic plumbing system in a cave below the main vent of the fissure eruption at Thríhnúkagígur, together with surficial structures form the basis for deciphering eruptive style and process. Whole rock chemical and isotopic compositions of erupted lavas, their corresponding intrusive units, and some of the intruded country rock provide insights into the mantle sources for Thríhnúkagígur magmas and the crustal processes that drove their evolution.

Chapter 1 is an overview of the geodynamics and volcanism in Iceland that provides context for the following chapters. With no eruptions on the Reykjanes Peninsula since the 13th century, the best analogs for eruptive process are other fissure eruptions in Iceland. Yet, these comparisons are imperfect because the Reykjanes Peninsula lacks central volcanoes or large magma storage chambers. In addition, few eroded cones or vents exist on the Reykjanes Peninsula because it has been largely resurfaced by Holocene lava flows since the end of the last glaciation. Few places, therefore, expose the shallow plumbing system of fissure eruptions that would reveal information about eruptive processes and vent development. Thríhnúkagígur, the main vent of a monogenetic fissure eruption in the Brennisteinsfjöll fissure swarm, is a unique place to study eruptive process on the Reykjanes Peninsula. The uppermost ~120 meter of the conduit remained evacuated following the eruption, revealing a cross-section though the shallow magmatic plumbing system.

In Chapter 2, direct observations of the internal structure of the Thríhnúkagígur magmatic plumbing system and surface geology forms the basis for describing the eruption, the development of the vent, and the formation of the cave. While one goal of this project is to understand what processes might be common for Reykjanes Peninsula fissure eruptions, the lung-shaped cave below the main vent is highly unusual. This structure warrants consideration of how the eruption at Thríhnúkagígur is also uncharacteristic of monogenetic fissure eruptions in this setting. A buried tephra cone is preserved at depth in the cave. The potential incorporation of this unconsolidated material into the erupting magma is investigated in this chapter.

With constraints on eruptive process in the uppermost crust, geochemical and isotopic analyses in Chapter 3 are used to evaluate the mantle sources of these magmas as well as their storage and evolution in the crust between where melts were generated and where they were erupted. Lavas from the Reykjanes Peninsula have been well-characterized geochemically, but seldom have individual eruptions with both intrusive and extrusive samples been studied in detail. A comprehensive whole rock major and trace element and Sr-Nd-Pb isotope data set is herein presented. Competing views of unadulterated mantle melts and significant contamination of these melts in crustal magma chambers have been presented for Reykjanes Peninsula lavas in previous literature. Chapter 3 evaluates these ideas by investigating a single small volume eruption in detail.

1.2 Regional tectonic setting

1.2.1 The Mid-Atlantic Ridge and the Icelandic plume

Iceland is a remarkably active volcanic province that straddles the Mid-Atlantic Ridge (MAR). This substantially thickened, buoyant oceanic crust is the result of increased melt production related to the concurrence of a mantle plume with the MAR. Its location at a divergent plate boundary has caused the Icelandic hotspot track to trail both east to the Faroe Islands on the Eurasian plate and west to Greenland on the North American plate. These tracks suggest that the Icelandic hotspot is at least as old as the opening of the North Atlantic around 56 Ma, as determined by magnetic anomalies (Nunns et al., 1983) and the geochronology of flood basalts and picrites in eastern Greenland (Larsen et al., 1992; Saunders et al., 1997).

Numerous geophysical studies, such as ICEMELT (Bjarnason et al., 1996; Wolfe et al., 1997) and HOTSPOT (Foulger et al., 2000), have used comprehensive seismic tomography surveys to image the plume beneath Iceland. These studies and others converge on a vertical, cylindrical thermal anomaly of approximately 150° C above ambient mantle temperature extending to at least 400 km depth in the mantle (Bjarnason et al., 1996; Wolfe et al., 1997; Foulger et al., 2000; Bjarnason, 2008; Brandsdóttir and Menke, 2008). The lack of an observable, deep-seated mantle plume extending to the 660 km discontinuity or D” beneath Iceland has led some authors to create alternative models for enhanced melt production in Iceland. Foulger and Anderson (2005) argue that the seismically observed structure can be explained by a complex tectonic model, whereby subducted oceanic crust from the closure of the Iapetus Ocean is trapped in Laurasian continental lithosphere, giving rise to an especially fertile mantle in a location where the geotherm is already elevated due to the presence of the MAR. However, the vast majority of data for Iceland have been interpreted within a hotspot framework since the advent of the fixed mantle hotspot hypothesis by Wilson (1963) and Morgan (1971). The work presented herein likewise assumes the existence of a mantle plume with geochemical properties similar to those of an ocean island basalt (OIB) source when discussing mantle sources.

The locus of the plume is assumed to be under the thickest crust, which reaches a maximum of approximately 40 km thick beneath Europe's largest ice cap, Vatnajökull, slightly to the east of Iceland's center (Figure 1.1). The average crustal thickness is 25-26 km (Darbyshire et al., 1998; Darbyshire et al., 2000; Björnsson et al., 2005; Bjarnason and Schmeling, 2009), whereas the thinnest crust is 18-20 km thick (Figure 1.1) and may be as thin as 14 km where the Reykjanes Peninsula goes offshore (Weir et al., 2001).

1.2.2 Neovolcanic zones

Much of the present day magmatism in Iceland exists within four main neovolcanic zones. Three of these are rift zones that comprise the subaerial MAR: the Western Volcanic Zone (WVZ), the Eastern Volcanic Zone (EVZ), and the Northern Volcanic Zone (NVZ). The fourth major volcanic zone, the Reykjanes Peninsula (RP), is a transtensional plate boundary that connects the southern tip of the WVZ to the submarine Reykjanes Ridge (Figure 1.1).

The plate boundaries and volcanic zones shown in Figure 1.1 are herein described from north to south. In the modern plate configuration, the submarine Kolbeinsey Ridge north of Iceland connects to the NVZ by the Tjörnes Fracture Zone. The NVZ ends beneath Vatnajökull and two rift zones continue to the southwest. The EVZ forms a continuous boundary with the NVZ that extends south of Vatnajökull. The WVZ is offset from the NVZ to the west by the E—W oriented Mid-Iceland Belt extending from Vatnajökull to Langjökull. From there, the WVZ extends to the southwest where it terminates at the eastern end of the transtensional Reykjanes Peninsula. The RP consists of a series of NE-SW trending parallel volcanic systems aligned in an E—W lineament connecting the subaerial expression of the MAR at the WVZ to the submarine Reykjanes Ridge to the west. The EVZ and the WVZ are connected in the south by a young non-transform fault system, the South Iceland Seismic Zone (SISZ). The SISZ extends east from the Hengill volcanic system on the Reykjanes Peninsula and intersects the EVZ between Hekla volcano and Torfajökull caldera (Geirsson et al., 2012). Additionally, there are two off-rift volcanic centers, Öræfajökull in the east and Snæfellsnes in the west.

Spreading of Iceland’s rift zones occurs at a rate of ~17-18 mm/yr total in the MORVEL model (DeMets et al., 2010), making it an ultraslow spreading center. LaFemina et al. (2005) used geodetic GPS measurements to characterize spreading rates along axis of the WVZ and EVZ. They determined that rates in the EVZ decrease to the south along the rift zone from the full North American-Eurasian spreading rate at the juncture with the NVZ (19.0 ± 2.0 mm/yr) to 11.0 ± 0.8 mm/yr in the southern EVZ. This decrease correlates with a spreading rate increase moving south along the WVZ (2.6 ± 0.9 mm/yr to 7.0 ± 0.4 mm/yr). The EVZ now accommodates two-thirds of the MAR spreading rate in south Iceland (LaFemina et al., 2005), which has led some authors to suggest that the WVZ is dying out as another ridge jump is made from the WVZ to the EVZ (Hardarson et al., 1997). The North American-Eurasian plate boundary continues to reconfigure to the southeast as the plates drift WNW over the stationary Icelandic plume (Hardarson et al., 1997; Mittelstaedt et al., 2008; Walters et al., 2013). In this framework, the GPS geodetic data of LaFemina et al. (2005) demonstrate that ridge reconfiguration is a transitional process rather than an instantaneous one as the EVZ continues to propagate to the south in the present day.

1.2.3 Deglaciation and volcanism

The Weichselian glaciation lasted from 113 ka to ~ 13-9 ka in Iceland (Fronval and Jansen, 1997). When the glaciation began to wane and the ice retreated, there was a large, rapid pulse of magmatism resulting from isostatic rebound and decompression melting. Therefore, a decrease in melt production in the WVZ related to the ridge relocation described in the previous section may not be observable in the postglacial Holocene because the signal would be masked by the sudden, extreme increase in melt production associated with deglaciation (Sinton et al., 2005). Immediately following the rapid removal of ice following the last glacial maximum, a spike in decompression melting spawned abundant and voluminous volcanism, which tapered off abruptly after only one to two thousand years (Jull and McKenzie, 1996; Maclennan et al., 2002). This phenomenon has been documented on the Reykjanes Peninsula (Guðmundsson, 1986), the WVZ (Sinton et al., 2005) and in all the other volcanic zones with production rates up to 30 times that of equilibrium melting (Maclennan et al., 2002). This phenomenon has also given rise to markedly different compositions in lavas erupted in interglacial periods and those erupted immediately following deglaciation (Gee et al., 1998b; Maclennan et al., 2002; Sinton et al., 2005).

1.3 Regional geochemical overview

As an ocean island on a mid-ocean ridge, Iceland is dominantly (although by no means entirely) basaltic in composition. Geochemical differences have been recognized globally between mid-ocean ridge basalts (MORB) and ocean island basalts (OIB; Sun and McDonough, 1989), but these differences were not initially understood to have originated from separate mantle sources. Schilling (1973) invoked multiple mantle sources to explain chemical variation in Iceland. He noted a gradual depletion in light rare earth elements (REEs) moving southwest along the Reykjanes Ridge away from Icelandic plume. Large ion lithophile elements (LILEs) (such as K, Rb, Cs, Ba, U, and Th) and light to intermediate REE ratios (notably La/Sm) in Reykjanes Ridge basalts followed a similar gradational trend (Figure 1.2). Not only did Schilling (1973) suggest a more primordial source beneath Iceland, but he used this evidence to argue for a two component mixing model between melts from both MORB and a plume (OIB) source in the mantle.

Contemporaneously, Jakobsson (1972) recognized a geographic correlation between variations in major element compositions across Iceland. He proposed three igneous rock series and linked them to their proximity to the MAR rift zones. These remain the defining rock series of Iceland today and are correlated to tectonic environment (Sigmarsson and Steinthórsson, 2007; Jakobsson et al., 2008). Alkali and transitional alkali basalts are confined to the off-rift volcanic zones and near the south tip of the propagating EVZ rift. Tholeiites, the most common of the basaltic rock series, are found along the neovolcanic rift zones. These rock series correlate with the melt fraction and volume, with tholeiites representing greater melt fraction and alkali basalts indicating small batches of more localized melt. These major element compositions are probably controlled more by tectonic environment and melting regime rather than variable mantle sources.

A great deal of research has gone into determining the number and compositions of different mantle domains contributing to Icelandic magmas. Among trace elements, niobium seems to be the most robust tracer of primordial mantle contributions because Nb is depleted in both depleted MORB-source upper mantle and in the crust relative to primitive mantle (McKenzie and O'Nions, 1991; Fitton et al., 1997). Elevated Nb/Zr ratios (≥0.08) in Iceland and at other North Atlantic hotspots relative to MAR ridge segments (≤0.05) is consistent with theoretical Nb systematics (Figure 1.2; Fitton et al., 1997; Hanan et al., 2000).

Helium isotope ratios are also broadly considered to be a robust tracer of a primitive mantle component. The primordial mantle theoretically has a higher $^{3}He/^{4}He$ ratio than degassed upper mantle because ^{4}He will be replenished in a degassed mantle by alpha decay of radionuclides, whereas ^{3}He will not, driving $^{3}He/^{4}He$ to lower values over time. Ratios are typically expressed relative to the atmospheric ratio (R/Ra) and it has long been recognized that Iceland has R/Ra, as much as three times greater (R/Ra = 24) than MORB and that these values are typically higher close to the center of the plume in east-central Iceland, although this distribution is non-uniform (Condomines et al., 1983; Kurz et al., 1985).

Indeed, the increasing consensus in the literature favors the mixing of multiple (2-4) source domains within the plume based on Sr-Nd-Pb-Hf isotope systematics. Some propose the range of compositions of Icelandic lavas arises without contribution from a MORB source and that the plume contains at least one depleted (unradiogenic Pb, radiogenic Nd, and moderate to unradiogenic Sr) component (Chauvel and Hémond, 2000; Thirlwall et al., 2004; Kokfelt et al., 2006). Rather than have a mid-ocean ridge contaminated by a plume source, they posit that the plume itself is responsible for heterogeneity in Iceland and instead, it contaminates the surrounding MAR. Regardless of whether there are contributions from a MORB source (Hanan and Schilling, 1997; Hanan et al., 2000) or not, most recent studies converge on the involvement of ancient recycled oceanic crust or lithosphere (Chauvel and Hémond, 2000; Thirlwall et al., 2004; Kokfelt et al., 2006; Peate et al., 2010; Koornneef et al., 2012).

Two dominant models for the origins of Icelandic magmas are best summarized by Manning and Thirlwall (2014). The first results from the melting of a zoned plume or one that contains veins or blobs of fertile material within depleted lithologies (Chauvel and Hémond, 2000; Kokfelt et al., 2006; Koornneef et al., 2012). Either fertile pyroxenite is incorporated into ambient peridotite or the structure of recycled oceanic lithosphere is preserved, giving rise to bilaterally zoned plume with melts from both fertile basaltic and refractory gabbroic compositions. The second model advocates convective mixing between numerous, isotopically distinct sources within the plume (Thirlwall et al., 2004; Peate et al., 2009; Peate et al., 2010). Excluding Öræfajökull, which requires the melting of minor amounts of pelagic sediment (Manning and Thirlwall, 2014), the Iceland array in $^{87}Sr/^{86}Sr$ and $^{143}Nd/^{144}Nd$ supports a binary mixing model. Lead isotope work has provided the most robust evidence for a third enriched mantle source (Sigmarsson & Steinthórsson 2007, and references therein) although Koornneef et al. (2012) argue that one dimensional polybaric melting models with mixing of melts from two sources at different depths can give rise to the full range of isotope compositions.

Oxygen isotopes in Icelandic lavas are commonly up to 2‰ lighter than mantle $\delta^{18}O$ values. This observation has also been used as evidence for a recycled oceanic crustal component interspersed in the mantle below Iceland (Kokfelt et al., 2006). Sigmarsson & Steinthórsson (2007), on the other hand, argue that contributions from the altered Icelandic crust to magmatic systems may limit the use of oxygen isotopes to identify mantle sources. Assimilation of altered basalt or hyaloclastite may drive Icelandic lavas to $\delta^{18}O$ several ‰ lighter than mantle values based on observed extreme negative $\delta^{18}O$ (<-10‰) in hydrothermal systems (Muehlenbachs et al., 1974; Hattori and Muehlenbachs, 1982) and more moderate depletions in $\delta^{18}O$ in the ubiquitous hyaloclastite formations in the EVZ (Bindeman et al., 2008).

1.4. The Reykjanes Peninsula and the Brennisteinsfjöll volcanic system

1.4.1 Reykjanes Peninsula tectonics and volcanism

The Reykjanes Peninsula, in southwest Iceland is a oblique transtensional plate boundary that arcs onshore to Iceland from the Reykjanes Ridge. It connects the offshore Reykjanes Ridge with the onshore Western Volcanic Zone (a ridge) and the South Iceland Seismic Zone (a “transform”) at a triple junction at Hengill. It consists of 4 NE-SW trending *en echelon* volcanic systems that form the plate boundary (Figure 1.3). Pioneering microseismic observations showed that both strike-slip and normal faults are present across the peninsula (Klein et al., 1973; Klein et al., 1977), which was supported by geodetic data that indicated both left-lateral and extensional motion (Brander et al., 1976). These studies demonstrated that the RP was not simply a transform plate boundary connecting the Reykjanes Ridge to the WVZ, but rather an extensional transform zone or what is sometimes referred to as a leaky transform (Taylor et al., 1994).

A variety of techniques have been implemented to understand the distribution of faults, volcanic fissures, and fractures on the Reykjanes that partition strain. These methods include the use of seismic data (Keiding et al., 2009), GPS geodesy (Hreinsdóttir et al., 2001; Clifton et al., 2002; Árnadóttir et al., 2006; Keiding et al., 2008), InSAR (Clifton et al., 2002), analog models (Clifton and Schlische, 2003), structural analysis (Villemin and Bergerat, 2013), and high resolution DEM mapping of fissures (Clifton and Kattenhorn, 2006).

Geodetic GPS work focuses on determining how NUVEL-1A spreading rates of 19-20 mm/yr between the North American and Eurasian plate are partitioned on the oblique divergent Reykjanes Peninsula. From 1993-1998 GPS velocities, Hreinsdóttir et al. (2001) observed 16.8 ± 0.9 mm/yr of left-lateral motion on the RP, but not the expected extensional component. They postulate that extension is accommodated during episodic rifting events that are thought to be cyclical with a ~1000 year periodicity (Clifton and Kattenhorn, 2006; Keiding et al., 2008). The last eruption on the RP occurred in the 13th century and the peninsula is presently in a quiescent period. However, recent work by Árnadóttir et al. (2006) models 1992-2000 GPS velocities with a best-fit locking depth of 8 km, and 19 mm/yr of left-lateral transcurrent motion, and ~9 mm/yr of extension at depth.

The motion and orientation of the plate boundary at depth gives rise to more complex deformation in the brittle regime and expression of structures at the surface. Clifton and Katterhorn (2006) use high resolution digital elevation maps (DEM) to map the surface expression of faults, fissures, and fractures on the Reykjanes. They find that the major strike-slip faults are oriented N-S, rotated 80-90° clockwise from the orientation of plate motion, and are primarily to the SE of the volcanic systems. The normal faults, on the other hand, are oriented NE-SW, parallel or sub-parallel to the trend of eruptive fissures and rotated ~60-70° counterclockwise to the direction of plate motion. North trending right-lateral strike-slip faults are *en echelon* and accommodate the E-W sinistral shear across the plate boundary; this style of faulting is referred to as bookshelf faulting and is most developed on the eastern Reykjanes. This style of faulting is characteristic of the SISZ to the east of the triple junction at Hengill (Bergerat and Angelier, 2003; Clifton and Einarsson, 2005; Clifton and Kattenhorn, 2006), however there is no observed extension in the SISZ. The commonality between the well-developed

N-S oriented dextral faulting in the SISZ and the eastern RP suggests that the volcanic systems of Brennisteinsfjöll and Hengill are governed by a tectonic regime intermediate between that of the RP and the amagmatic SISZ.

1.4.2 Reykjanes Peninsula lava chemistry

Except for rare silicic rocks from the Hengill volcanic system, the Reykjanes Peninsula is uniformly basaltic in composition. High MgO lavas on the RP fall broadly into two geochemical groups: depleted and enriched basalts (Gee et al., 1998a; Thirlwall et al., 2004; Peate et al., 2009). Depleted lavas have Nb/Zr < 0.08, $^{87}Sr/^{86}Sr < 0.70311$, and $^{143}Nd/^{144}Nd > 0.51307$ (Gee et al., 1998a). Peate et al. (2009) sampled all of the historic lavas on the Reykjanes (since the settlement of the island circa 871 C.E.). These are uniformly enriched, but are subdivided into "less enriched" (Nb/Zr 0.10-0.13, La/Yb_N 1.3-2.0) and "more enriched" (Figure 1.4; Nb/Zr 0.13-0.14, La/Yb_N 2.2-2.6, $^{206}Pb/^{204}Pb$ >18.8).

While many authors have focused on depleted picrites because they are the most primitive compositions on the RP and therefore perhaps most accurately reflect primary mantle melts, these are not representative and occur in rare, small volume flows (Jakobsson et al., 1978; Peate et al., 2009). In fact, these lavas are constrained primarily to 9-13 ka, during and immediately following deglaciation. The local stress state on magma bodies is likely to have fluctuated during glacial unloading, which may have caused eruptions to occur with increased frequency. Gee et al (1998b) argue that reduced residence times immediately following deglaciation prevent RP lavas from acquiring enriched trace element and isotope compositions from crustal contamination. Additionally, they posit that shorter residence times in the crust of smaller volumes of magma diminished the potential for magma mixing to occur, thereby preserving the depleted melt.

While crustal assimilation has been demonstrated to be an important magmatic process on the Reykjanes Peninsula (Gee et al., 1998a), the composition of these lavas has been reinterpreted to reflect binary mixing of melts derived from depleted and enriched components in the Icelandic plume. The enriched component dominates, comprising 50-90% of the mix for majority of RP lavas (Thirlwall et al., 2004; Peate et al., 2009) and the preservation of the depleted melts may be facilitated by the reduced residence times and decreased probability of magma mixing (Gee et al., 1998b). Nevertheless, there is a strong correlation between lava chemistry and age over the last 20 ka, with modern compositions at or approaching those before the deglaciation in southwest Iceland (Figure 1.5).

Rifting seems to be confined to one part of the northern Reykjanes Ridge or the RP at any given time and the estimated recurrence interval of these rifting episodes and associated volcanism is ~1000 years (Clifton and Kattenhorn, 2006; Keiding et al., 2008). The historic lavas from 940-1340 C.E. capture one of these intervals, within which enrichment in lavas increases to the east (Peate et al., 2009). These authors explicitly refrain from suggesting a causation for this correlation by stating that the full range of enriched values has been expressed on the Reykjanes over the last 9 ka (Gee et al., 2000). However, no other authors explore coincident rifting episodes across volcanic systems on the Reykjanes, so this correlation cannot be yet be dismissed as chance. Crustal thickness, subtle variations in tectonics and/or magmatic processes, and proximity to the plume center in the EVZ among other factors cannot yet be ruled out.

Figure 1.1. Map of Iceland and its neovolcanic zones. These zone trace the plate boundary between North America (NA) and Eurasia (EU). KR = Kolbeinsey Ridge; TFZ = Tjörnes Fracture Zone; NVZ = Northern Volcanic Zone; EVZ = Eastern Volcanic Zone; MIB = Mid-Iceland Belt; WVZ = Western Volcanic Zone; RP = Reykjanes Peninsula; RR = Reykjanes Ridge; R = Reykjanes; K = Krísuvík; BSF = Brennisteinsfjöll; H = Hekla; VME = Vestmannaeyjar. Volcanic zones are composed of many individual volcanic systems (Einarsson and Sæmundsson, 1987). Contours mark the approximate depth to the Moho as determined by Darbyshire et al. (2000).

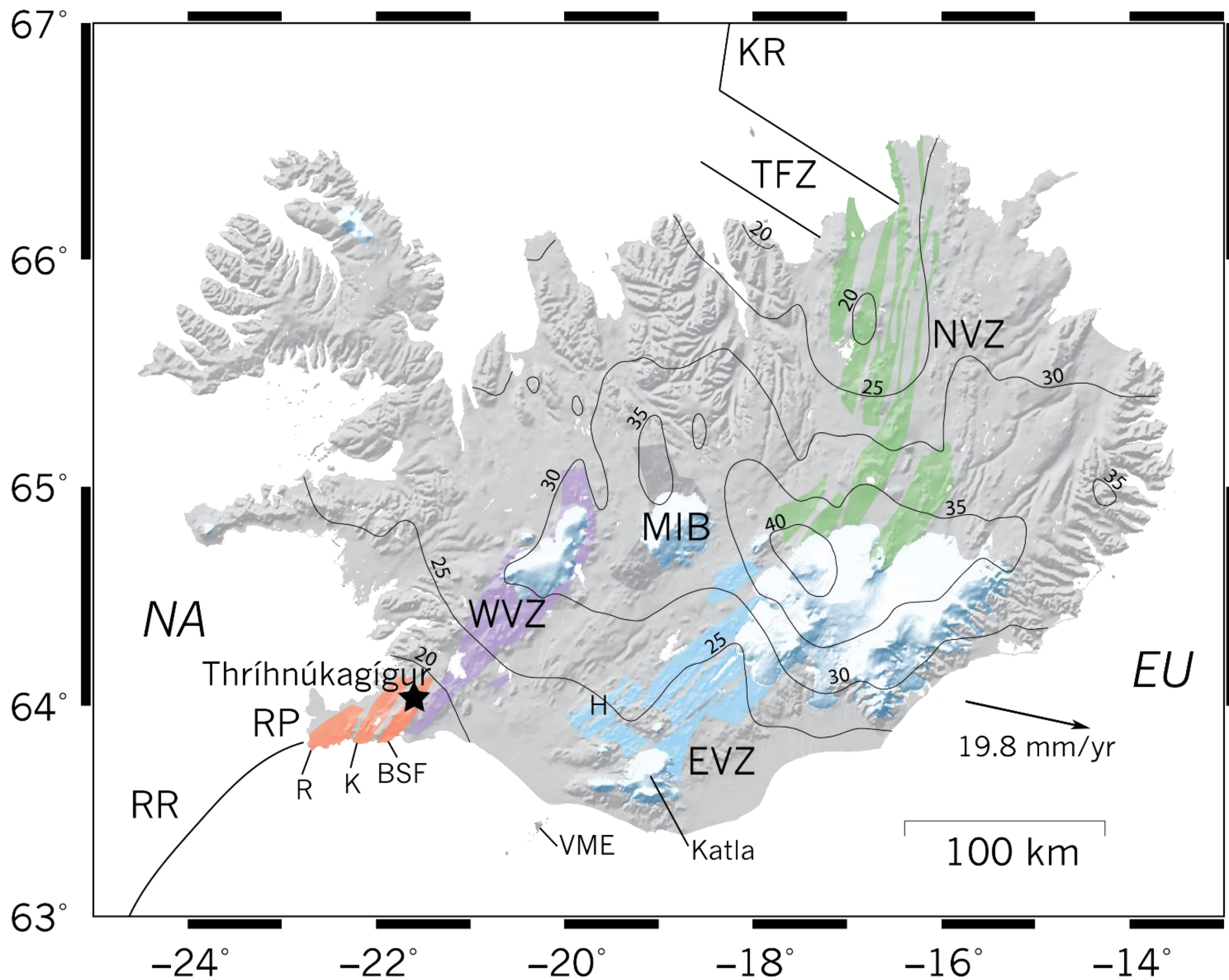

Figure 1.2. Variations along the Mid-Atlantic Ridge in La/Sm and Nb/Zr. Values are <1 for La/Sm on the South Reykjanes Ridge (SRR) and the Kolbeinsey Ridge (KR) and <0.05 for Nb/Zr. These ratios are greater than 1.5 and 0.08 for mainland Iceland (I). The North Reykjanes Ridge (NRR) is transitional between ambient MORB compositions and those in lavas derived from the Icelandic plume. Data from (Hanan et al., 2000).

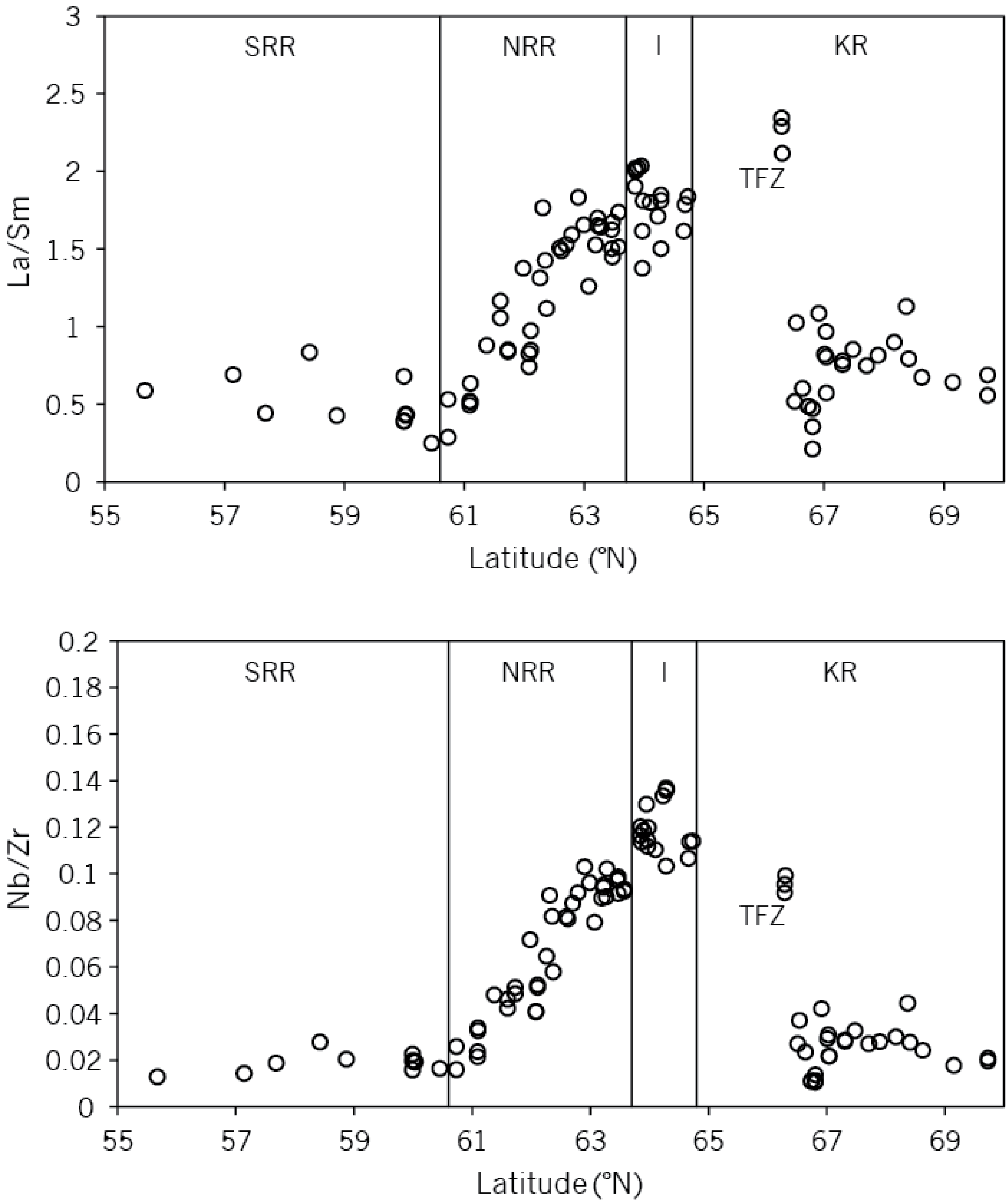

Figure 1.3. Map of the Reykjanes Peninsula showing the four fissure systems (shaded grey). From east to west they are the Reykjanes, Krísuvík, Brennisteinsfjöll, and Hengill volcanic systems. Thríhnúkagígur is located in Brennisteinsfjöll. Reykjavík and Thríhnúkagígur are shown in black stars. Outlines of the volcanic systems are from Einarsson & Sæmundsson (1987).

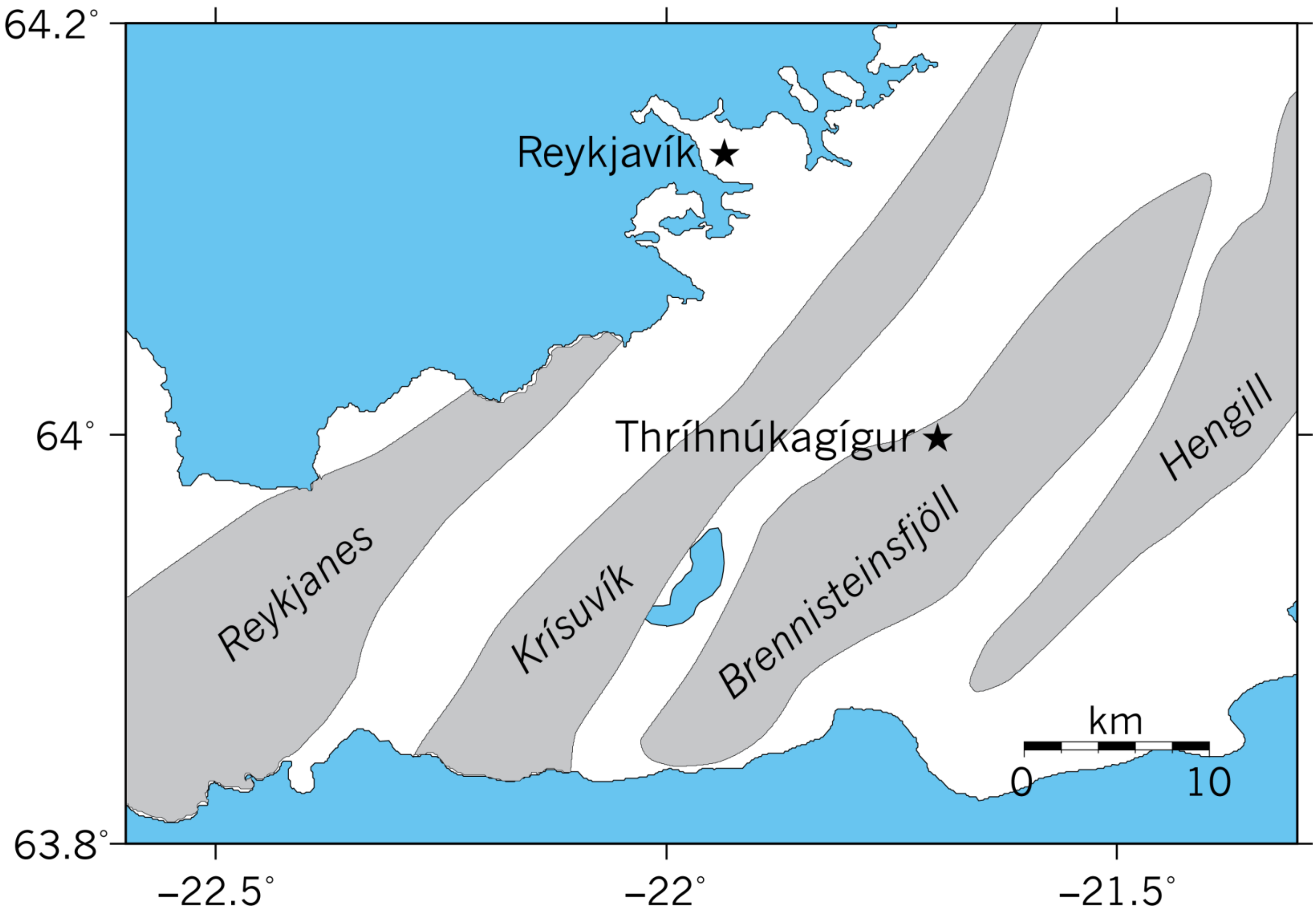

Figure 1.4. Enriched historic Reykjanes Peninsula lavas plotted on Nb/Zr vs. 87Sr/86Sr (a) and Nb/Zr vs. 143Nd/144Nd. Data from Peate et al. (2009) fall into “more enriched” and “less enriched” categories. More enriched sample correlate with lavas from Brennisteinsfjöll, while less enriched data are from the eastern Reykjanes Peninsula fissure swarms of Reykjanes and Krísuvík (b).

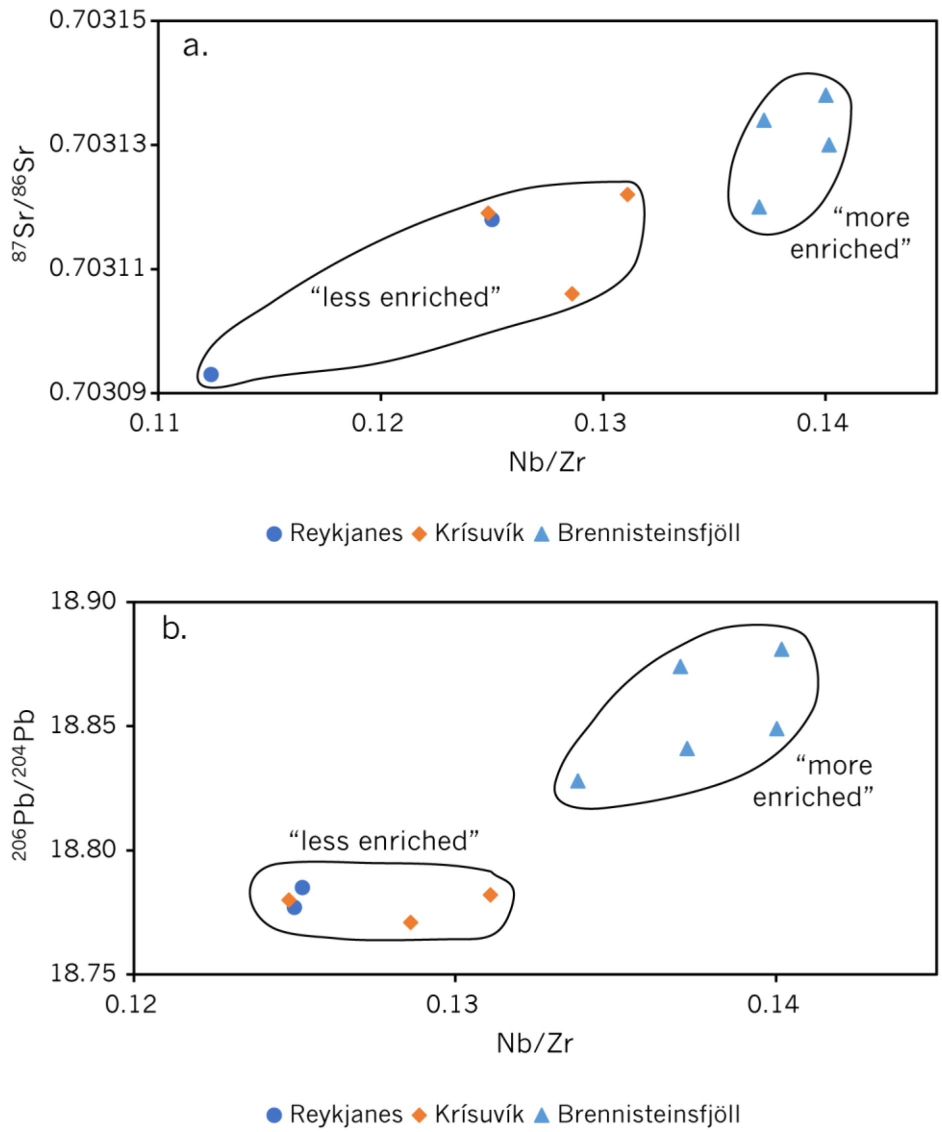

Figure 1.5. Changes in lava chemistry on the Reykjanes Peninsula through time from Gee et al. (1998b). Plots of lava age vs. Mg# (a), $^{87}Sr/^{86}Sr$ (b), Nb/Zr (c), and $^{143}Nd/^{144}Nd$ (d). The period during and immediately following deglaciation (13-9 ka) produced more primitive, depleted magmas with higher Mg# and $^{87}Sr/^{86}Sr$ and lower Nb/Zr ratios and $^{143}Nd/^{144}Nd$.

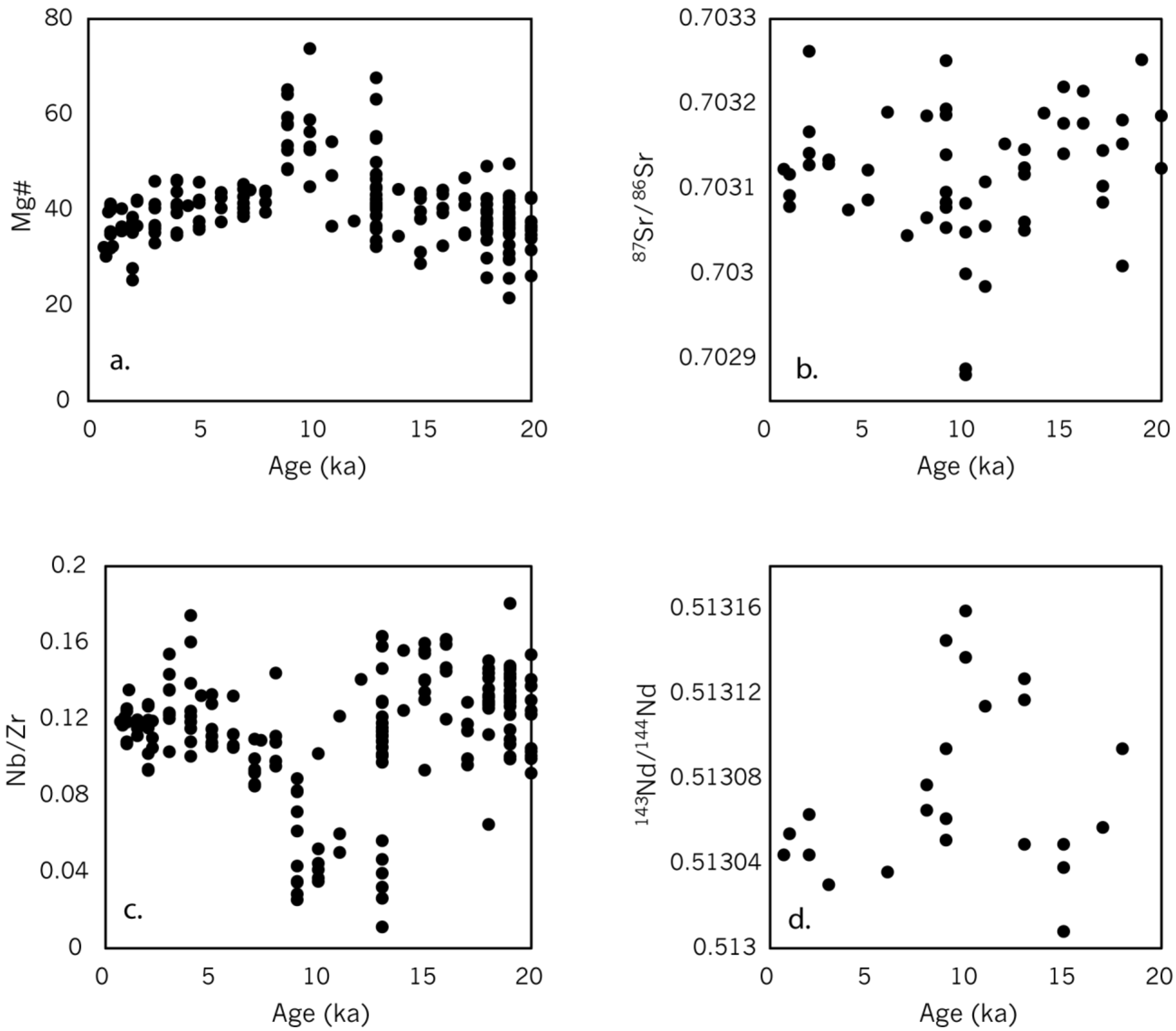

References

Árnadóttir T., Jiang W., Feigl K. L., Geirsson H. and Sturkell E. (2006) Kinematic models of plate boundary deformation in southwest Iceland derived from GPS observations. *J. Geophys. Res.* **111**, 1–16.

Bergerat F. and Angelier J. (2003) Mechanical behaviour of the Árnes and Hestfjall Faults of the June 2000 earthquakes in Southern Iceland: Inferences from surface traces and tectonic model. *J. Struct. Geol.* **25**, 1507–1523.

Bindeman I., Gurenko A., Sigmarsson O. and Chaussidon M. (2008) Oxygen isotope heterogeneity and disequilibria of olivine crystals in large volume Holocene basalts from Iceland: Evidence for magmatic digestion and erosion of Pleistocene hyaloclastites. *Geochim. Cosmochim. Acta* **72**, 4397–4420.

Bjarnason I. T. (2008) An Iceland hotspot saga. *Jökull*, 3–16.

Bjarnason I. T. and Schmeling H. (2009) The lithosphere and asthenosphere of the Iceland hotspot from surface waves. *Geophys. J. Int.* **178**, 394–418.

Bjarnason I. T., Wolfe C. J. and Solomon S. C. (1996) Initial results from the ICEMELT experiment : Body-wave delay times and shear-wave splitting across Iceland. *Geophys. Res. Lett.* **23**, 459–462.

Björnsson A., Eysteinsson H. and Beblo M. (2005) Crustal formation and magma genesis beneath Iceland: Magnetotelluric constraints. *Geol. Soc. Am. Spec. Pap. 388*, 665–686.

Brander J. L., Mason R. G. and Calvert R. W. (1976) Precise distance measurements in Iceland. *Tectonophysics* **31**, 193–206.

Brandsdóttir B. and Menke W. H. (2008) The seismic structure of Iceland. *Jökull* **58**, 17–34.

Brounce M., Feineman M., LaFemina P. C. and Gurenko A. (2012) Insights into crustal assimilation by Icelandic basalts from boron isotopes in melt inclusions from the 1783-1784 Lakagígar eruption. *Geochim. Cosmochim. Acta* **94**, 164–180.

Chauvel C. and Hémond C. (2000) Melting of a complete section of recycled oceanic crust: Trace element and Pb isotopic evidence from Iceland. *Geochemistry, Geophys. Geosystems* **1**, n/a–n/a.

Clifton A. E. and Einarsson P. (2005) Styles of surface rupture accompanying the June 17 and 21, 2000 earthquakes in the South Iceland Seismic Zone. *Tectonophysics* **396**, 141–159.

Clifton A. E. and Kattenhorn S. A. (2006) Structural architecture of a highly oblique divergent plate boundary segment. *Tectonophysics* **419**, 27–40.

Clifton A. E. and Schlische R. W. (2003) Fracture populations on the Reykjanes Peninsula, Iceland: Comparison with experimental clay models of oblique rifting. *J. Geophys. Res.* **108**.

Clifton A. E., Sigmundsson F., Feigl K. L., Gunnar Guðmundsson and Árnadóttir T. (2002) Surface effects of faulting and deformation resulting from magma accumulation at the Hengill triple junction, SW Iceland, 1994-1998. *J. Volcanol. Geotherm. Res.* **115**, 233–255.

Condomines M., Muehlenbachs K., O'Nions R. K., Óskarsson N. and Oxburgh E. R. (1983) Helium, oxygen, strontium and neodynium isotopic relationships in Icelandic volcanics. *Earth Planet. Sci. Lett.* **66**, 125–136.

Darbyshire F. A., Bjarnason I. T. and White R. S. (1998) Crustal structure above the Iceland mantle plume imaged by the ICEMELT refraction profile. *Geophys. J. Int.* **135**, 1131–1149.

Darbyshire F. A., White R. S. and Priestley K. F. (2000) Structure of the crust and uppermost mantle of Iceland from a combined seismic and gravity study. *Earth Planet. Sci. Lett.* **181**, 409–428.

DeMets C., Gordon R. G. and Argus D. F. (2010) Geologically current plate motions. *Geophys. J. Int.* **181**, 1–80.

Einarsson P. and Sæmundsson K. (1987) Earthquake epicenters 1982-1985 and volcnaic systems in Iceland (map). In *I hlutarins eðli: Festschrift for Thorbjorn Sigurgeirsson* (ed. Þ. Sigfússon).

Fitton J. G., Saunders A. D., Norry M. J., Hardarson B. S. and Taylor R. N. (1997) Thermal and chemical structure of the Iceland plume. *Earth Planet. Sci. Lett.* **153**, 197–208.

Foulger G. R. and Anderson D. L. (2005) A cool model for the Iceland hotspot. *J. Volcanol. Geotherm. Res.* **141**, 1–22.

Foulger G. R., Pritchard M. J., Julian B. R., Evans J. R., Allen R. M., Nolet G., Morgan W. J., Bergsson B. H., Erlendsson P., Jakobsdóttir S., Ragnarsson S., Stefansson R. and Vogfjo K. (2000) The seismic anomaly beneath Iceland extends down to the mantle transition zone and no deeper. *Geophys. J. Int.* **142**, F1–F5.

Fronval T. and Jansen E. (1997) Eemian and Early Weichselian (140–60 ka) Paleoceanography and paleoclimate in the Nordic Seas with comparisons to Holocene conditions. *Paleoceanography* **12**, 443.

Gee M. A. M., Taylor R. N., Thirlwall M. F. and Murton B. J. (2000) Axial magma reservoirs located by variation in lava chemistry along Iceland's mid-ocean ridge. *Geology* **28**, 699–702.

Gee M. A. M., Taylor R. N., Thirlwall M. F. and Murton B. J. (1998) Glacioisostacy controls chemical and isotopic characteristics of tholeiites from the Reykjanes Peninsula, SW Iceland. *Earth Planet. Sci. Lett.* **164**, 1–5.

Gee M. A. M., Thirlwall M. F., Taylor R. N., Lowry D. and Murton B. J. (1998) Crustal Processes: Major Controls on Reykjanes Peninsula Lava Chemistry, SW Iceland. *J. Petrol.* **39**, 819–839.

Geirsson H., Bennett R. A., LaFemina P. C., Árnadóttir T., Sturkell E., Sigmundsson F., Travis M., Schmidt P., Lund B. and Hreinsdóttir S. (2012) Volcano deformation at active plate boundaries: Deep magma accumulation at Hekla volcano and plate boundary deformation in south Iceland. *J. Geophys. Res.* **117**, B11409.

Guðmundsson A. (1986) Mechanical Aspects of Postglacial Volcanism and Tectonics of the Reykjanes Peninsula, Southwest Iceland. *J. Geophys. Res.* **91**, 12711–12721.

Hanan B. B., Blichert-Toft J., Kingsley R. and Schilling J.-G. (2000) Depleted Iceland mantle plume geochemical signature: Artifact of multicomponent mixing? *Geochemistry, Geophys. Geosystems* **1**.

Hanan B. B. and Schilling J.-G. (1997) The dynamic evolution of the Iceland mantle plume: the lead isotope perspective. *Earth Planet. Sci. Lett.* **151**, 43–60.

Hardarson B. S., Fitton J. G., Ellam R. M. and Pringle M. S. (1997) Rift relocation - a geochemical and geochronological investigation of a palaeo-rift in northwest Iceland. *Earth Planet. Sci. Lett.* **153**, 181–196.

Hattori K. and Muehlenbachs K. (1982) Oxygen Isotope Ratios of the Icelandic Crust. *J. Geophys. Res.* **87**, 6559–6565.

Hreinsdóttir S., Einarsson P. and Sigmundsson F. (2001) Crustal deformation at the oblique spreading Reykjanes Peninsula, SW Iceland: GPS measurements from 1993 to 1998. *J. Geodyn.* **106**, 13803–13816.

Jakobsson S. P. (1972) Chemistry and distribution pattern of Recent basaltic rocks in Iceland. *Lithos* **5**, 365–386.

Jakobsson S. P., Jónasson K. and Sigurdsson I. A. (2008) The three igneous rock series of Iceland. *Jökull* **58**, 117–138.

Jakobsson S. P., Jonsson J. and Shido F. (1978) Petrology of the Western Reykjanes, Peninsula. *J. Petrol.* **19**, 669–705.

Jull M. and Mckenzie D. (1996) The effect of deglaciation on mantle melting beneath Iceland. *J. Geophys. Res.* **101**, 21815–21828.

Keiding M., Árnadóttir T., Sturkell E., Geirsson H. and Lund B. (2008) Strain accumulation along an oblique plate boundary: The Reykjanes Peninsula, southwest Iceland. *Geophys. J. Int.* **172**, 861–872.

Keiding M., Lund B. and Árnadóttir T. (2009) Earthquakes, stress, and strain along an obliquely divergent plate boundary: Reykjanes Peninsula, southwest Iceland. *J. Geophys. Res. Solid Earth* **114**, 1–16.

Klein F. W., Einarsson P. and Wyss M. (1973) Microearthquakes on the Mid-Atlantic Plate Boundary on the Reykjanes Peninsula in Iceland. *J. Geophys. Res.* **78**, 5084.

Klein F. W., Einarsson P. and Wyss M. (1977) The Reykjanes Peninsula, Iceland, Earthquake Swarm of September 1972 and Its Tectonic Significance. *J. Geophys. Res.* **82**, 865–888.

Kokfelt T. F., Hoernle K., Hauff F., Fiebig J., Werner R. and Garbe-Schönberg D. (2006) Combined Trace Element and Pb-Nd-Sr-O Isotope Evidence for Recycled Oceanic Crust (Upper and Lower) in the Iceland Mantle Plume. *J. Petrol.* **47**, 1705–1749.

Koornneef J. M., Stracke A., Bourdon B., Meier M. A., Jochum K. P., Stoll B. and Grönvold K. (2012) Melting of a Two-component Source beneath Iceland. *J. Petrol.* **53**, 127–157.

Kurz M. D., Meyer P. S. and Sigurdsson H. (1985) Helium isotopic systematics within the neovolcanic zones of Iceland. *Earth Planet. Sci. Lett.* **74**, 291–305.

LaFemina P. C., Dixon T. H., Malservisi R., Árnadóttir T., Sturkell E., Sigmundsson F. and Einarsson P. (2005) Geodetic GPS measurements in south Iceland: Strain accumulation and partitioning in a propagating ridge system. *J. Geophys. Res.* **110**, B11405.

Larsen L. M., Pedersen A. K., Pedersen G. K. and Piasecki S. (1992) Timing and duration of early Tertiary volcanism in the North Atlantic: new evidence from West Greenland. *Magmat. causes Cont. Break.* **68**, 321–333.

Maclennan J., Jull M., McKenzie D., Slater L. and Grönvold K. (2002) The link between volcanism and deglaciation in Iceland. *Geochemistry, Geophys. Geosystems* **3**, 1–25.

Manning C. J. and Thirlwall M. F. (2014) Isotopic evidence for interaction between Öræfajökull mantle and the Eastern Rift Zone, Iceland. *Contrib. to Mineral. Petrol.* **167**, 959.

McKenzie D. and O'Nions R. K. (1991) Partial Melt Distributions from Inversion of Rare Earth Element Concentrations. *J. Petrol.* **32**, 1021–1091.

Mittelstaedt E., Ito G. and Behn M. D. (2008) Mid-ocean ridge jumps associated with hotspot magmatism. *Earth Planet. Sci. Lett.* **266**, 256–270.

Morgan W. J. (1971) Convection Plumes in the Lower Mantle. *Nature* **230**, 42–43.

Muehlenbachs K., Anderson A. T. and Sigvaldason G. E. (1974) Low-O18 basalts from Iceland. *Geochim. Cosmochim. Acta* **38**, 577–588.

Nunns A. G., Talwani M., Lorentzen G. R., Vogt P. R., Sigurgeirsson T., Kristjánsson L., Larsen H. C. and Voppel D. (1983) Magnetic anamolies over Iceland and surrounding seas. In *Structure and Development of the Greenland-Scotland Ridge* pp. 661–678.

Peate D. W., Baker J. A., Jakobsson S. P., Waight T. E., Kent A. J. R., Grassineau N. V. and Skovgaard A. C. (2009) Historic magmatism on the Reykjanes Peninsula, Iceland: a snap-shot of melt generation at a ridge segment. *Contrib. to Mineral. Petrol.* **157**, 359–382.

Peate D. W., Breddam K., Baker J. A., Kurz M. D., Barker A. K., Prestvik T., Grassineau N. V. and Skovgaard A. C. (2010) Compositional Characteristics and Spatial Distribution of Enriched Icelandic Mantle Components. *J. Petrol.* **51**, 1447–1475.

Saunders A. D., Fitton J. G., Kerr A. C., Norry M. J. and Kent R. W. (1997) The North Atlantic Igneous Province. In *Large Igneous Provinces: Continental, Oceanic, and Planetary Flood Volcanism* pp. 45–93.

Schilling J.-G. (1973) Iceland Mantle Plume: Geochemical Study of Reykjanes Ridge. *Nature* **242**, 565–571.

Sigmarsson O. and Steinthórsson S. (2007) Origin of Icelandic basalts: A review of their petrology and geochemistry. *J. Geodyn.* **43**, 87–100.

Sinton J., Grönvold K. and Sæmundsson K. (2005) Postglacial eruptive history of the Western Volcanic Zone, Iceland. *Geochemistry, Geophys. Geosystems* **6**, n/a–n/a.

Sun S. -s. and McDonough W. F. (1989) Chemical and isotopic systematics of oceanic basalts: implications for mantle composition and processes. *Geol. Soc. London, Spec. Publ.* **42**, 313–345.

Taylor B., Crook K. and Sinton J. (1994) Extensional transform zones and oblique spreading centers. *J. Geophys. Res.* **99**, 19707–19718.

Thirlwall M. F., Gee M. A. M., Taylor R. N. and Murton B. J. (2004) Mantle components in Iceland and adjacent ridges investigated using double-spike Pb isotope ratios. *Geochim. Cosmochim. Acta* **68**, 361–386.

Villemin T. and Bergerat F. (2013) From surface fault traces to a fault growth model: The Vogar Fissure Swarm of the Reykjanes Peninsula, Southwest Iceland. *J. Struct. Geol.* **51**, 38–51.

Walters R. L., Jones S. M. and Maclennan J. (2013) Renewed melting at the abandoned Húnafloí Rift, northern Iceland, caused by plume pulsing. *Earth Planet. Sci. Lett.* **377-378**, 227–238.

Weir N. R. W., White R. S., Brandsdóttir B., Einarsson P., Shimamura H. and Shiobara H. (2001) Crustal structure of the northern Reykjanes Ridge and Reykjanes Peninsula, southwest Iceland. *J. Geophys. Res.* **106**, 6347.

Wilson J. T. (1963) Continental Drift. *Sci. Am.* **208**, 86–103.

Wolfe C. J., Bjarnason I. T., VanDecar J. C. and Solomon S. C. (1997) Seismic structure of the Iceland mantle plume. *Nature* **385**, 245–247.

Chapter 2

Inside the Volcano: Rapid entrainment of unconsolidated crust during a monogenetic fissure eruption

2.1 Introduction

Small volume basaltic eruptions (<1 km^3) produce tephra and scoria cones and/or lava fields that are among the most abundant subaerial volcanic landforms on Earth (Wood, 1980; Keating et al., 2007). As commonplace geologic features, it is important to understand how their structure and development are controlled by the preexisting structures relative to the far field stresses that typically control dike propagation and orientation. These eruptions occur in a variety settings including monogenetic fields, at the sites of fissure eruptions, and on the flanks of stratovolcanoes and shield volcanoes. Recent rifting events have been well-observed and well-imaged geodetically (Wright et al., 2006; Calais et al., 2008; Biggs et al., 2013; Sigmundsson et al., 2015), but are not able to fully resolve the geometry and development of the uppermost eruptive conduit. Data from older, eroded fissure systems have been described in detail (Németh and White, 2003; Keating et al., 2007; Genareau et al., 2010; Valentine, 2012; Harp and Valentine, 2015; Németh and Kereszturi, 2015). These suggest that decrease in the vertical stress field in the very uppermost crust allows dikes to widen in the upper 50-150 m (Keating et al., 2007; Valentine, 2012). Yet, most observations of the internal structure of monogenetic cones are limited to eroded systems at the surface of the Earth. Rarely is the full length of the shallow magma plumbing observed in entirety.

Thríhnúkagígur is a monogenetic, small volume basaltic fissure eruption on the Reykjanes Peninsula. It is unique in Iceland, and perhaps in the world, in that a large cave directly below the main cone exposes a cross-section of the uppermost magma plumbing system, as well as the regional stratigraphy. This vertically oriented lung-shaped cave offers a unique a view into some non-unique magmatic and eruptive processes. First, the uppermost ~150 m of architecture provides insights into the eruptive process and the behavior of dikes in the shallow subsurface. Second, the remnants of a buried tephra cone near the bottom of the cave provides insights to one way a crustal contaminant may be added to mantle-derived magmas. The buried tephra cone is evaluated for both its role in focusing the flux of magma to a single vent at the surface and as a crustal material that could have been entrained by the erupting magma, thereby creating a vacancy below the main cone.

2.2 Field descriptions

2.2.1 Surface geology

Thríhnúkar is a NNE-SSW trending fissure system in the Brennisteinsfjöll volcanic system. Its name is derived from the three peaks, Vesturhnúkur, Miðhnúkur, and Thríhnúkagígur that mark different eruptive episodes (Figure 2.1; Sæmundsson, 2006). Vesturhnúkur, the oldest and westernmost of the peaks, sits on the edge of a plateau that descends steeply to the northwest. It is associated temporally with the late Weichselian glaciation (Sæmundsson et al., 2010) and consists primarily of basaltic hyaloclastite. Thin dikes are pervasive on the western slope of the hyaloclastite and three dolerite plugs occur at the summit, representing potential eruptive centers.

Miðhnúkur is a basaltic spatter cone between Vesturhnúkur and Thríhnúkagígur that is estimated to be approximately 5 ka in age (Sæmundsson, 2006; and references therein). Flows from Miðhnúkur (H-145; Figure 2.1) are the most extensive of the three Thríhnúkar eruptions with some outcrops appearing up to 6.5 km away from the main cone (Sæmundsson et al., 2010). Most of the flow extends off the plateau to the west and northwest. Its full extent is unknown because it has been largely buried by subsequent lava flows from other eruptive fissures. A 300 meter long depression formed east of the Miðhnúkur cone during the event, and looks like a collapsed lava tube. It is elongate parallel to the strike of the fissure and at least partially filled with lavas from the Miðhnúkar eruption.

The eruption of Thríhnúkagígur is estimated to be 3.5 ka in age (Sæmundsson, 2006). Soil profiles overlying Thríhnúkagígur lavas included Katla tephras from >2500 bp (Sæmundsson, 2006; Sæmundsson, 2008).The easternmost of the Thríhnúkur peaks, its main cone is an amalgamation of two vents from a fissure eruption. Smaller disparate spatter cones associated with the fissure eruption occur up to 1.5 km from the main cone (Figure 2.1). Thríhnúkagígur lavas can be distinguished in the field by the presence of macroscopic plagioclase phenocrysts as opposed to olivine in the Miðhnúkar lavas. The main flow from Thríhnúkagígur (H-146) covers roughly 0.34 km^2 (Figure 2.1). Three additional small lava fields are present along the fissure and were fed by small spatter cones. One is immediately adjacent to the main cone to the SSW and the other two lava fields are 1.5 km to the NNE on the flank of the plateau (Figure 2.1). These three flows total to just under 0.1 km^2 in area. The one proximal to the main cone is only ~0.015 km^2 in area.

Lavas flows are relatively thin, about 15-30 cm in height. The flow tops are vesicle-poor, but become increasing vesicular towards the base of the flow where individual vesicles are up to several centimeters in diameter and become more interconnected. Lavas from the main cone flowed primarily to the north and east, but also filled the depression to its west that had formed originally during the Miðhnúkar eruption. The depression filled to a height of about 1-1.5 m leaving behind a terrace (bathtub ring) after it drained to the east by a lava tube.

The main spatter cone is relatively symmetrical, but elongate along the azimuth of the fissure. The summit consists of a pair of similarly sized vents at the north and south ends of the cone. The southern vent remained open, whereas the northern vent became plugged towards the end of the eruption. The cone formed from the coalescence of the fissure into a couple of main vents during a Strombolian eruption with low viscosity, gas-rich lavas (Figure 2.2). Pele's tears and oxidized scoriaceous vent spatter of various colors around and at the top of the cone support this eruptive style. There are also several tens of vesicle-poor 2-5 cm rheomorphic flows draining back into the vent (Figure 2.3). These thin flows back into the vent contrast the surrounding highly vesicular H-146 flows. The vent itself is ~8 m in diameter at the surface, but narrows rapidly with increasing depth, in places less than 3 by 2 meters, elongated along the fissure azimuth reflecting the overall cone structure (Figure 2.2).

2.2.2 Subsurface Geology

The eruptive conduit provides the only entrance to the subsurface of Thríhnúkagígur (Figure 2.4). The narrow cylindrical section of the conduit extends vertically 60 m down from the summit. This section does not expose much of the subsurface stratigraphy as it is coated by flowback of lava into the conduit. Flowback is characterized by rivulet textures (Figure 2.5) and stalactites of lava (Figure 2.6) that are a few centimeters to tens of cm in scale. Part way down the conduit there is a narrow, continuous tunnel that diverts off and reconnects to the main conduit in the shape of a teacup handle.

Further down the conduit from the surface, the cave broadens and flowback features no longer coat the cave walls. As the cylindrical conduit opens up into the main, lung-shaped hollow of the cave, it transitions from a focused oblong tube into a 2 m wide planar dike exposed in the cave walls. The majority of the exposed rock consists of sub-horizontal basalt flows that have been altered to a mustard yellow (Figure 2.7). These flows are commonly a few tens of cm in thickness, and are generally not more than a meter thick.

Underlying the succession of lava flows is a buried pile of tephra, which has previously been interpreted as a laterally continuous, gently dipping layer of hyaloclastite that breaks the surface at Vesturhnúkar (Sæmundsson, 2006). This unconsolidated material observed in the cave beneath Thríhnúkagígur appears to be a separate geologic unit from the hyaloclastite. Instead, it is interpreted herein as the remnant of a subaerially erupted tephra cone rather than a hyaloclastite ridge. The photo in Figure 2.8 shows the contrast in physical characteristics between these two units. Although these two units may represent different stages the hyaloclastite succession, rare bomb sags in the buried tephra suggest a subaerial eruption. The buried is only exposed in the NW wall of the cave and not on the SE wall, until deeper down in the cave. The contact with the overlying lavas dips toward the NE and SW in wall, which is consistent with a tephra cone that would dip in all directions from its highest point. The buried tephra cone is seen interfingering with the overlying lava pile in the NW wall of the cave, but the slope of the tephra remains relatively constant until it grades into a >1.5 m thick tephra sheet exposed at the northern end of the cave (Figures 2.9, 2.10). Bombs and bomb sags in the tephra apron suggest that the eruption that formed the tephra cone was subaerial. The constant slope of the buried tephra cone and lack of reworking, other than minor interfingering with subsequent lava flow, also suggests rapid burial by lava since the tephra is unconsolidated. Because this relatively unconsolidated material is preserved at all, its eruption and burial under ~120 m of lava flows likely occurred within an interglacial period. Otherwise glaciers would have likely modified or removed the tephra cone.

The buried tephra primarily consists of unconsolidated, 1-5 mm glass shards with rare macroscopic plagioclase crystals. Locally within the tephra pile pieces of scoria are common, but no larger than 10 centimeters and rarely greater than 5 cm. The buried tephra displays no major internal structures, but it is locally heterogeneous in size, color and composition. For example, there is a 20 cm layer within the tephra that is well consolidated with a quasi-foliated clay matrix around larger scoria clasts up to ~5 cm, which suggests this tephra was reworked in the presence of water. Separately, in the massive portions of the unit that lack evidence of reworking, there are zones that exhibit 1-2 cm wide spots that have been partially palagonitized.

The age of the buried tephra cone is unknown, but may be constrained by the periodicity of magmatism and rifting on the Reykjanes Peninsula, which is thought to be on the order of 1000 years (Sæmundsson et al., 2010). Lava flows in the cave are rarely greater than 1 m thick. By assuming a rate of 1 meter of burial per 1000 years, and accounting for the thickness of the lavas overlying the tephra apron (~120 m), an approximate age of 100 ka is calculated. This assumes eruptions occurred in this location during each rifting cycle and produced a lava flow thicker than the average flows observed in the cave, so this is a minimum age estimate. The Eemian interglacial ended approximately 113 ka with the onset of the Weichselian glaciation in northern Europe (Fronval and Jansen, 1997), further suggesting that 100 ka is a minimum age.

Within the lava flows that lie stratigraphically above the top of the tephra cone in the western wall of the cave there is a 5 m wide black to purple oval-shaped plug of crystalline basalt with a large gas cavity in the center (Figure 2.11). It has an oxidized red contact aureole and is interpreted to be an intrusion associated with the ~3.5 Ka Thríhnúkagígur eruption. Although it has no surface expression, it is close enough to the surface that it is probable that it vented to the surface and then was subsequently buried during the formation of the main cone of Thríhnúkagígur. The plug itself is too high in the ceiling to collect samples directly. Large boulders of oxidized, purple basalt beneath the plug are interpreted as having fallen from the plugged conduit rather than the dike for two reasons. First, some boulders have greater dimensions that the width of the dike. Second, these boulders are not below the dike and are higher up on debris pile (the cave floor) than any locations directly below the dike.

From the floor of the cave, the larger structure of the dike that fed the 3500 bp eruption can be observed. The dike arcs across the ceiling tracing a vertical plane through the center of the cave. It trends NNE-SSW, which is consistent with the regional extensional fissures and crater rows of the Brennisteinsfjöll fissure swarm. The dike is similar to the plugged conduit in that it is oxidized from black to purple and the baked margins of country rock adjacent to the dike are red to a reddish-purple. About half way down from the narrowing of the conduit to the floor of the cave, the dike has an *en echelon* structure (Figure 2.7). Towards the floor of the cave on the northeast side, the dike decreases in width to 0.5-1 m and develops a more complex structure. Further down towards the floor on the northeast end of the cave, decimeter wide splays are developed. In other segments, it separates into two thinner dikes then recombines into a single larger dike. At the lowest exposure, the dike can be seen cross-cutting the tephra apron (Figure 2.9).

At the southwest end of the cave, a narrow gap between the debris pile and the ceiling of the cave extends down along the strike of the dike. In one segment of the dike there is a nearly 0.5 m long, 5 cm wide gas pocket that pinches out at both its ends (Figure 2.11). Roughly 20 m down into this gap becomes a series of crawl spaces between boulders. Here the dike can be seen crosscutting the tephra pile, but the structure of the dike is difficult to trace because of the dike splays into many smaller dikes at this depth and the exposure is much more limited. The best exposures of the dike are where it fed vertical cylindrical pipes, or proto-conduits, that extend up into the buried tephra (Figure 2.12). These proto-conduits have flowback features along their walls, suggesting that their formation was a result of magmatic scouring of the poorly consolidated tephra. These cylindrical cavities are typically immediately adjacent to the dike and range in diameter from 0.25 to 2 m. The largest is mapped (Stefánsson, 1992; Sæmundsson, 2006) and penetrates more than 30 m up into the overlying tephra (Figure 2.12).

2.3 Methods

Measuring the volume of the cave can help constrain the amount of tephra that once filled the cave if it formed by the removal of unconsolidated buried tephra by an erupting magma. Measuring the volume of the Thríhnúkagígur spatter cone and estimating the lava volumes and their density can constrain the dense rock equivalent (DRE) of the erupted products, which can help to constrain the relative proportion of tephra that could have been entrained and incorporated into the lavas.

2.3.1 Light Detection and Ranging (LiDAR)

The cave at Thríhnúkagígur was scanned to gain an understanding of its overall shape and structure and to relate that to the dynamics of the fissure eruption to which it is likely related. The scans also serve the purpose of giving robust constraints on the volumes of the cave and the main cone. Twelve locations from inside the cave at Thríhnúkagígur were used to collect high resolution Light Detection and Ranging (LiDAR) data to create a digital elevation model of the cave in 2011. The exterior of the cone was also scanned. Data was collected with a Leica C-10 scanner. The resulting DEM from the interior and exterior scans is accurate to <4 cm, yielding an accurate and precise volume estimate of the main chamber of the cave and the spatter cone at the surface.

2.3.2 Density Measurements

In order to compare the mass of erupted lavas and the mass of the buried tephra that may have once filled the volume of the cave, the dense rock equivalent (DRE) volumes of the two units must be determined. Vesicles in the lava samples were determined to have a modal percentage of 29% by point counting. Most vesicles were at least 1 mm in diameter; therefore lava chips were crushed with a mortar and pestle into fragments that were <3 mm in any dimension and hand selected to ensure that all vesicles were open. A Mettler electronic balance was used to weigh ~4 g of lava rock chips. A similar mass of the better consolidated, yet still representative tephra were also weighed. These samples were then placed in 10 ml and 50 ml graduated cylinders partially filled with water, respectively, to measure the volume. Because the error on the 50 ml cylinder was greater, a larger duplicate sample of the same tephra sample was also weighed and its volume measured.

2.4 Results

The LiDAR derived DEM allows us to estimate that the volume of the cave is ~40,000 m^3 (Figures 2.4, 2.12). The surface area of the lavas extruded from the Thríhnúkagígur eruption can be estimated at 350,000 m^2 from the geologic map by Sæmundsson (2006). With a minimum estimated thickness of the lava flows, and cone height and radius, a minimum erupted volume can be estimated. For this calculation, a 30 m high cone with a radius of 50 m and a lava flow thickness 0.25 m thick are used (Table 2.1). These estimates yield an erupted volume of $1.67 \cdot 10^5$ m^3. The proportion of incorporated tephra by mass that may have been entrained in the erupted lava can then be determined using the DRE of the buried tephra and erupted lavas (Table 2.2). This eruptive volume and a density of 2150 kg/m^3 yields a total eruptive mass of 3.57 x 10^8 kg of lava. The maximum possible mass fraction of tephra in the erupted Thríhnúkagígur lavas is therefore 29%.

2.5 Discussion

A challenge for evaluating crustal assimilation in Iceland, and more generally at ocean islands, is that these components have the same basaltic bulk compositions as the magmas that intrude them. Without any knowledge of the physical and chemical characteristics of potential crustal contaminants, it is nearly impossible to constrain their contribution to mantle-derived magmas. The buried tephra could not have been identified as a component in the Thríhnúkagígur lavas if only the lavas had been examined in isolation. The unique exposure provided in the cave where the buried tephra is exposed allows for it to be identified as a possible basaltic crustal contaminant. Direct field observations and the physical properties of the crustal contaminant (fine-grained, poorly consolidated, glassy, etc.) are critical to interpreting their role in magma production and eruption dynamics.

2.5.1 Cave formation

Without a major edifice loading the crust at Thríhnúkar, and in the absence of a central magma chamber, local asperities in the uppermost crust should be the secondary control on the orientation of the dike after the regional stress field. Indeed, this is observed in Thríhnúkagígur's internal structure. The vertical sheet-like structure of the dike along the length and height of the cave supports a dominant regional stress field even in the uppermost crust, with the minimum stress in the north-northeast direction (Clifton et al., 2002; Clifton and Kattenhorn, 2006; Keiding et al., 2008; Keiding et al., 2009). The dike ruptured the surface up to 1.5 km away from Thríhnúkagígur to the north-northeast where several smaller volume cones are mapped as part of the Thríhnúkagígur event (Figure 2.1; Sæmundsson, 2006) demonstrating that it or a series of *en echelon* dikes behaved uniformly over at least a couple of kilometers.

In addition to this primary control on dike orientation, the unconsolidated buried tephra is much less competent than the overlying laterally continuous basalt flows, acting as a less resistant pathway for magma to travel to the surface. This preexisting structure is a local heterogeneity that likely guided and concentrated the magma during its final ascent to the surface. Evidence of magmatic erosion or scouring of the tephra is preserved in proto-conduits that penetrate into the buried tephra. These structures are seen in contact with or immediately adjacent to the dike and are always seen intruding into the tephra. The flowback-lined walls of proto-conduits in the deepest extent of the SW end of the cave suggest that magma acted as an erosive fluid that entrained the fine-grained, poorly consolidated buried tephra.

The location of the plugged conduit directly above the highest point in the remnant buried tephra cone is consistent with the idea that at initial stages of eruption, flow of magma could have been funneled by the tephra's cone-like geometry to the surface. Without a corresponding surface feature, the plugged conduit either did not actually feed an eruption, or any cone that it may have constructed was subsequently buried by the main cone of Thríhnúkagígur. Ultimately, the dike became more favorable than the plugged conduit for erupting lavas at the surface. The location of the buried tephra cone directly below the main cone may indicate that the tephra still acted to concentrate the eruption at this location. This may also explain why the main cone of three different monogenetic eruptions – the Thríhnúkar complex – all occur within a few hundred meters of each other.

The eruption at Thríhnúkagígur was likely Hawaiian to mildly Strombolian in style. Fire fountaining associated with the opening of the fissure would have focused into the main cone over time. This would have also focused rising gas pockets, such as the 0.5 m long gas bubble observed in the dike deep at the SW end of the cave and may reflect a shift to a more Strombolian eruption with punctuated explosions. Repeated, extremely thin (2-5 cm) lava flows indicate flow back (Figure 2.3) into the vent and are consistent with repeated bursts of lava erupting through the main conduit. Punctuated explosions associated with slug flow would allow lava to drain back into the conduit repeatedly. These observations point towards a low viscosity magma with intermediate to high gas content, which is also consistent with the thin (~0.25 m), vesicle-rich lava flows and Pele's tears observed on the surface of the cone.

A plausible scenario to explain the formation and preservation of the cave beneath Thríhnúkagígur is that unconsolidated or poorly consolidated material (the buried tephra) was entrained by the erupting magma as the diking event progressed. Assuming that the volume of the present day cave represents the maximum amount of tephra that could have been incorporated into Thríhnúkagígur lavas, 10-29% of the lava could be derived from the buried tephra cone. The buried tephra under Thríhnúkagígur, coupled with the vacancy below the main cone, demonstrates that incorporation of poorly consolidated, low-density material can occur rapidly, even during the course of an eruption if conditions are favorable. Up to 29% by mass of tephra may be incorporated in this manner.

The schematic diagram in Figure 2.13 illustrates a conceptual model for cave formation in two views. The diagram on the left is a cross-section within the plane of the dike that fed the eruption of Thríhnúkagígur. The right hand side is a diagram of a cross-section perpendicular to the dike. The model begins with the eruption of a tephra cone (Figure 2.13a) and then buried by subsequent lava flows (Figure 2.13b), which continue to accumulate through time until 3500 BP. Figures 2.13c and 2.13d show the initial stages of eruption where the dike cross-cuts the buried tephra cone and lava flows, and then erupts at the surface. As the eruption progresses, tephra becomes entrained in the ascending magma; and simultaneously the fissure transitions from erupting along its entire length to focusing into a couple of vents (Figure 2.13e). At the final stage of eruption, the dike has focused into a pair of adjacent vents that form the main spatter cone (Figure 2.13f). Figure 2.13g shows the cave profile at present after cave-ins have filled in part of the remnant buried tephra cone with debris.

2.6 Conclusions

Monogenetic fissure eruptions typically accommodate far field stresses, but the orientation and propagation of dikes that intrude the crust or result in eruptions may also be affected by a local stress field or preexisting crustal structures (Muirhead et al., 2015). At Thríhnúkagígur, the orientation of the eruptive fissure was consistent with accommodation of the far field stress regime, ascending to the surface as a vertical planar dike. The preexisting buried tephra cone did not affect the geometry or orientation of the dike as it propagated into the overlying lava flows to the surface; however, the location of the main cone of Thríhnúkagígur probably resulted from the anisotropy produced by the presence of a buried tephra cone at depth. The low density, fine-grained unconsolidated tephra is less competent than the surrounding and lava flow that bury it, as demonstrated by the numerous proto-conduits extending into it. The buried tephra very likely provided a preferential pathway for the ascending magma thereby concentrating flow through fissure at the main cone of Thríhnúkagígur. Here, evidence suggests that small-scale structures in the shallow crust do not influence the orientation or geometries of fissure eruption, but they may play a role in the location of the main vents that develop as the eruption progresses.

Moreover, as the flow of magma was focused through the buried tephra, the ascending magma scoured out, entrained, and erupted the unconsolidated buried tephra with it. This the preferred model for the development of the subterranean cave below the Thríhnúkagígur cone. Numerous proto-conduits fingers extend off the dike up into the overlying tephra dike at depth in the cave, providing evidence for erosion of the buried tephra by the ascending magma. A minimum estimate of the erupted volume of lava from Thríhnúkagígur from field observations and a geologic map by Sæmundsson (2006) were compared to the volume of the cave from LiDAR scans. The DRE of the buried tephra and lava were then used to find that the maximum percent by mass of tephra that could be in the lavas is 29%.

The rapid incorporation of the buried tephra into the erupting magma demonstrates that magmas may be contaminated rapidly and to a significant extent by shallow crustal components. If not for this unique exposure of the tephra in the cave, the buried tephra could not have been identified as a component in the Thríhnúkagígur lavas and this shallow crustal contamination would have been untraceable. The unconsolidated, poorly crystalline, and fine-grained nature of the tephra facilitated its ingestion and similar properties are advantageous for deeper crustal assimilation as well.

Table 2.1. Estimates of Thríhnúkagígur lavas volumes and calculation of tephra contents.

Cone Height (m)	Cone Radius (m)	Cone Volume (m^3)	Flow Area (m^2)	Flow Thickness (m)	Minimum Erupted Volume (m^3)	Dense Rock Equivalent (kg/m^3)	Minimum Erupted Mass (kg)	Cave Volume (m^3)	Tephra Density (kg/m^3)	Maximum Tephra Mass (kg)	% Tephra by Mass
30	50	78,500	350,000	0.25	166,500	2150	3.57E+08	40,000	2550	1.02E+08	29%

Table 2.2. Densities of Thríhnúkagígur lava and buried tephras.

	Sample ID	Mass (g)	Volume (mL)	Density (kg/m^3)
Lava	TNG-14-33	4.268	1.5	2850
Buried tephra	TNG-14-22	4.071	1.6	2540
Buried tephra	TNG-14-32	13.801	5.4	2560

Figure 2.1. Map of the Thríhnukar fissure system modified from Sæmundsson (2006). Samples are shown in black stars. Subterranean samples are excluded from this map, but are generally located underneath the Thríhnúkagígur spatter cone in red.

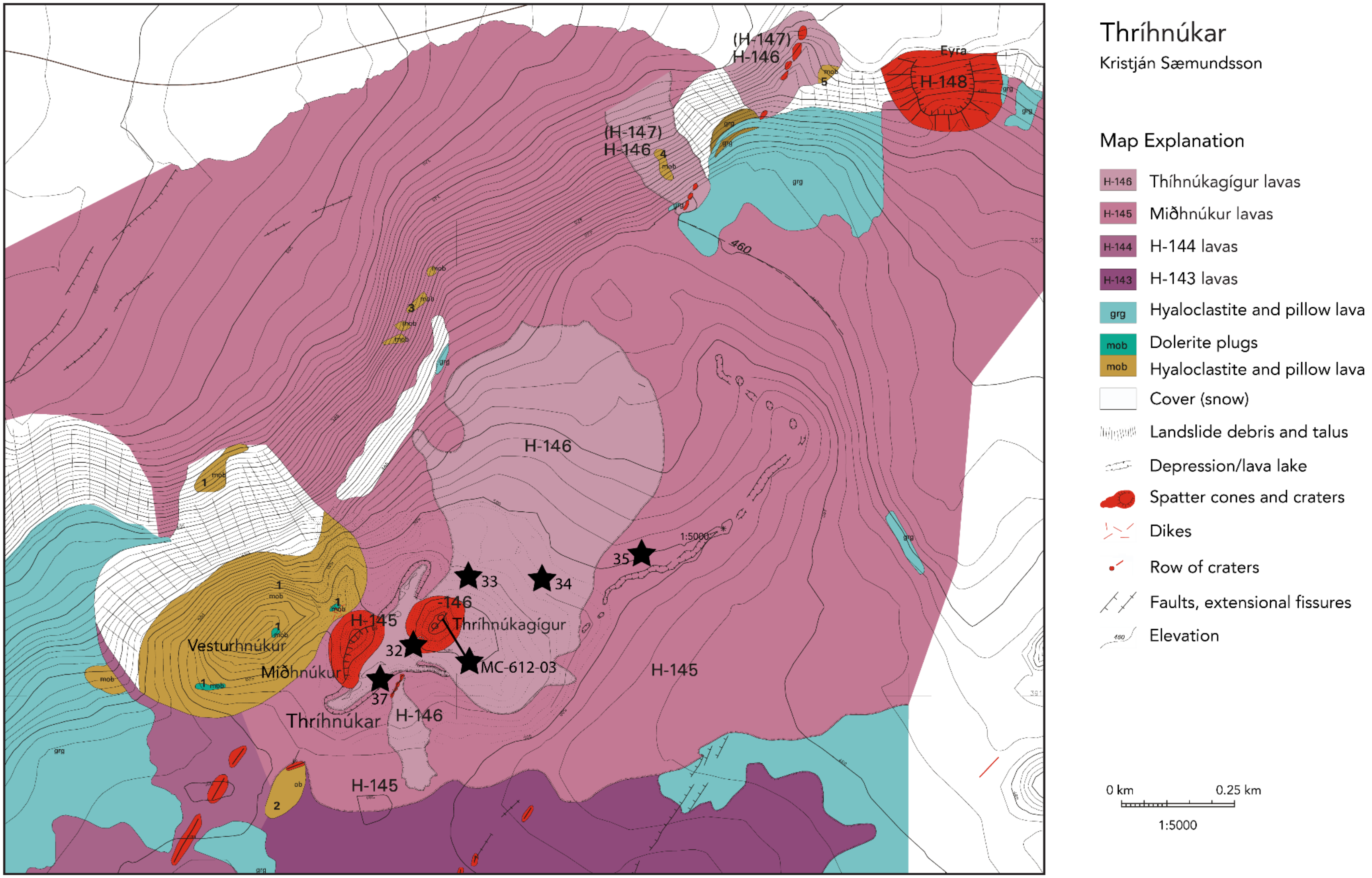

Figure 2.2. Two vents comprise the main cone of Thríhnúkagígur. The northern vent (left) became plugged towards the end of the eruption, while the southern vent (right, with scaffolding) remained open, providing an entrance to the cave below. Photo from P. LaFemina.

Figure 2.3. Succession of thin (2-5 cm) lava flows back into the vent at the summit of Thríhnúkagígur. Photo from P. LaFemina.

Figure 2.4. LiDAR scan of the interior of the cave at Thríhnúkagígur. Green and blue coloring represents different reflectivities of the rock. The dike, plugged conduit, and the buried tephra appear in blue. The image on the left is a view parallel to the orientation of the dike. The view on the right is perpendicular to the orientation of the dike.

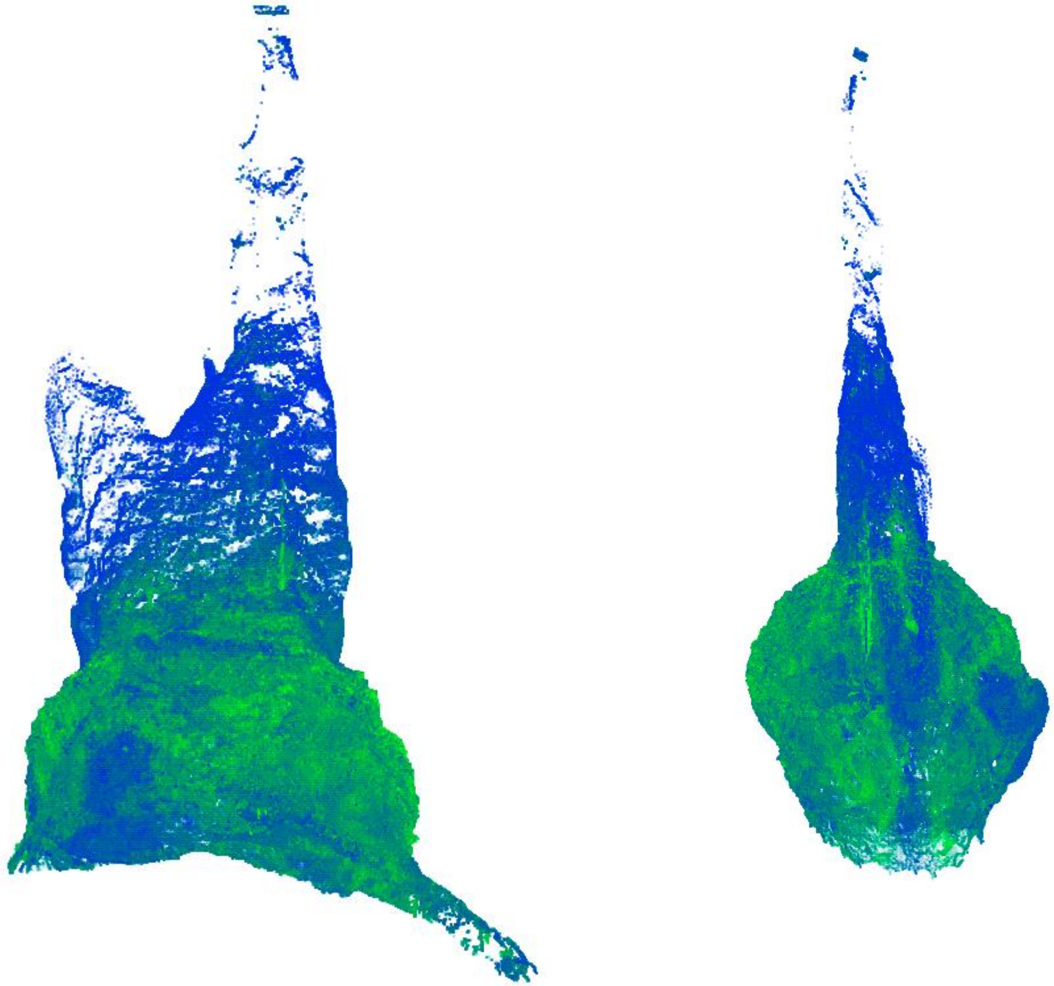

Figure 2.5. Magma flowback rivulets on a fallen block in the cave. Photo from P. LaFemina.

Figure 2.6. Stalactites of lava that dripped back into the cave during and/or following the eruption. Photo from P. LaFemina.

Figure 2.7. The NNE cave wall. A photo mosaic by P. LaFemina is simplified in a cartoon depicting the dike and tephra with sample locations.

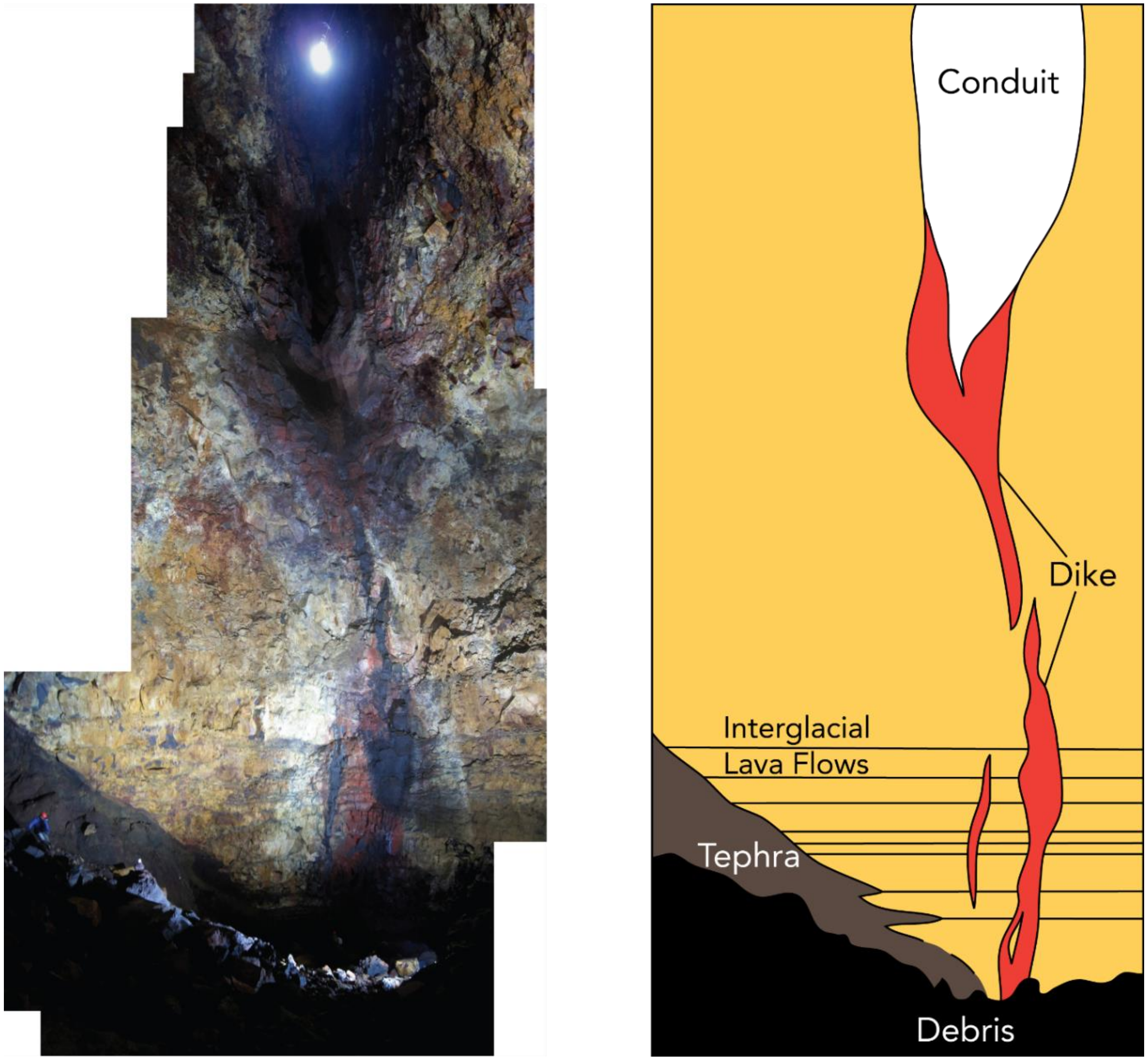

Figure 2.8. Representative buried tephra (right; TNG-14-15) is poorly consolidated compared to the well-welded hyaloclastite (left) collected at the from the gentle dipping hyaloclastite unit postulated by Sæmundsson (2006).

Figure 2.9. A panorama of the dike at the north end of the cave. Here it cross-cuts the tephra apron and to the left interfingering between the buried tephra and subsequent lava flows can be seen. Photo from P. LaFemina.

Figure 2.10. Photograph of the interior of the cave. The plugged conduit is the roundish purple feature on the left. The dike is the vertical purple-black feature on the right. The buried tephra cone on the bottom left if black.

Figure 2.11. A ~0.5 m long gas pocket in the center of the dike.

Figure 2.12. LiDAR scan of the Thríhnúkagígur cone and cave with the location of the largest of the proto-conduits indicated (a). A LiDAR scan of the main proto-conduit shows its geometry in greater detail (b).

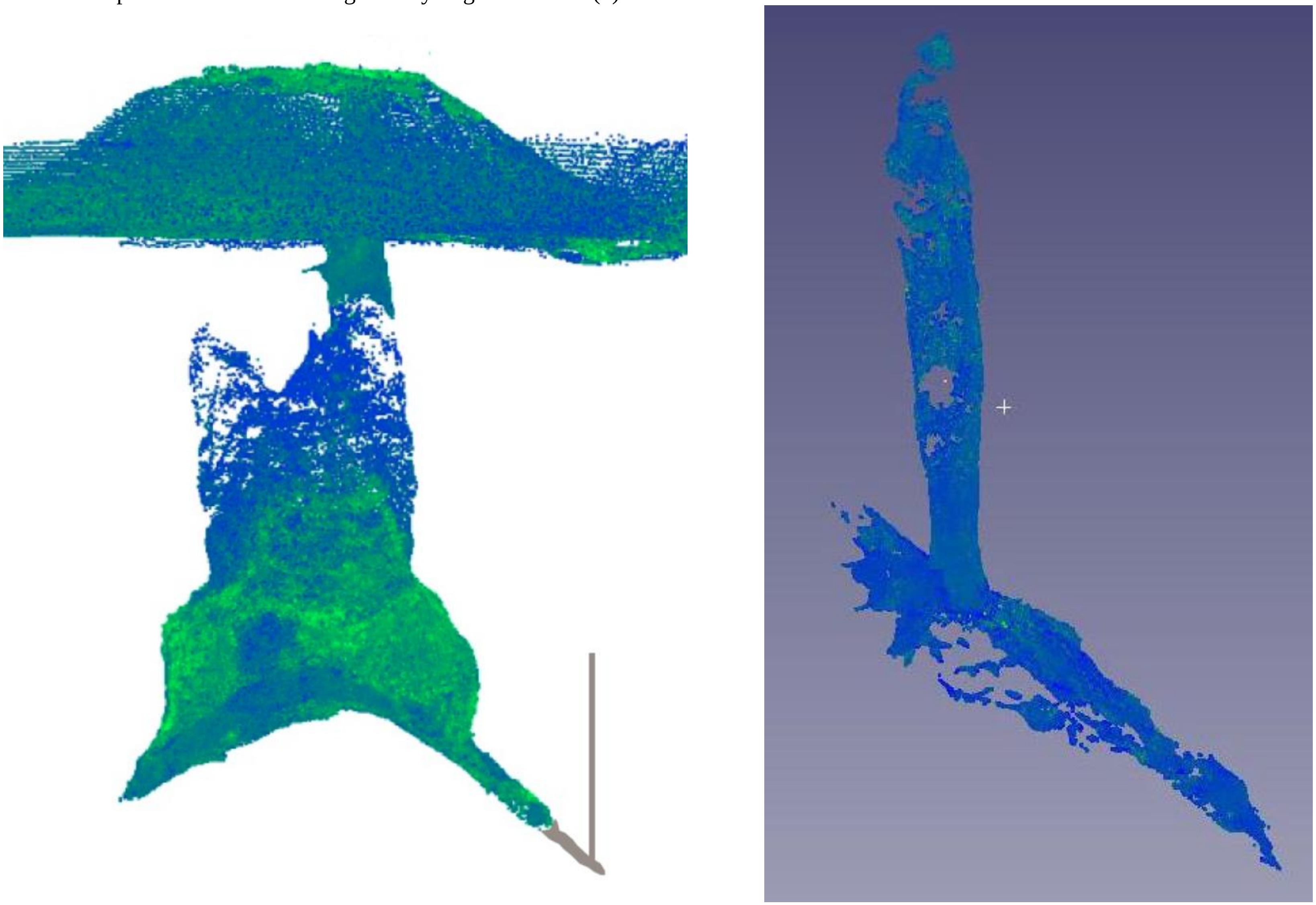

Figure 2.13. Stages of Thríhnúkagígur formation starting with the formation (a) and burial of the tephra cone (b), followed by dike injection (c) and eruption along a fissure (d). As the eruption continues, the magma both progressively entrains more tephra from depth and narrows from a fissure into a couple of vents (e anf f). Part g shows the present day outline of the cave. The left hand side of the diagram shows a cross-section within the plane of the dike. The left shows a cross-section perpendicular to the dike.

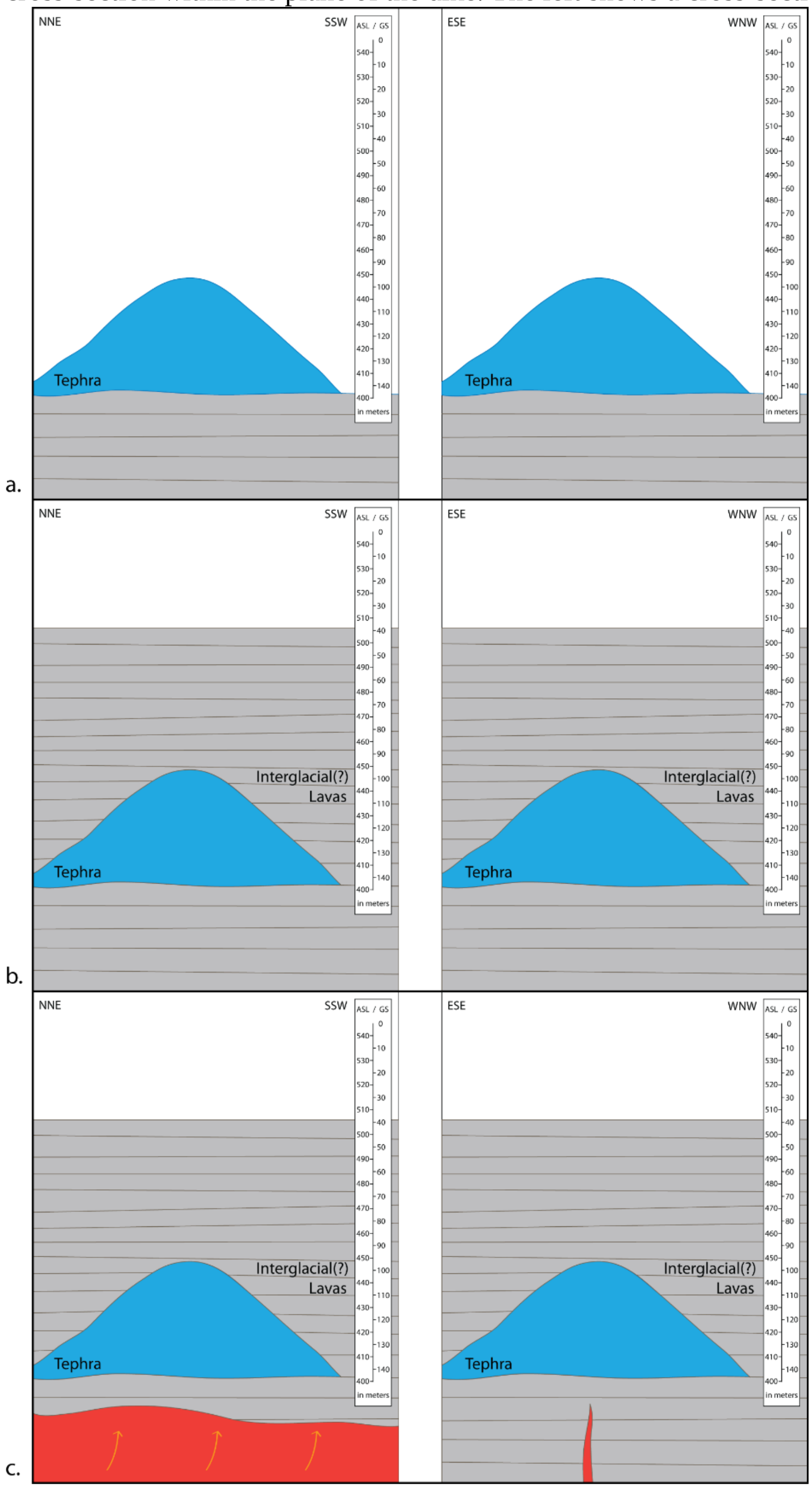

Figure 2.13 (d-f) continued.

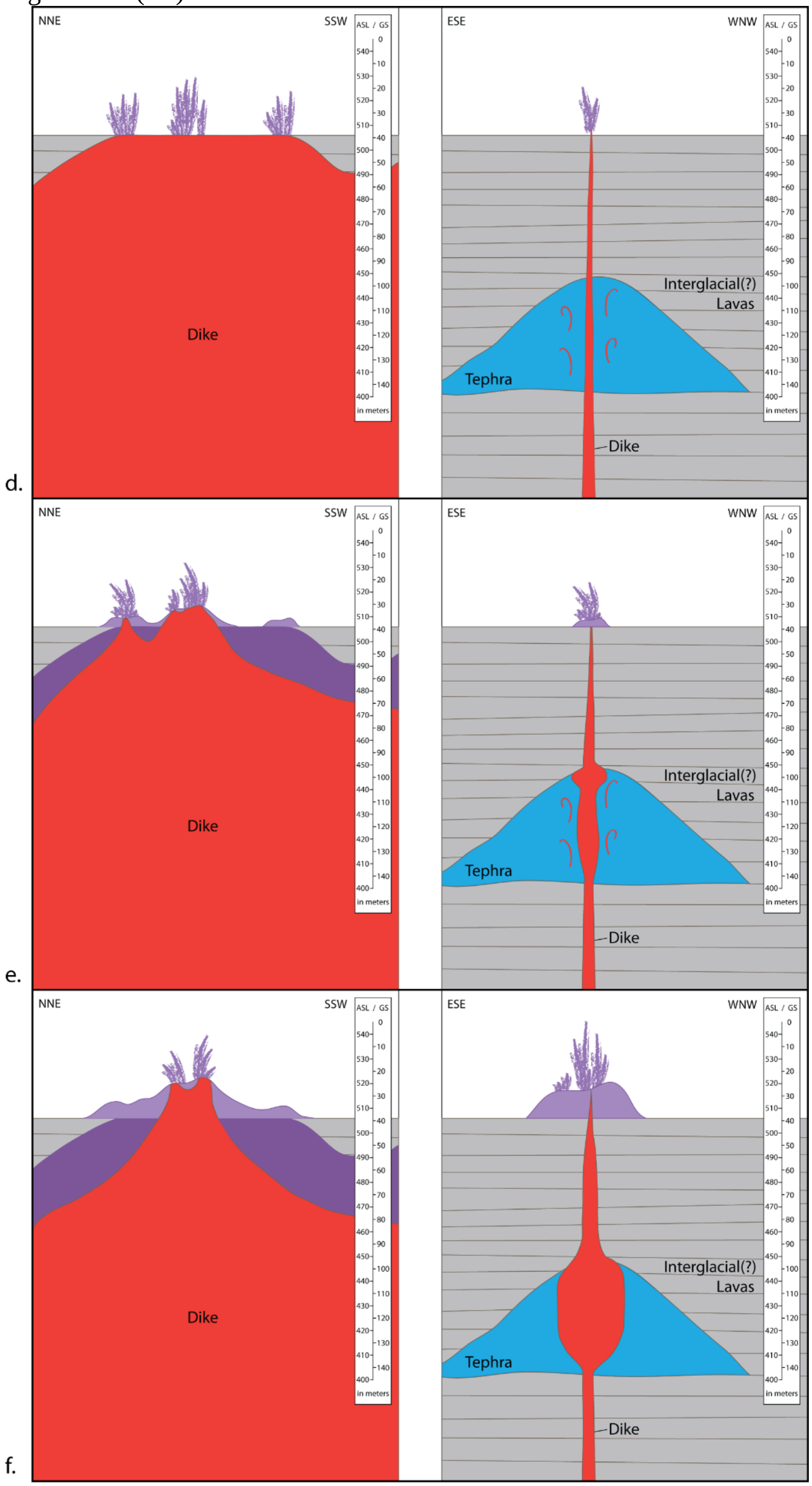

Figure 2.13 (g) continued.

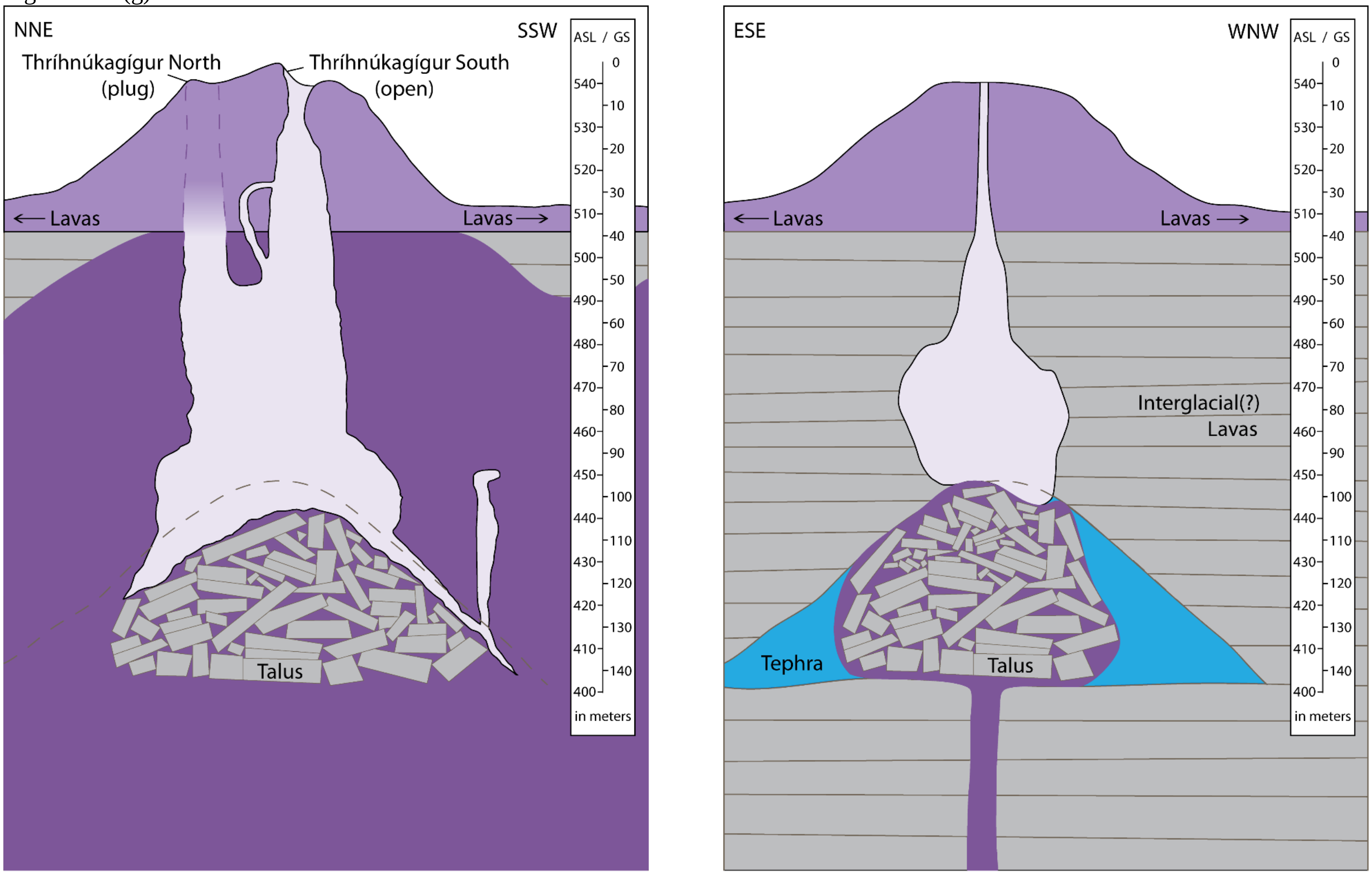

Cross section parallel to dike

Cross section perpendicular to dike

References

Biggs J., Chivers M. and Hutchinson M. C. (2013) Surface deformation and stress interactions during the 2007-2010 sequence of earthquake, dyke intrusion and eruption in northern Tanzania. *Geophys. J. Int.* **195**, 16–26.

Calais E., D'Oreye N., Albaric J., Delvaux D., Déverchère J., Ebinger C., Ferdinand R. W., Kervyn F., Macheyeki A. S., Oyen A., Perrot J., Saria E., Smets B., Stamps D. S. and Wauthier C. (2008) Strain accommodation by slow slip and dyking in a youthful continental rift, East Africa. *Nature* **456**, 783–788.

Clifton A. E. and Kattenhorn S. A. (2006) Structural architecture of a highly oblique divergent plate boundary segment. *Tectonophysics* **419**, 27–40.

Clifton A. E., Sigmundsson F., Feigl K. L., Gunnar Guðmundsson and Árnadóttir T. (2002) Surface effects of faulting and deformation resulting from magma accumulation at the Hengill triple junction, SW Iceland, 1994-1998. *J. Volcanol. Geotherm. Res.* **115**, 233–255.

Fronval T. and Jansen E. (1997) Eemian and Early Weichselian (140–60 ka) Paleoceanography and paleoclimate in the Nordic Seas with comparisons to Holocene conditions. *Paleoceanography* **12**, 443.

Genareau K., Valentine G. A., Moore G. M. and Hervig R. L. (2010) Mechanisms for transition in eruptive style at a monogenetic scoria cone revealed by microtextural analyses (Lathrop Wells volcano, Nevada, U.S.A.). *Bull. Volcanol.* **72**, 593–607.

Harp A. G. and Valentine G. A. (2015) Shallow plumbing and eruptive processes of a scoria cone built on steep terrain. *J. Volcanol. Geotherm. Res.* **294**, 37–55.

Keating G. N., Valentine G. A., Krier D. J. and Perry F. V. (2007) Shallow plumbing systems for small-volume basaltic volcanoes. *Bull. Volcanol.* **70**, 563–582.

Keiding M., Árnadóttir T., Sturkell E., Geirsson H. and Lund B. (2008) Strain accumulation along an oblique plate boundary: The Reykjanes Peninsula, southwest Iceland. *Geophys. J. Int.* **172**, 861–872.

Keiding M., Lund B. and Árnadóttir T. (2009) Earthquakes, stress, and strain along an obliquely divergent plate boundary: Reykjanes Peninsula, southwest Iceland. *J. Geophys. Res. Solid Earth* **114**, 1–16.

Muirhead J. D., Kattenhorn S. A. and Le Corvec N. (2015) Varying styles of magmatic strain accommodation across the East African Rift. *Geochemistry Geophys. Geosystems*, 1541–1576.

Németh K. and Kereszturi G. (2015) Monogenetic volcanism : personal views and discussion. *Int. J. Earth Sci.* **104**, 2131–2146.

Németh K. and White J. D. L. (2003) Reconstructing eruption processes of a Miocene monogenetic volcanic field from vent remnants: Waipiata Volcanic Field, South Island, New Zealand. *J. Volcanol. Geotherm. Res.* **124**, 1–21.

Sæmundsson K. (2008) Þríhnúkagígur Helstu niðurstöður kjarnaborana.

Sæmundsson K. (2006) *Þríhnúkagígur Jarðfræðirannsóknir og tillögur*.,

Sæmundsson K., Jóhannesson H., Hjartarson Á., Kristinsson S. G. and Sigurgeirsson M. Á. (2010) Geological Map of Southwest Iceland, 1:100,000.

Sigmundsson F., Hooper A., Hreinsdóttir S., Vogfjörd K. S., Ófeigsson B. G., Heimisson E. R., Dumont S., Parks M., Spaans K., Gudmundsson G. B., Drouin V., Árnadóttir T., Jónsdóttir K., Gudmundsson M. T., Högnadóttir T., Fridriksdóttir H. M., Hensch M., Einarsson P., Magnússon E., Samsonov S., Brandsdóttir B., White R. S., Ágústsdóttir T., Greenfield T., Green R. G., Hjartardóttir Á. R., Pedersen R., Bennett R. a, Geirsson H., La Femina P. C., Björnsson H., Pálsson F., Sturkell E., Bean C. J., Möllhoff M., Braiden A. K. and Eibl E. P. S. (2015) Segmented lateral dyke growth in a rifting event at Bárðarbunga volcanic system, Iceland. *Nature* **517**, 191–5.

Stefánsson Á. B. (1992) Þríhnúkagígur. *Náttúrufræðingurinn* **61**, 229–242.

Valentine G. A. (2012) Shallow plumbing systems for small-volume basaltic volcanoes, 2: Evidence from crustal xenoliths at scoria cones and maars. *J. Volcanol. Geotherm. Res.* **223-224**, 47–63.

Wood C. A. (1980) Morphometric evolution of cinder cones. *J. Volcanol. Geotherm. Res.* **7**, 387–413.

Wright T. J., Ebinger C., Biggs J., Ayele A., Yirgu G., Keir D. and Stork A. (2006) Magma-maintained rift segmentation at continental rupture in the 2005 Afar dyking episode. *Nature* **442**, 291–294.

Chapter 3

Magma genesis at Thríhnúkagígur, Reykjanes Peninsula, Iceland: Implications for magmatic plumbing structure at monogenetic volcanic fields

3.1 Introduction

The Reykjanes Peninsula, in the absence of central volcanoes and large homogenizing magma chambers, is dominated by monogenetic basaltic fissure eruptions. With a few exceptions (Gee et al., 1998a; Gee et al., 2000), the geochemistry of lavas on the Reykjanes Peninsula has been interpreted to primarily reflect the mantle sources that generated these melts. Recent unrest in the region (Clifton et al., 2002; Michalczewska et al., 2012) reflects that magma is injected and stored in the crust, so it is necessary to understand both the magmatic plumbing structure of these intrusions and the effect of magma storage in has on the geochemical evolution of these magmas.

Radiogenic isotope analysis has traditionally formed the bulk of the mantle source characterization for Reykjanes Peninsula lavas, and lavas across Iceland more generally because of the plume-ridge interactions and intrinsic chemical heterogeneities within the plume. However, some authors suggest that these isotopes, and Sr in particular, could be affected by interaction with or assimilation of hydrothermally altered basalts during a magma's residence in the crust (Gee et al., 1998a; Gee et al., 2000). Because mantle sources have been debated extensively with samples from a much greater geographic area than the single location of Thríhnúkagígur (Condomines et al., 1983; Hanan and Schilling, 1997; Chauvel and Hémond, 2000; Skovgaard et al., 2001; Stracke et al., 2003;

Kokfelt et al., 2006; Kitagawa et al., 2008; Peate et al., 2010; Koornneef et al., 2012; Rudge et al., 2013; Shorttle et al., 2013; Manning and Thirlwall, 2014), source geochemistry is not the main focus of this study. Rather, results of Sr-Nd-Pb isotope ratios in lavas from Thríhnúkagígur are discussed primarily within the context of the literature that has attempted to define specific mantle source compositions on the Reykjanes Peninsula (Hanan and Schilling, 1997; Thirlwall et al., 2004; Kokfelt et al., 2006; Kitagawa et al., 2008), to evaluate the potential to use Sr as a tracer of crustal contamination of Thríhnúkagígur magmas.

Using a combined major and trace element and Sr-Nd-Pb isotope geochemical approach this work seeks to understand, from source to surface, the evolution of magma erupted at Thríhnúkagígur. The unique exposure offered by the cave below the main cone of Thríhnúkagígur allows sampling of the intrusive part of the system and older buried tephra in addition to the surficial lavas. Heterogeneity in the compositions from different part of the system suggests a magmatic plumbing structure that does not homogenize mantle-derived melts. Geophysical and geodetic observations of other intrusions and fissure eruptions provide a context in which to invoke a magmatic plumbing system that may preserve geochemical variations.

3.2 Sample descriptions

At the surface, one Miðhnúkur and four Thríhnúkagígur lava samples were collected for analysis (Figure 2.1). A sample of vent spatter at the summit of Thríhnúkagígur from a previous sampling campaign was also prepared for analysis. Within the cave, 5 dike samples, one sample of the fallen intrusive plug, and 6 buried tephra samples were collected for geochemical analysis. Photograph mosaics and sketches provide sample locations within the main chamber of the cave (Figures 2.4, 2.5).

3.2.1 Surface lavas

Lavas from Thríhnúkagígur are highly vesicular (18-36.5% by volume) and relatively glassy with <15% plagioclase phenocrysts (Table 3.1; Figure 3.1a, b). Samples TNG-14-33 and TNG-14-34 were collected from some of the thicker flow tops (~20 cm) in the area as outcrops with exposures of the interior of the H146 flow were not found. TNG-14-37 was taken from the lip of a former lava lake. TNG-14-32 is from a small flow from a flank vent on the main cone that traveled into the lava lake depression after the lava had cooled and/or drained.

One sample, TNG-14-35, was collected from a laterally more extensive, older Holocene flow from Miðhnúkar (H145). Miðhnúkar flows are easily distinguishable from the Thríhnúkagígur lavas as they contain macroscopic olivine phenocrysts (Figure 3.1f) rather than plagioclase.

3.2.2 Dikes

The dike is heterogeneous and samples were taken from a variety of different outcrops. Samples were taken from the interior of the dike, a 6 cm thin dike that splays off of the main dike, and a chilled margin of the dike. Samples from the interior of the dike tend to be more vesicular, have larger plagioclase phenocrysts, and courser groundmass compared to the margin of the dike. These changes are typically gradational, but TNG-14-27e (exterior; Figure 3.1c) and TNG-14-27i (interior; Figure 3.1d) shared a sharp contact. These two samples are the most contrasting dike samples as TNG-14-27i has flow banding and interstitial clinopyroxene between the plagioclase phenocrysts, while TNG-14-27e is devoid of phenocrysts and vesicles, and has a fine-grained groundmass.

3.2.3 Plugged conduit

This is the only sample that was not collected *in situ*. TNG-14-18 was collected immediately below an intrusive, partially hollow structure on the cave ceiling. Weathering of the cave walls to a yellow color contrasted the reddish-purple altered surfaces of this feature. It is notable for being aphanitic with very few phenocrysts.

3.2.4 Buried tephras

Tephra samples consist of primarily glassy, vesicular clasts (Figure 2.8); however, the total crystallinity, gas content, grain size distribution, and degree of alteration of the clasts is variable. Samples may contain clasts that are exclusively fresh and black or have a mixture of black and brown glasses. Clasts that are larger than 5 mm are present in most samples although they rarely exceed 2-3 cm. Grain mounts were made for 4 of the 6 tephra samples. The grain mounts excluded clasts larger than 5 mm. The two exceptions for which no grain mounts were made are TNG-14-17, which is a fist sized scoria clast and TNG-14-28, which was consolidated and contained some sedimentary structure. Neither is representative of the bulk tephra pile. Free whole crystals of plagioclase and olivine occur, while broken fragments of large plagioclase crystals are the most common crystalline clast type. There are also rare plagioclase and plagioclase-olivine glomerocrysts.

3.3 Methods

Samples were cut into centimeter thick slabs and the weathered edges were trimmed off of the slabs with a ceramic tile saw and polished to remove saw marks. Thin section billets were cut from the slabs and sent to Spectrum Petrographics to make standard 30 μm microprobe polished thin sections. The remaining slabs for each sample were chipped into millimeter sized pieces with a ceramic jaw crusher. Tephras were rinsed in an ultrasonic bath of milliQ water for 1 hour and dried. Tephras and rock chips were transferred into a tungsten carbide shatterbox and run for 20-30 seconds to create a fine powder.

3.3.1 Point counting

Mineral modes were determined by point counting of thin sections under a petrographic microscope. Grids of 10 by 20 were used to achieve 200 total counts per thin section. For the grain mounts of the buried tephra, point counting continued until 150 spots on grains had been counted. For the other thin sections, vesicles were included in the total of 200 counts.

3.3.2 Major element analytical methods

Bulk rock major and trace element compositions were determined at the Laboratory for Isotopes and Metals in the Environment at The Pennsylvania State University. Lithium metaborate fusions were made and prepared in nitric acid for major element analysis. Splits of 100 mg sample powder were weighed and mixed with 1.000 g of lithium metaborate in preweighed vials. After gently shaking the mixture, it was transferred to graphite crucibles and placed in a furnace preheated to 900°C. The crucibles were heated to 1000°C for 10 minutes, then cooled back to 900°C. The resulting melts were added to 100 ml of 5% HNO_3 solutions in Teflon vials with magnetic stir bars. The solutions were stirred for at least 15 minutes before being transferred to polyethylene containers for storage. These solutions were analyzed for major element concentrations using a Perkin-Elmer Optima 5300DV Inductively Coupled Plasma Atomic Emission Spectrometer (ICP-AES).

3.3.3 Trace element analytical methods

For trace element analysis, 100 mg of powder were weighed out for each sample. Powders were subsequently digested in three steps; first with a combination of 6N HF and 8N HNO_3, then with 2N HCl, and finally with 4N HNO_3. Samples were dried down between each stage of digestion. Following the final dry down, samples were taken up in HNO_3 and diluted with milliQ water to 2000 times their original weight in a matrix of ~2% HNO_3. High concentrations of Ba and Sr required a separate dilution to 5000 times the original sample weight, also in a ~2% HNO_3 solution in milli-Q water. This procedure was also followed for a method blank and five rock standards: BHVO-1, BCR-1, BR, BIR-1, and JA-1.

Trace elements were analyzed using a Thermo X-Series II Quadrupole Inductively Coupled Plasma Mass Spectrometer (ICP-MS). The instrumental background was determined using a 2% HNO_3 solution in milli-Q water. Background was found to be ≤0.01 for all elements except Ni and Sc, which were less than 0.1 ppb, and Cu, Cr, and Zn, which were less than 0.54 ppb. The experimental design started with a method blank and the five rock standards. The method blank was run again before the samples were analyzed as unknowns. Calibration lines with an R^2 value of greater than or equal to 0.999 were used for determining concentrations of elements in the unknowns. One standard data point was removed to produce curves for several transition metals and rare earth elements. Two standard data points had to be removed from the Co, and Ho curves to produce an R^2 of 0.999. The true dilution factors for each sample were determined based on the initial mass of the powdered sample and the mass of the final diluted sample for analysis. The concentrations in solution were then multiplied by the dilution factor (~2000 except for ~5000 for Ba and Sr) to determine the concentration of each analyte in the bulk rock.

Samples were digested and analyzed in two separate batches. Samples TNG-14-18 and TNG-14-27e were duplicated in the second analysis. For these replicate analyses, reported values for most analytes are within 5.0%. The elements Sc, V, Co, Cu, Sr, Ce, Lu, and U were all within 8.0%. Only Cs (39.0%) and Ta (18.3%) had larger errors. These two elements occur in concentrations of < 0.5 ppm in these samples and are not used to predicate any arguments presented herein.

3.3.4 Pb, Sr, and Nd isotope analytical methods

Acid digestion, ion exchange chromatography, and isotope ratio measurements of Pb, Sr, and Nd were conducted at the Consiglio Nazionale delle Ricerche (CNR), Pisa, Italy. Splits of 200 mg were weighed out for each sample and dissolved in a combined concentrated HF and HNO_3 solution, then HNO_3, followed by 7N HCl, and finally with 0.7N HBr. Sample solutions were dried down between each step. Samples were transferred to centrifuge tubes and centrifuged to remove any residuum before ion exchange chromatography. Acid digestion and ion exchange chromatography procedures are described in Appendix A.

Isotope ratios were measured on a Finnigan MAT 262 multi-collector thermal ionization mass spectrometer (TIMS) running in static mode for Pb and dynamic mode for Sr and Nd. For Pb isotopic analysis, mass discrimination corrections of 0.15 ± 0.01% per mass unit relative to the NIST SRM 981 reference standard were applied to experimental data (Todt et al., 1993). Following this correction, Pb isotope analyses have 2SD within 0.025% per mass unit. Laboratory Pb blanks are routinely between 0.2-0.4 ng, and no blank correction is made.

Ratios of $^{87}Sr/^{86}Sr$ are normalized to $^{86}Sr/^{88}Sr$ of 0.1194 and the mean $^{143}Nd/^{144}Nd$ ratios are normalized to $^{146}Nd/^{144}Nd$ of 0.7219. The results of 19 analyses of Sr standard NIST SRM 987 ($SrCO_3$) gave an average of 0.710227 ± 20 (2SD). Measured values are corrected to $^{87}Sr/^{86}Sr = 0.710250$. Blanks for Sr are <0.3 ng and are negligible. Twenty-seven analyses of the Nd standard is JNdi-1 yield 0.512104 ± 10 (2SD) and no correction was made.

3.4 Results

3.4.1 Major elements

Lavas from the two eruptions in Thríhnúkagígur fissure system and the buried tephras exposed at depth within the cave are basalts (Table 3.2; Figure 3.2; Le Bas and Le Maitre, 1986) with 46.70 – 49.25 wt.% SiO_2 and 6.03 – 9.58 wt.% MgO (Mg# 47 – 61). This range is broadly consistent with tholeiitic Holocene lavas of the Reykjanes Peninsula (Jakobsson et al., 1978; Gee et al., 1998a; Peate et al., 2009). The dike from the most recent eruption has 47.23 – 49.25 wt.% SiO_2 and 10.78 – 13.20 wt.% Fe_2O_3T at relatively constant MgO content (7.54-8.04 wt.%). The buried tephra is the only rock unit with samples that have a non-zero LOI (0.69 – 2.79 wt.%), suggestive of variable alteration or weathering. These samples have 14.42 – 16.09 wt.% Al_2O_3 and 46.70 – 48.38 wt.% SiO_2. By comparison, the lavas fed by the main dike are more homogeneous (Al_2O_3 = 15.2-15.8 wt.%; SiO_2 = 47.7-48.2 wt.%). All unaltered samples have CIPW norms that are olivine normative (Table 3.3).

Plots of major elements versus MgO show a compositional gap between the Holocene basalts (MgO ≥ 7.25 wt.%) and the older buried tephras (MgO ≤ 6.78 wt.%). Thríhnúkagígur lavas and dikes have a steep, positive linear trend for Al_2O_3 vs MgO, differing from the buried tephra, which have relatively constant Al_2O_3. For CaO, the lava and dike samples show limited compositional range (12.00-13.38 wt.%), while the buried tephras have lower concentrations (9.79-11.43) that give the whole suite a weakly positive trend. TiO_2 and Fe_2O_3 increase linearly with decreasing MgO, although several samples depart from the overall trend (Figure 3.3). The chilled margin (TNG-14-27e) has low TiO_2 and Fe_2O_3 for its MgO while the plugged conduit (TNG-14-18) and Miðhnúkar (TNG-14-35) have high TiO_2 and Fe_2O_3 for their MgO contents. Concentrations of SiO_2 increase with decreasing MgO, but this trend is not continuous across the entire sample suite (Figure 3.3). Rather, the lava flows and dike samples form a separate trend that is offset to higher silica for their MgO content relative to the buried tephra samples. One dike sample from the chilled margin (TNG-14-27e) markedly departs from that slope with ~1 wt.% more SiO_2 than the other lava and dike samples. The alkalis form linear negative trends with MgO.

The chemical index of alteration (CIA; Nesbitt and Young, 1982) was used to evaluate the extent of alteration (Figure 3.3). The CIA is defined as $100*[Al_2O_3/(Al_2O_3 + CaO + Na_2O + K_2O)]$. Two visibly altered samples – a surface vent spatter sample (MC-03-612) and a reworked, partially palagonitized tephra (TNG-14-28) – had a CIA of 58, compared to CIAs of ≤53 in all other samples. These samples depart from otherwise linear trends in several major elements when plotted against MgO (Figure 3.3). Values of CIA for fresh basalts are typically 30-45 (Nesbitt and Young, 1982), so the samples in this study may have all experienced mild alteration or may have incorporated altered crust during their ascent through the crust.

3.4.2 Trace elements

Concentrations of the compatible trace elements Ni and Cr decrease with decreasing MgO. Scandium varies by rock type; buried tephras show a positive trend with MgO while the Holocene lavas and dikes show a negative correlation.

Concentrations of the incompatible elements Sr, Eu, and Pb are inversely correlated with MgO (Figure 3.4; Table 3.4).

Primitive mantle normalized multi-element diagrams are characterized by strong positive Nb and Ta anomalies, a positive Ba anomaly, and a large negative Pb anomaly for all samples (Figure 3.5; Sun and McDonough, 1989). The vent spatter (MC-612-03 with CIA = 58) is the sole exception with a positive Pb anomaly, which is interpreted to be the result of contamination. The average values for each of the rock units yield similar patterns for most incompatible trace elements. The buried tephras are enriched relative to the lava and dike suite, but form generally parallel trends. Strontium has a negative anomaly in the buried tephras and a positive anomaly for the chilled margin (TNG-14-27e) and the plugged conduit (TNG-14-18).

Chondrite normalized rare earth element (REE) diagrams display relatively smooth patterns, decreasing steadily from the light REEs to the heavy REEs (Figure 3.6; Sun and McDonough, 1989). The chilled margin (TNG-14-27e) and plugged conduit (TNG-14-18) have the flattest REE patterns ($[La/Yb]_N$ = 1.92 and 1.68, respectively) in samples from Thríhnúkagígur. The buried tephras are the most enriched in all REEs, but are relatively more enriched in the LREEs, giving rise to a steeper pattern ($[La/Yb]_N$ > 2.75). The lavas and the dike samples are intermediate between the buried tephras and the plugged conduit in terms of REE composition. There is a very subtle positive Eu anomaly in the chilled margin of the dike (TNG-14-27e). However, no other samples from Thríhnúkagígur have Eu anomalies, positive or negative.

3.4.3 Pb, Sr, and Nd isotopes

There is a positive relationship in the $^{206}Pb/^{204}Pb$ – $^{208}Pb/^{204}Pb$ data (Figure 3.7a). The most radiogenic samples are the buried tephras, although one Holocene Thríhnúkagígur sample has higher $^{208}Pb/^{204}Pb$ (Table 3.5). The least radiogenic sample is the vent spatter (MC-612-03). This sample has exceptionally high Pb concentration (2.40 ppm) and a CIA of 58. It has a large positive Pb anomaly on the primitive mantle normalized diagram, while all other samples have strong negative Pb anomalies (Figure 3.5). The vent spatter has very similar major and trace element abundances to other lavas and dikes. This suggests that Pb contamination was added to the sample, so it will not be considered as representative of any trend or end member. The most unradiogenic sample considered to be primary is from the dike (TNG-14-24). In general, the Holocene lavas and dikes have a greater range of $^{206}Pb/^{204}Pb$ and $^{208}Pb/^{204}Pb$ than the buried tephra, especially to lower $^{206}Pb/^{204}Pb$ ratios.

Ten of eighteen samples plot in a relatively narrow range in $^{206}Pb/^{204}Pb$ and $^{207}Pb/^{204}Pb$ (Figure 3.7b). In these 10 samples, ratios of $^{206}Pb/^{204}Pb$ are between 18.79 and 18.95 and $^{207}Pb/^{204}Pb$ ratios range from 15.47 and 15.55 (Table 3.5). All but one of the buried tephras fall within this range. Two additional dike samples fall within this range of $^{206}Pb/^{204}Pb$, but with higher $^{207}Pb/^{204}Pb$ ratios. The remaining six samples form a negative linear trend (Figure 3.7b).

Ratios of $^{143}Nd/^{144}Nd$ range from 0.512982 to 0.513066. Despite the narrow range, the buried tephras are distinct from the lavas and dike samples. With the exception of the most altered buried tephra sample (TNG-14-28 with CIA = 58), the buried tephras do not exceed 0.513018 ± 0.000010. A single lava sample has a $^{143}Nd/^{144}Nd$ value within the tephra range, while all other dike and lava samples have ratios greater than 0.513021. There is some slight overlap between the buried tephra suite and the dike and lava samples when error is considered (Table 3.5). The plugged conduit (TNG-14-18) has a ratio of 0.513039 ± 0.000008, placing it at the high end of the measured $^{143}Nd/^{144}Nd$ values.

Three dike samples define the lowest $^{87}Sr/^{86}Sr$ values of 0.703135 to 0.703143 (Figure 3.8). The other lavas and dikes span the same range of Sr isotope ratios as the buried tephra. Aside from the buried tephra with the high CIA, only a single lava sample falls within the reported values for the buried tephras in Nd ratios. The most depleted (unradiogenic Sr and radiogenic Nd) sample is the same as the most depleted Pb sample, dike sample TNG-14-24.

3.5 Discussion

3.5.1 Source geochemistry

3.5.1.1 Trace element characteristics

High field strength (HSFE) and rare earth element (REE) ratios illustrate important differences between SW Iceland (RP and WVZ) and the Eastern Volcanic Zone. The Reykjanes Peninsula and the Western Volcanic Zone comprise a steeper positive trend separate from the EVZ on a plot of $(La/Yb)_N$ vs. Nb/Zr (Figure 3.9), suggesting a uniquely Nb-enriched source component in the west. Thríhnúkagígur buried tephras have the highest $(La/Yb)_N$ among the RP and some of the highest Nb/Zr in all of

Iceland. Their Nb/Zr ratios are comparable to those of the most enriched EVZ volcanics, but at much lower $(La/Yb)_N$. If similar mantle source geochemistry is assumed, then incompatible trace element ratios differences may attributed to melting in the presence of garnet. The thicker lithosphere in the EVZ should generate deeper mantle melts than on the RP, so the difference in the SW Iceland and EVZ slopes on the $(La/Yb)_N$ vs. Nb/Zr plot could possibly be attributed to the relative compatibility of Yb garnet in southern EVZ source region. This is consistent with the slow spreading rates associated with incipient rifting in the southern EVZ as it propagates to the south (LaFemina et al., 2005).

Ratios of Nb/U, like Nb/Zr, suggest that Nb is anomalously enriched in the RP mantle relative to the rest of Iceland (Kokfelt et al., 2006; Koornneef et al., 2012), pointing to different geochemical source domains across the southern Iceland mantle. Globally, magmas produced at ocean islands and mid-ocean ridges have Nb/U ratios of 47 ± 10 irrespective of Nb bulk concentrations, yet lavas from SW Iceland depart markedly from this range, with Nb/U as high as 100 (Figure 3.10a; Hofmann et al., 1986).

A similar pattern is observed for Ce on the RP. Ratios of Ce/Pb remain remarkably constant for OIBs (25 ± 5; Hofmann et al., 1986), but the Reykjanes Peninsula and the WVZ are more enriched with values commonly up to 40 (Figure 3.10b; Hofmann et al., 1986). Rare samples have even higher Ce/Pb ratios up to 51 in the Western Volcanic Zone and on the RP (Koornneef et al., 2012), including two Thríhnúkagígur samples.

Strong enrichments in Nb/U and Ce/Pb ratios cannot be attributed to the melting process because both of these ratios use elements that are nearly equally incompatible.

Unlike Yb, which is preferentially compatible in garnet, the source mineralogy does not exert a differentiating effect on Nb relative to U, or Ce relative to Pb. This suggests that there is a mantle component unique to the RP that contributes strongly to Thríhnúkagígur magmas, and the RP more broadly.

3.5.1.2 Sr-Nd-Pb isotope systematics: mantle sources

The melt fraction, melting depth, and source mineralogy can strongly affect trace element ratios, but do not affect isotope ratios. Several studies have proposed Sr-Nd-Pb isotopic compositions for mantle sources in Iceland (Hanan and Schilling, 1997; Thirlwall et al., 2004; Kokfelt et al., 2006; Kitagawa et al., 2008). They converge on three main sources – an enriched plume source, an EM1-like source, and a depleted (MORB-like) source. The EM1-like source is specific to the Reykjanes Peninsula in Holocene basalts (Thirlwall et al., 2004), but is recorded in Tertiary basalts in eastern Iceland (Hanan and Schilling, 1997; Kitagawa et al., 2008).

Lavas from south Iceland plot primarily along an array between the enriched plume source and the depleted source in Sr-Nd-Pb isotope space and are subparallel to the Northern Hemisphere Reference Line on Pb-Pb plots (NHRL; Hart, 1984). The Reykjanes, Krísuvík, and Brennisteinsfjöll fissure swarms, all part of the Reykjanes Peninsula, define largely overlapping fields on the $^{206}Pb/^{204}Pb$ vs. $^{208}Pb/^{204}Pb$ plot (Figure 3.11; Thirlwall et al., 2004; Kokfelt et al., 2006; Peate et al., 2009). These three fissure swarms are bracketed by the less radiogenic Pb composition of southern Reykjanes Ridge (Thirlwall et al., 2004) and the more radiogenic Pb compositions of the volcanic systems of Hekla (Park 1990; Furman et al., 1995) and Vestmannaeyjar (Furman et al., 1991;

Chauvel & Hémond, 2000; Kokfelt et al., 2006; Peate et al., 2010) in the southern EVZ. Katla has the most radiogenic Pb isotope ratios in south Iceland (Park 1990; Furman et al., 1995) and acts as the enriched regional end member for both Pb-Pb plots. However, some Reykjanes Peninsula lavas with lower $^{206}Pb/^{204}Pb$ are pulled off the NHRL to higher $^{208}Pb/^{204}Pb$ relative to $^{206}Pb/^{204}Pb$, towards the EM1-like component.

Thríhnúkagígur lavas and dikes plot with other Reykjanes Peninsula lavas on the $^{206}Pb/^{204}Pb$ vs. $^{208}Pb/^{204}Pb$ plot (Figure 3.11). The buried tephras and the majority of Thríhnúkagígur lavas and dikes fall on the binary mixing array defined by south Iceland lavas between an enriched plume source and a depleted MORB-like source, although several Thríhnúkagígur lava and dike samples (MC-612-03, TNG-14-24, TNG-14-34, TNG-14-18, and TNG-14-17) extend slightly off of the array and off of the NHRL towards the EM1-like source.

The lowest $^{206}Pb/^{204}Pb$ sample (MC-612-03) is vent spatter from the summit of Thríhnúkagígur, however, it is not shown on figures in this section because it is considered to be contaminated (see section 3.4.3). Thríhnúkagígur lavas and dikes define a field at $^{206}Pb/^{204}Pb$ ratios consistent with previously reported Brennisteinsfjöll compositions. Excluding the vent spatter, the field defined by this single eruption at Thríhnúkagígur is as broad as the entire reported range of previously reported data from Brennisteinsfjöll (n = 9). Contributions from the EM1-like component are consistent with some the Thríhnúkagígur lavas and dikes and other Reykjanes Peninsula lavas being pulled off the NHRL. The buried tephra on the other hand, does not require a contribution from this source.

While only a single enriched plume sources is revealed by the Pb-Pb isotope plot, an enriched, high-Nb component unique to SW Iceland was identified on the basis of Nb/U ratios. Plotted against $^{206}Pb/^{204}Pb$ (Figure 3.12a) and $^{208}Pb/^{204}Pb$ (Figure 3.12b), there is a positive correlation between Nb/U ratios and Pb isotope ratios on the Reykjanes, suggesting that there is a second enriched plume source in south Iceland with the same Pb isotope compositions but with enriched Nb.

As with the Pb-Pb plots, Figure 3.13 shows that $^{87}Sr/^{86}Sr$ vs. $^{143}Nd/^{144}Nd$ ratios from south Iceland form an array that is bracketed by Katla (relatively radiogenic Sr and unradiogenic Nd; Park, 1990; Furman et al., 1995) on one end and the southern Reykjanes Ridge (unradiogenic Sr and radiogenic Nd; Thirlwall et al., 2004) on the other. Again, the enriched plume source and depleted MORB-like source bound the array, which includes the Reykjanes Peninsula fissure swarms. Aside from a single Krísuvík sample that plots with the EM1-like source at higher $^{87}Sr/^{86}Sr$, there is no systematic trend towards this mantle component in the RP data.

Thríhnúkagígur lavas and dikes with the lowest $^{87}Sr/^{86}Sr$ ratios cluster closely with previously reported compositions at Brennisteinsfjöll on a plot of $^{87}Sr/^{86}Sr$ vs. $^{143}Nd/^{144}Nd$ (Figure 3.13). Most of the other lava and dike samples fit more broadly with other Reykjanes and Krísuvík lavas, but fall outside the previously defined range of Brennisteinsfjöll Sr-Nd isotope compositions (Thirlwall et al., 2004; Kokfelt et al., 2006; Peate et al., 2009). One lava and one buried tephra fall outside of the previously recognized Reykjanes Peninsula fields, extending in the direction of the EM1-like component.

The Thríhnúkagígur data overlap on Sr-Nd-Pb isotope plots not only with other Reykjanes Peninsula fissure swarms, but also with lavas from Vestmannaeyjar. The relatively enriched buried tephra field overlaps with the depleted end of the Vestmannaeyjar field on the ^{206}Pb/^{204}Pb vs. ^{208}Pb/^{204}Pb plot (Figure 3.11), and the Thríhnúkagígur lavas, dikes, and buried tephras all fall within the Vestmannaeyjar field in Sr-Nd isotope space (Figure 3.13). This affinity with Vestmannaeyjar suggests that similar mantle components may contribute to magma genesis across south Iceland. Vestmannaeyjar may be the mostly likely location to express geochemical similarities to the Reykjanes Peninsula because neither the RP nor Vestmannaeyjar have central volcanoes or are thought to have large magma chambers (unlike Hekla or Katla). Therefore, their magmas are likely to experience similar processes and evolve by similar pathways. For example, injections of magma into the crust are have short residence times in both locations, on the order of decades, and feed small volume (<1 km^3) monogenetic fissure eruptions (Sigmarsson, 1996; Higgins and Roberge, 2007; Koerberle et al., 2015).

Assuming similar isotopic sources, variations between these volcanic systems may be ascribed to the relative proportions of the different mantle sources contributing to melt generation, which may be affected by differences in melting depth and melt fraction. (While this explains isotopic similarities, it still fails to reconcile the differences in Nb/U between the RP and Vestmannaeyjar as expressed in Figure 3.9, requiring an additional mantle source.) Additionally, continuous melt extraction at the neovolcanic zones like the Reykjanes Peninsula could gradually deplete enriched mantle sources. As an enriched mantle component is repeatedly melted and becomes increasingly less fertile, its proportional contribution relative to the depleted component is also likely to decrease.

The buried tephra is conservatively estimated to be at least 100 ka in age and likely older because it is believed to have formed during the previous interglacial, which ended at 113 ka (Fronval and Jansen, 1997). Therefore, one possible explanation for the subtle difference in the Pb and Nd isotopes in the buried tephra and the Holocene lavas and dikes may be their age difference and the depletion of the enriched plume source beneath the Reykjanes Peninsula through time.

In addition to the enriched, depleted, and EM1-like mantle sources already discussed, Thirlwall et al. (2004) propose a fourth mantle source that falls along the south Iceland array of lava compositions on Pb-Pb and Sr-Nd isotope plots. The contributions of this source are unclear. This component would have a more moderate $^{87}Sr/^{86}Sr$ ratio (~0.7032) than the EM1-like component, and may explain the trend of Thríhnúkagígur samples on a Sr-Pb isotope plot (Figure 3.14). As with previous isotope plots, the southern Reykjanes ridge is the most depleted of the south Iceland volcanic systems and Katla is the regionally enriched end member. The Thríhnúkagígur data fall within the enriched end of the Reykjanes field, beyond the Brennisteinsfjöll field, with two samples recording higher $^{87}Sr/^{86}Sr$ ratios than previously reported for the Reykjanes Peninsula at $^{206}Pb/^{204}Pb \geq 18.4$. While this proposed mantle end member appears promising in Sr-Pb isotope space, it cannot explain the high $^{87}Sr/^{86}Sr$ ratios of the sample suite at more radiogenic Nd ratios. This suggests that the previously defined fourth end member of Thirlwall et al. (2004) is not the main source of the Sr isotope signature in Thríhnúkagígur lavas, dikes, or buried tephra, but neither can it be ruled out as a potential contributor. Another source is still necessary to explain the radiogenic Sr isotope signature.

3.5.1.3 Sr isotopes: potential crustal contributions

The low $^{206}Pb/^{204}Pb$ lava and dike samples that may require an EM1-like component are not the same samples that trend toward the EM1-like source in Sr-Nd isotope space. Dike sample TNG-14-24 has lowest $^{206}Pb/^{204}Pb$ (excluding vent spatter, which is interpreted to be contaminated) and *lowest* $^{87}Sr/^{86}Sr$ and highest $^{143}Nd/^{144}Nd$ of the lava and dikes. If TNG-14-24 reflected a larger contributions from an EM1-like source, it would be expected to have the *highest* or among the higher $^{87}Sr/^{86}Sr$ samples measured. Likewise, the buried tephra extend more radiogenic Sr ratios (Figure 3.13), but do not extend towards the EM1-like component on Pb-Pb plots (Figure 3.11). The inconsistent behavior of individual samples and the buried tephra in regards to EM1-like source contributions suggests that Sr isotopes may be decoupled from Pb and Nd isotopes and that the EM1-like source is in fact relatively minor at Thríhnúkagígur.

The lack of a systematic trend in any of the RP fissure swarms towards the EM1-like component on the $^{87}Sr/^{86}Sr$ vs. $^{143}Nd/^{144}Nd$ (Figure 3.13) or $^{206}Pb/^{204}Pb$ vs. $^{87}Sr/^{86}Sr$ (Figure 3.14) plots lends support to the hypothesis that altered crust contributes to the genesis of Reykjanes Peninsula magmas (Gee et al., 1998a). A crustal component hydrothermally altered by seawater, as given by Gee et al. (1998a) plots near the EM1-like component (Figure 3.13). The broad array defined by Icelandic lavas in the Sr-Nd isotopes compared to the tight array in Pb-Pb isotopes is consistent with variable contributions to mantle-derived magmas by a highly radiogenic $^{87}Sr/^{86}Sr$ hydrothermally seawater-altered crustal component. With $^{87}Sr/^{86}Sr$ ratios in excess of 0.7042 in drill cores from modern RP geothermal systems (Elderfield and Greaves, 1981), even small amounts of contamination to these lavas could produce notable changes to the parental Sr isotopic composition. Hydrothermally altered crust (HAC) is likely to have a much stronger effect on Sr isotopes than Nd or Pb isotopes because it is both fluid mobile and there is a large and highly radiogenic reservoir of Sr in the ocean. So although a single point is plotted for HAC on Figure 3.23, small contributions from seawater-altered crust may shift magma compositions towards more radiogenic $^{87}Sr/^{86}Sr$ values at invariant $^{143}Nd/^{144}Nd$ ratios.

3.5.1.4 Summary

The anomalous Nb/U and Ce/Pb ratios in lavas on the Reykjanes Peninsula may not be adequately explained by the three major sources proposed for Iceland. The isotopically enriched plume source is common to all of Iceland and contributes more to lavas in the southern EVZ, such as Hekla and Katla, than on the RP. Therefore, Nb/U or Ce/Pb ratios would be expected to be higher in the southern EVZ than on the RP if it were a signature of the enriched plume component. Based on the Pb isotope vs. Nb/U plots (Figure 3.12), high Nb does not seem to be a characteristic of the depleted component, which is partially defined by its depletion in trace elements, particularly Nb (Thirlwall et al., 2004). An additional source with Pb isotopic compositions similar to the enriched mantle plume source must be present beneath the RP, characterized by unusually high Nb/U and Ce/Pb that sets it apart from the enriched component beneath the Eastern Volcanic Zone.

Of the Sr-Nd-Pb isotope systematics, only Pb hints at the EM1-like component's contribution to Thríhnúkagígur lavas and dikes with slightly higher $^{208}Pb/^{204}Pb$ in some samples for their $^{206}Pb/^{204}Pb$ ratios. This component does not contribute to the buried tephras on the $^{206}Pb/^{204}Pb$ vs. $^{208}Pb/^{204}Pb$ plot, contradicting the Sr-Nd isotope plot where the high $^{87}Sr/^{86}Sr$ component contributed equally to the buried tephra as to the lavas and dikes. It is therefore unlikely that the EM1-like source is responsible for the highly radiogenic Sr isotope ratios. Similarly, the sample (TNG-14-24) with the seemingly largest EM1-like signature on the Pb-Pb plot, has the least radiogenic Sr composition, further demonstrating that the Sr isotopes are decoupled from Pb and Nd isotopes. The highly radiogenic $^{87}Sr/^{86}Sr$ ratios observed at Thríhnúkagígur suggest a basaltic crustal component that has been hydrothermally altered by seawater.

On the basis of radiogenic isotopes and Nb/U ratios, there may be up to 5 mantle sources that contribute to Thríhnúkagígur magmas as well as a hydrothermally altered crustal component. These are 1) the depleted source, 2) the EM1-like source, 3) the enriched plume source with Nb/U ratios more typical of MORB and OIB lavas, 4) the enriched plume source with enriched Nb, and 5) the source proposed by Thirlwall et al. (2004) similar to the depleted source, but with $^{87}Sr/^{86}Sr$ ratios between the depleted and the EM1-like source. It is more likely that there are 2 mantle source domains – the depleted source common to all of southern Iceland and Nb-enriched plume source unique to the Reykjanes Peninsula – that are significant in generating Thríhnúkagígur magmas, possibly with minor contributions from an EM1-like source. A fourth component characterized by high $^{87}Sr/^{86}Sr$ that is decoupled from Nd and Pb isotope values likely has its origins in the crust.

3.4.2 Magmatic processes

3.5.2.1 Fractional crystallization

The samples from Thríhnúkagígur form a nearly horizontal trend on a plot of CaO/Al_2O_3 vs. MgO (Figure 3.4), which indicates olivine-dominated fractional crystallization and removal in this system. The slight decrease in CaO/Al_2O_3 with decreasing MgO in the buried tephra is consistent with removal of clinopyroxene. Some lava and dike samples show a range to higher Ca/Al_2O_3 over a limited range of MgO, which suggests that plagioclase may have been removed from these samples.

Fractional crystallization is evident from the major and trace element variations with MgO in Thríhnúkagígur lavas and dikes as well as in the buried tephra. Both Ni and Cr show a positive correlation with MgO, indicating that olivine is the dominant mafic phase during fractional crystallization (Figure 3.4), as these elements are all compatible in olivine. Scandium, which is compatible in clinopyroxene, decreases with decreasing MgO in the buried tephras (Figure 3.4). Conversely, there is a negative trend in Sc with MgO in the Thríhnúkagígur lavas and dikes, which is consistent with an increase of incompatible elements in the residual magma as olivine (but not clinopyroxene) is partitioned out of the system.

Strontium and europium are generally incompatible in mafic phases, but are compatible in anorthitic plagioclase. Strontium anomalies behave similarly to those in Eu (Figure 3.5), but whereas the Eu anomalies were subtle if present, the negative Sr anomaly in the buried tephra and the positive anomalies in the lavas and dikes are obvious on multielement diagrams (Figure 3.5). Primitive mantle normalized Sr values converge on a relatively narrow range of values (8.37-12.1) across sample suites compared to other elements. Plagioclase accumulation or removal could possibly explain the variations in the Sr and Eu data. Alternatively, these data could be interpreted as being consistent with lithospheric buffering of magma before its injection into the crust. If the melt was generated in or approached equilibrium with plagioclase-bearing peridotite in the lithospheric mantle prior to intruding the crust (Gee et al., 1998a), a more discrete range of Sr and Eu would be expected. Regardless of possible lithospheric interaction, the Eu/Eu* values close to unity suggest that plagioclase fractionation plays a relatively small role in the evolution of lavas, dike, and buried tephras.

3.5.2.2 Assimilation of hydrothermally altered basaltic crust

Hydrothermal alteration by seawater shifts basaltic compositions towards more radiogenic $^{87}Sr/^{86}Sr$ ratios. Previous studies have used Sr isotope ratios to argue that assimilation of crust altered by seawater contributes in excess of 20% to magmas in south Iceland during their residence in the crust (e.g. Sigmarsson et al., 1991; Sigmarsson et al., 1992; Gee et al., 1998a). Oxygen has also been used to investigate the assimilation of altered crust (Bindeman et al., 2006; Bindeman et al., 2008), because the major element oxygen is a more robust tracer than trace-level Sr. But even oxygen isotopes are not a well-agreed upon proxy. Other authors alternatively interpret anomalously light oxygen isotope ratios to be a reflection of a recycled oceanic crustal component in the mantle plume beneath Iceland (Kokfelt et al., 2006).

Hydrothermally altered crust contains secondary and hydrated minerals that give it a lower density than unaltered basalt, and perhaps a lower density than basaltic magmas. This density contrast can cause the ascending magma to stall and form sill-like bodies (Taisne et al., 2011). Mechanisms that may allow for continued ascent include increasing the pressure in the magma body, magmatic etching of a pathway through the altered crust, or the assimilation of altered crust until the density of the magma is lowered enough to continue to ascend buoyantly. Given that the altered crust plays a role in stalling magmas in the crust, perhaps it should be expected that there is some amount of interaction with a crustal component that may contribute to Icelandic magmas.

Nevertheless, there are few geochemical tools available to unambiguously trace the bulk assimilation of basaltic crust in basaltic magma. The preponderance of seawater-dominated hydrothermal systems on the Reykjanes Peninsula allows for $^{87}Sr/^{86}Sr$ ratios to be used to model contamination of magmas in this part of Iceland (Raffone et al., 2008; Marks et al., 2015). This is because seawater has much more radiogenic Sr than Icelandic basalts and it has been shown to impart ratios as high as 0.7042 on altered basalts in the Reykjanes fissure system (Elderfield and Greaves, 1981). If the Thríhnúkagígur Sr isotopes are assumed to be derived partially from a hydrothermally altered basaltic component at depth, a maximum estimate of crustal contamination can be determined. This model builds off of the work of previous studies that use a hydrothermally altered crustal component to explain the range of $^{87}Sr/^{86}Sr$ and $\delta^{18}O$ in fresh basalts on the Reykjanes Peninsula; they measure compositions extending to radiogenic values of $^{87}Sr/^{86}Sr = 0.703295$, and very light values of $\delta^{18}O = +3‰$ on the Reykjanes Peninsula (Gee et al., 1998a; Gee et al., 1998b; Peate et al., 2009).

In order to assess the possible contributions of hydrothermally altered crust, potential mixing between Sr and Nd end members in the Thríhnúkagígur system are modeled. The model in Figure 3.15 shows two binary mixing trends on a Sr-Nd isotope plot. The first is a single, nearly horizontal mixing curve between dike sample TNG-14-24 and a conservative hydrothermally altered crustal component proposed by Gee et al. (1998a). The dike sample is chosen as a mixing end member because it has the least radiogenic Sr isotopic composition (as well as the least radiogenic Pb and most radiogenic Nd isotopes) of any of the lavas and dikes. The large range of $^{87}Sr/^{86}Sr$ ratios reported in modern geothermal systems (Elderfield and Greaves, 1981) makes a ratio of 0.7036 a probable minimum estimate. The combination of the most depleted dike sample and a minimum estimate for the crustal component will yield a maximum estimate for the amount of assimilated hydrothermally altered crust in the suite of Thríhnúkagígur lavas and dikes.

The mixing curve between the theoretical altered crustal composition and the dike show that a maximum of 25% hydrothermally altered crust may explain the full range of Thríhnúkagígur lavas and dike compositions in Sr-Nd isotope space. The majority of the samples may be explained by less than 15% of the crustal component. It is important to emphasize that these represent maximum estimates. True quantities of crustal contamination could be much lower if the altered crust has a more radiogenic $^{87}Sr/^{86}Sr$ value than 0.7036; which seems likely given the observed values in modern geothermal systems (Elderfield and Greaves, 1981), or if there is a range of $^{87}Sr/^{86}Sr$ in the primary mantle melts. Indeed, more extensive alteration by seawater could both drive the $^{87}Sr/^{86}Sr$ to higher ratios and make it easier to assimilate by facilitating the growth of more secondary and hydrous minerals. In this case small amounts of a hydrothermally altered crustal component could explain the observed $^{87}Sr/^{86}Sr$ ratios at Thríhnúkagígur and on the rest of the Reykjanes Peninsula.

3.5.2.3 Buried tephra as a component in Thríhnúkagígur lavas

Evidence from direct field relationships observed in the cave below Thríhnúkagígur's main cone suggests that the buried tephra was physically scoured out and entrained by the magma that fed the eruption. One of the most convincing observations is the presence of hollow, cylindrical proto-conduits that extend vertically into the overlying tephra immediately adjacent to the cross-cutting dike. In order to evaluate this direct observation of processes occurring within the upper magmatic plumbing system, isotopic and trace element mixing models are used to evaluate the tephra assimilation hypothesis geochemically.

The Sr-Nd isotope data in this study do not form a simple binary mixing trend between the hydrothermally altered crust and the dike. In order to assess whether the buried tephra could provide an additional crustal component distinct from the hydrothermally altered crust, the buried tephra with the least radiogenic $^{87}Sr/^{86}Sr$ (TNG-14-26) was chosen as a third component. Given the positioning of the buried tephra ~100 m below the surface, a two-step mixing process is assumed. First, variable mixing with hydrothermally altered crust occurs at depths of a few kilometers. Then these variably affected magmas pick up the buried tephra immediately prior to or during the eruption. Thus, compositions reflecting variable mixtures between mantle-derived magma and hydrothermally altered crust (the near-horizontal curve in Figure 3.15 described in the previous section) are then mixed with the representative tephra component. All but a single outlier require less than 30% of the buried tephra, which is consistent with the maximum estimate of 29% obtained based on physical observations made in Chapter 2.

Immobile elements such as HFSEs and REEs can also be used to assess mixing between mantle-derived magma and the buried tephra. Ratios of HSFEs (Nb/Zr) and REEs (La/Yb) were chosen for two reasons. First, there is an observable contrast in these ratios between the buried tephra and the Holocene lavas and dikes. Second, the use of immobile trace elements helps to avoid the potential effects of low-temperature alteration to the buried tephra since it became exposed at depth in the damp cave. Secondary alteration could potentially overprint the systematics of fluid-mobile elements.

Three end members were chosen to represent possible original magma compositions. The plugged conduit, TNG-14-18, is used because it has the highest Mg# (61) of the sample suite. The chilled margin of the dike, TNG-14-27i, is used because of its low immobile trace element ratios. Finally, the most isotopically depleted dike sample used in the Sr-Nd modeling is implemented here for consistency. The average of five of six buried tephra samples is used to represent the buried tephra end member. Sample TNG-14-28 is excluded from this average because of its high CIA (58) and unique sedimentary structures, which are found only in two 20 cm thick outcrops out of tens of meters of exposed tephra in the cave. Therefore, it is not considered to be representative of the average buried tephra. End member compositions are given in Table 3.6.

Refractory trace element ratios Nb/Zr and La/Yb (Figure 3.16) were used to determine relative mixing proportions. Depending on the magmatic end member, estimates of tephra addition vary considerably. The plugged conduit yields the highest estimates of 28-35% tephra to explain lavas and dike compositions. The chilled margin gives more moderate estimates of 12-18%; and the dike used as the end member in the Sr-Nd modeling suggests 0-8% tephra addition to the erupting magma. The plugged conduit (TNG-14-18) represents a slightly more primitive magma (MgO > 9%) than that erupted during the majority of the eruption (MgO = 7.5-8%). It is not entirely consistent with the major element systematics of the rest of the system (see for example MgO vs. Al_2O_3 in Figure 3.3), and may result in an over-estimate of the inherited tephra component. Thus the maximum estimate from immobile trace element modeling is consistent with the maximum estimate of 29% buried tephra produced with volume estimates of the cave from a LiDAR-derived DEM and the erupted products.

The variability of these three estimates, none of which overlap, does not lend strong support to the hypothesis that the cave was formed by the erosion and entrainment of buried tephra into the erupting magma. The dike (TNG-14-24) used in the Sr-Nd isotope mixing model produces low estimate of tephra addition (0-8%). As this seems the most reasonable primitive mixing end member based on its isotopes ratios (as well as its wt% Al_2O_3 and Sc concentration; see Figures 3.2 and 3.3), the low estimate warrants some consideration. It is possible given the unconsolidated nature of the buried tephra that it may have been rapidly scoured, entrained, and erupted. The proximity of the buried tephra cone to the surface would not necessarily allow much time for the magma to have mixed entrained tephra homogeneously. Early lavas buried within the main cone may contain the bulk of the buried tephra, while tephra-poor lavas and dikes formed later in the eruption are the only ones currently available to sample.

The extent to which the buried tephra was entrained in the erupting magma is not clear from geochemical mixing models. The Sr-Nd isotope mixing model benefits from the addition of a tephra component. On the other hand, the immobile element mixing model does not necessarily require a tephra component to explain the observed compositions of the lavas and dikes. These lines of evidence, at best, weakly support the hypothesized entrainment of tephra to form the cave. At worst, they are not inconsistent with the hypothesis.

3.5.3 Brennisteinsfjöll plumbing system

Variations in lava geochemistry over the course of an eruption have been documented elsewhere in Iceland in basaltic (Furman et al., 1991) and intermediate systems (Sigmarsson et al., 2011). It is not unreasonable to suspect that a dike and sill system propagating towards the surface might contain semi-isolated sill-like bodies at different levels in the crust. These various pockets of magma may experience different geochemical evolutionary histories. Further, different injections of melt to the shallow crustal part of the system may be derived from different proportions of enriched and deplete mantle components. The lack of a central homogenizing magma chamber at Brennisteinsfjöll may facilitate production and/or preservation of a heterogeneous magma, and by extension the smaller fissure swarm of Thríhnúkagígur.

The heterogeneous nature of the major and trace element and radiogenic isotope geochemistry in the Thríhnúkagígur lavas and dikes reflects the lack of a large homogenizing magma chamber in the magmatic plumbing system. Instead, a network of interconnected sills and dikes could both preserve initial heterogeneity in mantle-derived magmas and facilitate the development of additional heterogeneity by independent evolution of small pockets of magma at multiple levels within the crust (Figure 3.17).

The absence of a central volcano in Brennisteinsfjöll is consistent with a conceptual model of a network of small sill-like magma bodies as well as the intrusion and eruption of magmas with variable geochemistry.

The top of the plumbing system exposed in the cave preserves moderate variations in magma composition at different intervals in a single eruption. For example, the plugged conduit is more than 1.5% higher in MgO than all other samples. The chilled margin of the main dike sampled from the wall of the cave anomalously high silica relative to the other unaltered Holocene samples (Table 3.2). These two samples also have markedly different incompatible trace element ratios relative to other Holocene lavas (e.g., lower Nb/Zr and La/Yb; Figure 3.16). It may be expected that these samples would have the most depleted isotopic compositions as well, but this is not the case. Their Sr-Nd-Pb isotopes are indistinguishable from the rest of the lava and dike samples.

Hydrothermally altered crust or hyaloclastites can be much less dense than crystalline basaltic lavas and could stall ascending magmas at many intervals in the crust (Taisne et al., 2011). The variable crustal assimilation estimates (0-25%) suggested by the Sr isotopic ratios in the Thríhnúkagígur lavas are consistent with the co-eruption of relatively unmixed magmas produced in separate sill-like intrusions. Different sills may incorporate variable amounts of hydrothermally altered crust. Further, the altered material itself likely has variable Sr isotopic compositions.

The independent evolution of many different pockets of magmas could allow for a wide range of compositions in a single eruption. This model, in the absence of a central homogenizing magma chamber at Brennisteinsfjöll, invokes an interconnected network of sills and dikes that may facilitate the development of chemical heterogeneity in different locations in the plumbing system. Once an eruption is triggered, these relatively isolated pockets of magma are unable to become well-mixed and compositional differences are preserve in the lavas and the shallow magmatic plumbing system.

This model is also consistent with observations made during and prior to the eruption at Eyjafjallajökull. Although this stratovolcano is markedly different in nature from the fissure swarms of the Reykjanes, the inflation or injection of a mafic sill-like from a deep source is likely to be the dominant intrusive style on the RP, which lacks large homogenizing magma chambers. The deformation at Eyjafjallajökull in 1994 and 1999 is modeled to have occurred at 3.5-6.5 km depth based on InSAR (Pedersen and Sigmundsson, 2004; Pedersen and Sigmundsson, 2006; Sigmundsson et al., 2010), GPS and tilt measurements (Sturkell and Sigmundsson, 2003), and seismic observations (Tarasewicz et al., 2014). A small volume flank eruption presumably sourced from this intrusion had a mafic composition. Interaction with a shallow more silicic chamber sparked the summit eruption (Sigmundsson et al., 2010; Sigmarsson et al., 2011). As the summit eruption progressed, the chemistry of the tephra changed composition hinting at mixing of the mafic component with various more evolved components at different times during ascent (Keiding and Sigmarsson, 2012). This observation is consistent with the observed microseismic earthquake swarms concentrated at particular depths propagating down from the middle crust to upper mantle with each renewal of eruptive explosivity (Tarasewicz, Brandsdóttir, et al., 2012). Collectively, these observations have led multiple authors to suggest a complex multi-sill magmatic plumbing system (Sigmundsson et al., 2010; Keiding and Sigmarsson, 2012; Tarasewicz, White, et al., 2012).

3.6 Conclusions

The lavas and dikes at Thríhnúkagígur have Sr-Nd-Pb isotopic ratios that fall within the range of data previously reported for the Reykjanes Peninsula and at Brennisteinsfjöll. These compositions can be explained by three component mixing of an isotopically and Nb enriched plume component and a depleted component, with minor contributions from an EM1-like component. The southern EVZ requires an isotopically indistinguishable enriched plume component from the one contributing to the RP, but without the unusually enriched Nb. Lavas and dikes at Thríhnúkagígur plot with more enriched RP compositions with a minor EM1-like signature. Unlike the Holocene lavas and dikes, the buried tephra does not have a discernable EM1-like contribution and cluster at the extreme enriched end of previously defined RP compositions. Although the buried tephra is more enriched than the Holocene lavas and dikes, the difference is small compared to the full range of compositions expressed on the RP. Because the buried tephra is ≥100 ka in age, this contrast may also reflect a gradual depletion or dilution of the enriched component under Brennisteinsfjöll through time.

The $^{87}Sr/^{86}Sr$ ratios, like the Nd and Pb isotope ratios, are generally consistent with Reykjanes Peninsula lavas, except that some samples have relatively high Sr isotope ratios at low $^{206}Pb/^{204}Pb$ and $^{143}Nd/^{144}Nd$ ratios. An additional mantle source may be invoked to explain this variation, but is only discernable on the $^{206}Pb/^{204}Pb$ vs. $^{87}Sr/^{86}Sr$ plot. The necessity of this additional mantle end member is difficult to evaluate because Sr isotopes seem to be decoupled from the Nd-Pb isotopes. The most EM1-like sample on the $^{206}Pb/^{204}Pb$ vs. $^{208}Pb/^{204}Pb$ plot is the least EM1-like in Sr-Nd space. Therefore, basaltic crust altered at depth in seawater-dominated hydrothermal systems is proposed as an alternative source for radiogenic Sr. Seawater has highly radiogenic Sr, so even minor contributions from the altered crust could affect $^{87}Sr/^{86}Sr$ ratios in erupted lavas.

The isotope, major, and trace element geochemistry of Thríhnúkagígur is similar to other erupted compositions on the Reykjanes Peninsula. However, the unique cave below the main vent of the 3500 BP eruption allows compositions from the shallow plumbing system to be constrained in addition to the surface lavas. The intrusive samples collected from dike exposures within the walls of the cave have a wider range in major and trace element abundances than the lavas. This demonstrates magma heterogeneity within the small volume of magma along its final ascent to the surface vent, which is not apparent in the majority of surficial flows. It is possible that during the peak of monogenetic fissure eruptions, the magma is well-mixed relative to the initial and final stages, when flow rates are lower. We propose that even in relatively homogeneous monogenetic eruptions, significant chemical variation may persist into the uppermost plumbing system, essentially to the point of the eruption. The surface lavas that represent this heterogeneity may be buried under subsequent lava flows or preserved only in very localized deposits near the vent, or they may be mixed out during the eruptive event itself.

The proposed magmatic plumbing system of interconnected dikes and sills stalled at hydrothermally altered layers in the middle to upper crust below Brennisteinsfjöll provides a mechanism that may both preserve variations in mantle derived magma compositions and facilitate additional magma heterogeneity. This type of plumbing system is consistent with geophysical observations at other volcanic systems in Iceland, as are the crustal residence times. The time scales of mafic magma storage, in particular, have implications for volcanic hazards. If deformation is identified, eruption could occur tens of years later.

Observations made from within the cave at Thríhnúkagígur suggest that buried tephra has been assimilated or simply excavated by the magma en route to the surface. Immobile trace element and radiogenic isotopes mixing models are used to test the conclusions of magmatic entrainment of the buried tephra presented in Chapter 2. These models produce similar estimates for the maximum amount of tephra that could have been entrained and erupted in the Thríhnúkagígur lavas. These models produce maximum estimates of ~28% and ~35% respectively, and 0-8% at minimum. Variation in initial magma compositions may partially explain the variation in the estimates from these models. Another possible source of variability is the extent of buried tephra incorporation as the eruption progresses. It is possible that during the initial phases of the eruption, likely more explosive with fire fountaining along a fissure, the buried tephra may have been blown out by the erupting magma. These lavas with a greater buried tephra component are likely at the base of the main cone at Thríhnúkagígur. Accordingly, the surficial lavas in this study may record less of a buried tephra component if the mass balance approach based on geophysical evidence is considered to be robust.

The lack of consensus about how to identify uniquely crustal tracers of contamination in Icelandic magmas remains a problem. Hydrated, palagonitized, or vitreous basaltic material, akin to the buried tephra beneath Thríhnúkagígur, is likely to have a lower melting temperature than holocrystalline basalt. Fine-grained, low-density, poorly consolidated materials (e.g. hyaloclastites, tephras, tillites) are easily disaggregated, increasing the probability of magma stalling, and have high surface area, which may encourage rapid digestion or entrainment. Nonetheless, even at Thríhnúkagígur, where there are reasonable physical constraints on the maximum mass of basaltic crustal component assimilated and completely characterized geochemistry, including the upper magmatic plumbing system in addition to surficial lava flow, mixing models are unable to provide internally consistent estimates of assimilation. The ability of magma compositions to preserve an unambiguous record of interaction with altered basaltic crustal materials may be limited to systems involving extreme hydrothermal alteration of the crust as recorded by stable isotopes and radiogenic seawater-derived strontium.

Table 3.1. Mineral and groundmass modes in percent. Modes are normalized to 100% after removing the vesicle mode, which is reported separately.

Sample ID	Plagioclase	Olivine	Oxides*	Groundmass/ Glass	Tephra/ Contaminant	Clinopyroxene	Vesicles
Dike							
TNG-14-14m	10.9	4.4	13.5	70.4		0.8	19.2
TNG-14-24	18.5	2.9		78.6			13.5
TNG-14-25	40.5	7.0	10.1	0.0		42.4	21
TNG-14-27i	44.3	10.2	10.2	0.0		35.2	12
Lavas							
TNG-14-32	18.3	4.9		59.8		17.1	18
TNG-14-33	17.8	5.6	10.5	61.4	4.0	0.6	24.5
TNG-14-34	15.4	6.3		74.8	3.6		36.5
TNG-14-37	15.8	6.1		70.1	7.2	0.7	27.5
Miðhnúkar							
TNG-14-35	6.3	7.4		78.1	8.2		27.5
Vent Spatter							
MC-612-03	11.7	1.3		87.0			
Plugged Conduit							
TNG-14-18	2.1	8.9		89.1			4
Tephra							
TNG-14-15	5.8	2.9		91.3			
TNG-14-17	10.0	2.9		87.1			
TNG-14-19							
TNG-14-22	10.7	1.3		88.0			
TNG-14-26	10.2	2.6		87.2			
TNG-14-28	3.6			96.4			

Table 3.2. Major element chemical analyses in weight percent oxides. Data were collected by a Perkin-Elmer Optima 5300DV ICP-AES for a representative sample set for the units present at Thríhnúkagígur. Mg# and the chemical index of alteration (CIA) are unitless numbers. Mg# is defined as 100 * Mg/(Mg + Fe) where Mg and Fe are molar abundances. CIA is defined as 100 * $Al_2O_3/(Al_2O_3 + CaO + Na_2O + K_2O)$. For plotting major element compositions, all samples were normalized to 100% after removing LOI. *Duplicate analysis. Duplicates are averaged for all figures.

Sample ID	TNG-14-14m	TNG-14-24	TNG-14-25	TNG-14-27e	TNG-14-27e*	TNG-14-27i	TNG-14-18	TNG-14-18*	TNG-14-15	TNG-14-17	TNG-14-19
Sample Type	Dike	Dike	Dike	Dike	Dike	Dike	Plugged conduit	Plugged conduit	Buried tephra	Buried tephra	Buried tephra
Description	Interior	Interior	Interior	Chilled margin	Chilled margin	Interior	Rockfall	Rockfall	Uncon-solidated	Bomb	Uncon-solidated
Location	Cave, NNE end	Cave, SSW end	Cave, SSW end	Cave, SSW end	Cave, SSW end	Cave, SSW end	Cave, N end	Cave, N end	cave, N/NNE	cave, N end	cave, NNW end
SiO_2	48.11	47.42	47.11	48.20	49.25	47.23	47.58	47.68	48.38	48.11	48.18
TiO_2	1.77	1.58	1.54	1.19	1.23	1.55	1.41	1.43	2.37	2.33	2.26
Al_2O_3	14.69	15.71	15.91	14.88	15.06	15.64	15.22	15.34	14.63	14.56	14.93
Fe_2O_3T	13.20	12.25	12.15	10.78	11.12	12.08	12.30	12.45	14.06	13.85	13.55
MnO	0.20	0.19	0.19	0.18	0.18	0.19	0.19	0.19	0.21	0.21	0.20
MgO	7.55	7.63	7.98	7.86	7.87	7.89	9.58	9.54	6.60	6.51	6.55
CaO	12.03	12.04	11.84	13.38	13.31	12.14	12.00	11.95	11.36	11.43	11.50
Na_2O	2.12	2.13	2.15	2.04	2.09	2.10	1.95	2.00	2.30	2.32	2.28
K_2O	0.18	0.13	0.14	0.10	0.08	0.15	0.10	0.07	0.28	0.28	0.30
P_2O_5	0.18	0.15	0.18	0.09	0.11	0.16	0.14	0.14	0.29	0.30	0.29
LOI	0.00	0.00	0.00	0.00	0.00	0.00	0.00	0.00	0.00	0.00	0.69
Total	100.03	99.26	99.22	98.69	100.32	99.12	100.47	100.81	100.53	99.94	100.74
Mg#	53	55	57	59	58	56	61	60	48	48	49
CIA	51	52	53	49	49	52	52	52	51	51	51

Table 3.2 continued.

Sample ID	TNG-14-22	TNG-14-26	TNG-14-28	TNG-14-32	TNG-14-33	TNG-14-34	TNG-14-37	MC-612-03	TNG-14-35
Sample Type	Buried tephra	Buried tephra	Buried tephra	Lava	Lava	Lava	Lava	Vent spatter	Miðhnúkar lava
Description	Uncon-solidated	Uncon-solidated	Palagon-itized	Flank vent flow	Main vent flow	Main vent flow	Main vent flow	Main vent scoria	Lava flow
Location	cave, NW end	cave SW/SSW	cave SW/WSW	N 63° 59.865' W 21° 42.015'	N 63° 59.958' W 21° 41.880'	N 63° 59.972' W 21° 41.658'	N 63° 59.836' W 21° 42.098'	top of main vent	N 63° 59.981' W 21° 41.455'
SiO_2 (%)	47.95	47.81	46.70	48.11	47.26	47.33	47.70	49.22	46.34
TiO_2 (%)	2.29	2.35	1.89	1.65	1.60	1.60	1.58	1.71	1.82
Al_2O_3 (%)	14.77	14.42	16.09	15.14	15.66	15.69	15.60	16.15	14.04
Fe_2O_3T (%)	14.09	13.84	13.45	12.73	12.29	12.28	12.20	13.04	13.55
MnO (%)	0.20	0.21	0.17	0.19	0.19	0.19	0.19	0.18	0.21
MgO (%)	6.20	6.76	6.03	7.66	7.66	7.67	7.74	7.21	8.62
CaO (%)	10.84	11.33	9.79	11.94	12.01	12.00	11.89	9.91	10.93
Na_2O (%)	1.95	2.29	1.65	2.07	2.05	2.09	2.07	1.65	2.01
K_2O (%)	0.31	0.29	0.20	0.14	0.15	0.16	0.15	0.11	0.19
P_2O_5 (%)	0.29	0.28	0.24	0.16	0.15	0.16	0.17	0.17	0.17
LOI(900C)	1.11	0.00	2.79	0.00	0.00	0.00	0.00	0.00	0.00
Total	99.99	99.62	99.00	99.82	99.03	99.17	99.29	99.37	98.34
Mg#	47	49	47	54	56	55	56	52	56
CIA	53	51	58	52	52	52	53	58	52

Table 3.3. CIPW norms. Calculated from major element data and trace element concentrations of Sr, Ba, Cr, Ni, and Zr. Samples TNG-14-22, TNG-14-28, and MC-612-03 are excluded from this table because they have been altered to an extent that makes their bulk chemistry fall outside the range of compositions for which norms can be calculated.

Sample ID	TNG-14-14m	TNG-14-24	TNG-14-25	TNG-14-27e	TNG-14-27i	TNG-14-18	TNG-14-15	TNG-14-17	TNG-14-19	TNG-14-26	TNG-14-32	TNG-14-33	TNG-14-34	TNG-14-37
Sample Type	Dike	Dike	Dike	Dike	Dike	Plugged conduit	Buried tephra	Buried tephra	Buried tephra	Buried tephra	Flank vent lava	Main vent lava	Main vent lava	Main vent lava
Plagioclase	48.49	51.83	52.52	49.48	51.62	49.46	48.58	48.76	49.46	48.33	49.79	51.43	51.62	51.24
Orthoclase	1.06	0.83	0.83	0.53	0.89	0.53	1.65	1.65	1.83	1.77	0.83	0.95	0.95	0.95
Diopside	23.65	21.55	20.25	28.34	22.07	21.24	21.43	22.01	21.39	21.94	22.07	21.35	21.30	20.93
Hyper-sthene	15.07	12.06	10.53	11.50	10.35	11.17	18.61	17.50	17.19	16.82	16.39	12.89	12.37	14.71
Olivine	4.98	7.60	9.80	5.14	9.05	11.87	1.43	1.48	2.15	2.88	4.56	7.20	7.57	6.03
Ilmenite	3.40	3.06	2.89	2.34	3.00	2.70	4.54	4.48	4.33	4.54	3.17	3.10	3.10	3.06
Magnetite	2.90	2.71	2.70	2.42	2.68	2.70	3.07	3.06	2.97	3.06	2.80	2.73	2.73	2.7
Apatite	0.42	0.37	0.42	0.23	0.37	0.32	0.67	0.70	0.67	0.65	0.39	0.37	0.39	0.39
Zircon	0.01	0.01	0.01	0.01	0.01	0.01	0.03	0.03	0.03	0.03	0.01	0.01	0.01	0.01
Chromite	0.06	0.07	0.07	0.07	0.07	0.09	0.03	0.03	0.03	0.03	0.07	0.06	0.06	0.06

Table 3.4. Trace element chemical analyses. Data were collected by a Thermo X-Series II Quadruple ICP-MS for samples from the Thríhnúkar fissure system. All concentrations are in ppm. NR = not reported. *Duplicate analysis.

Sample ID	TNG-14-14m	TNG-14-24	TNG-14-25	TNG-14-27e	TNG-14-27e	TNG-14-27i*	TNG-14-18	TNG-14-18*
Sample Type	Dike	Dike	Dike	Dike	Dike	Dike	Plugged conduit	Plugged conduit
Li	NR	4.24	4.41	NR	3.91	NR	NR	4.93
Sc	44.2	42.5	40.8	53.4	55.8	41.7	39.9	42.7
V	382	352	342	380	391	347	314	338
Cr	295	314	331	318	317	333	382	391
Co	74.4	75.3	95.9	63.1	67.7	67.6	73.2	79.5
Ni	93.3	113	123	74.8	75.6	117	187	191
Cu	116	167	96.6	79.9	85.0	119	92.5	98.8
Zn	102	97.3	96.2	72.2	74.8	93.6	92.4	95.3
Rb	3.71	3.17	3.14	1.94	1.90	3.26	1.89	1.88
Sr	189	208	208	183	189	203	166	187
Y	25.7	23.7	22.1	17.5	17.2	23.0	22.2	22.3
Zr	87.6	78.8	78.5	50.3	50.0	77.6	62.7	62.1
Nb	11.7	10.6	10.8	6.15	6.27	10.2	6.64	6.56
Cs	0.09	0.10	0.10	0.07	0.10	0.07	0.05	0.08
Ba	60.9	52.5	51.7	39.1	36.6	55.9	33.0	33.5
Hf	2.31	2.05	2.01	1.46	1.41	2.06	1.72	1.66
Ta	0.83	0.66	0.65	0.45	0.38	0.73	0.48	0.41
Pb	0.54	0.49	0.39	0.30	0.30	0.46	0.26	0.26
Th	0.48	0.42	0.41	0.25	0.24	0.43	0.25	0.25
U	0.15	0.13	0.13	0.08	0.07	0.13	0.08	0.08
La	7.77	6.97	6.81	4.41	4.29	7.01	4.87	4.88
Ce	18.8	17.0	16.4	10.9	10.6	17.0	12.7	12.6
Pr	2.77	2.37	2.25	1.65	1.51	2.48	1.95	1.84
Nd	12.7	11.6	10.8	7.80	7.57	11.3	9.24	9.42
Sm	3.57	3.25	2.99	2.34	2.21	3.18	2.77	2.76
Eu	1.29	1.19	1.11	0.94	0.90	1.17	1.04	1.03
Gd	4.19	3.78	3.48	2.84	2.71	3.75	3.37	3.32
Tb	0.71	0.64	0.60	0.49	0.47	0.64	0.59	0.58
Dy	4.50	4.01	3.77	3.05	2.93	4.00	3.79	3.72
Ho	0.92	0.85	0.79	0.63	0.61	0.83	0.78	0.78
Er	2.61	2.40	2.21	1.80	1.72	2.35	2.24	2.23
Tm	0.39	0.35	0.32	0.26	0.24	0.35	0.33	0.33
Yb	2.44	2.24	2.09	1.66	1.59	2.17	2.07	2.08
Lu	0.38	0.33	0.31	0.26	0.24	0.34	0.33	0.31

Table 3.4 continued.

Sample ID	TNG-14-15	TNG-14-17	TNG-14-19	TNG-14-22	TNG-14-26	TNG-14-28
Sample Type	Buried tephra	Buried tephra	Buried tephra	Buried tephra	Buried tephra	Buried tephra
Li	5.00	4.98	NR	NR	5.19	NR
Sc	43.8	44.3	43.4	41.7	48.5	40.4
V	403	408	406	387	445	343
Cr	139	141	143	136	160	224
Co	66.6	107	59.4	51.9	69.2	62.2
Ni	75.9	73.5	77.9	67.4	80.8	136
Cu	317	187	180	265	190	271
Zn	116	117	114	113	128	98.4
Rb	6.33	6.34	6.67	8.16	6.99	4.07
Sr	248	256	241	236	280	185
Y	33.5	31.4	30.1	35.2	36.5	24.7
Zr	132	133	131	130	145	97.8
Nb	21.8	21.7	21.2	20.9	23.9	14.4
Cs	0.17	0.18	0.15	0.20	0.18	0.13
Ba	93.8	94.5	96.3	95.0	103	75.4
Hf	3.24	3.31	3.34	3.30	3.54	2.55
Ta	1.31	1.33	1.48	1.44	1.42	1.00
Pb	0.81	0.85	0.81	0.86	0.65	0.63
Th	0.84	0.86	0.85	0.85	0.91	0.65
U	0.25	0.26	0.27	0.27	0.26	0.18
La	13.5	12.9	12.9	13.2	14.5	9.11
Ce	33.4	31.2	31.0	32.0	34.4	21.9
Pr	4.58	4.24	4.41	4.55	4.56	3.13
Nd	22.0	19.9	19.6	20.0	21.3	14.1
Sm	5.56	5.05	5.00	5.18	5.47	3.78
Eu	1.86	1.73	1.73	1.78	1.87	1.32
Gd	6.18	5.46	5.47	5.82	5.90	4.22
Tb	1.00	0.90	0.90	0.96	0.97	0.71
Dy	5.97	5.39	5.41	5.85	5.79	4.40
Ho	1.24	1.10	1.08	1.19	1.18	0.90
Er	3.40	3.05	3.03	3.32	3.27	2.53
Tm	0.48	0.44	0.44	0.48	0.46	0.38
Yb	3.06	2.82	2.70	2.94	2.99	2.37
Lu	0.45	0.41	0.42	0.45	0.43	0.37

Table 3.4 continued.

Sample ID	TNG-14-32	TNG-14-33	TNG-14-34	TNG-14-37	MC-612-03	TNG-14-35
Sample Type	Lava	Lava	Lava	Lava	Vent spatter	Miðhnúkar
Li	5.31	NR	NR	NR	4.68	NR
Sc	46.7	41.7	42.0	40.1	45.9	41.6
V	387	354	354	342	385	382
Cr	326	297	294	287	315	319
Co	99.0	76.4	164	170	72.8	84.1
Ni	120	114	114	110	117	161
Cu	176	159	149	150	159	149
Zn	105	97.7	96.5	92.5	107	109
Rb	3.52	3.48	3.54	3.29	3.64	4.19
Sr	221	192	193	194	179	176
Y	25.3	24.3	24.0	23.2	23.4	27.4
Zr	87.3	82.4	82.5	77.7	92.7	97.9
Nb	11.9	11.0	11.0	10.4	12.5	12.5
Cs	0.11	0.08	0.08	0.08	0.13	0.11
Ba	57.3	56.2	56.0	56.2	55.6	61.0
Hf	2.23	2.18	2.18	2.07	2.33	2.57
Ta	0.71	0.78	0.78	0.74	0.76	0.88
Pb	0.55	0.61	0.91	0.50	2.40	1.38
Th	0.46	0.46	0.48	0.43	0.52	0.55
U	0.14	0.15	0.15	0.13	0.16	0.18
La	7.65	7.54	7.24	7.08	7.65	8.28
Ce	18.6	18.4	17.9	17.3	18.5	20.5
Pr	2.58	2.68	2.63	2.53	2.53	3.00
Nd	12.5	12.3	12.0	11.5	12.2	13.8
Sm	3.42	3.43	3.37	3.23	3.27	3.87
Eu	1.26	1.24	1.25	1.20	1.19	1.37
Gd	4.01	4.00	3.93	3.83	3.81	4.46
Tb	0.68	0.68	0.68	0.65	0.65	0.77
Dy	4.29	4.31	4.20	4.08	3.99	4.81
Ho	0.90	0.88	0.87	0.85	0.84	0.99
Er	2.53	2.50	2.46	2.38	2.34	2.80
Tm	0.37	0.37	0.37	0.35	0.34	0.42
Yb	2.36	2.34	2.33	2.21	2.17	2.64
Lu	0.35	0.36	0.36	0.35	0.33	0.41

Table 3.5. Pb-Sr-Nd isotope ratios. Data were collected by Finnigan MAT 262 multi-collector thermal ionization mass spectrometer (TIMS). Two standard deviations are given in ten-thousandths for Pb ratios and one-millionths for $^{87}Sr/^{86}Sr$ and $^{143}Nd/^{144}Nd$.

Sample ID	TNG-14-14m	TNG-14-24	TNG-14-25	TNG-14-27e	TNG-14-27i	TNG-14-18	TNG-14-15	TNG-14-17	TNG-14-19
Sample Type	Dike	Dike	Dike	Dike	Dike	Plugged conduit	Buried tephra	Buried tephra	Buried tephra
$^{206}Pb/^{204}Pb$	18.9042	18.5182	18.8017	18.7945	18.8128	18.6805	18.9241	18.6840	18.9437
2σ	228	112	224	55	36	82	77	28	69
$^{207}Pb/^{204}Pb$	15.5892	15.5525	15.6302	15.4768	15.5031	15.5237	15.5355	15.5346	15.5381
2σ	192	97	184	44	30	72	63	23	57
$^{208}Pb/^{204}Pb$	38.5980	38.2656	38.5401	38.3135	38.3958	38.3395	38.5259	38.3471	38.5224
2σ	463	235	456	108	74	167	154	57	139
$^{87}Sr/^{86}Sr$	0.703187	0.703135	0.703143	0.703203	0.703141	0.703088	0.703174	0.703186	0.703223
2σ	7	7	8	9	8	30	7	7	15
$^{143}Nd/^{144}Nd$	0.513031	0.513040	0.513036	0.513021	0.513029	0.513039	0.513012	0.513010	0.513010
2σ	8	15	6	10	20	8	8	8	6

Table 3.5 continued.

Sample ID	TNG-14-22	TNG-14-26	TNG-14-28	TNG-14-32	TNG-14-33	TNG-14-34	TNG-14-37	MC-612-03	TNG-14-35
Sample Type	Buried tephra	Buried tephra	Buried tephra	Flank lava	Main vent lava	Main vent lava	Main vent lava	Vent Spatter	Miðhnúkar lava
$^{206}Pb/^{204}Pb$	18.9328	18.8634	18.8472	18.8418	18.8233	18.5738	18.8520	18.2889	18.4774
2σ	46	46	64	69	78	14	62	21	69
$^{207}Pb/^{204}Pb$	15.5411	15.4893	15.5191	15.5375	15.5338	15.5647	15.5352	15.5947	15.5628
2σ	37	38	52	56	62	11	54	18	58
$^{208}Pb/^{204}Pb$	38.5464	38.3865	38.4452	38.4790	38.4478	38.3561	38.4755	38.1947	38.2762
2σ	92	95	13	143	155	27	135	45	142
$^{87}Sr/^{86}Sr$	0.703305	0.703157	0.703191	0.703170	0.703213	0.703281	0.703178	0.703197	0.703184
2σ	8	8	10	7	9	8	8	6	7
$^{143}Nd/^{144}Nd$	0.513018	0.512991	0.513050	0.513000	0.513030	0.513044	0.513024	0.513022	0.513022
2σ	10	9	16	13	9	8	7	10	8

Table 3.6. Mixing end member compositions for Figures 3.14 and 3.15. HAC = hydrothermally altered crust; from Gee et al. (1998a).

End Member	$^{87}Sr/^{86}Sr$	$^{143}Nd/^{144}Nd$	Sr (ppm)	Nd (ppm)	La/Yb	Sm/Nd	Nb/Zr
HAC	0.7036	0.51305	300	10.6			
TNG-14-24	0.703135	0.513040	208	11.6	3.11	0.281	0.134
TNG-14-26	0.703157	0.512991	280	9.33	4.84	0.257	0.164
TNG-14-18	0.703188	0.513039	177	21.3	2.35	0.297	0.106
Avg. buried tephra					4.26	0.256	0.163

Figure 3.1. Photomicrographs of two phenocryst population, a more tabular euhedral one (a) and a high aspect ratio one (b) in lava TNG-14-14m; the phenocryst-poor chilled margin (c; TNG-14-27e) and flow banding with interstitial clinopyroxene in the interior the same dike (d; TNG-14-27i); aphanitic, phenocryst-poor plugged conduit, TNG-14-18 (e); and large olivine phenocrysts from the Miðhnúkar lava flow, TNG-14-35 (f).

Figure 3.2. Total alkali-silica plot (TAS). All Thríhnúkagígur samples analyzed are subalkaline basalts. Buried tephra samples are represented by triangle; lava and dike samples from the Holocene eruption are circles; the lava sample from Miðhnúkar is a cross. TAS diagram from Le Bas and Le Maitre (1986).

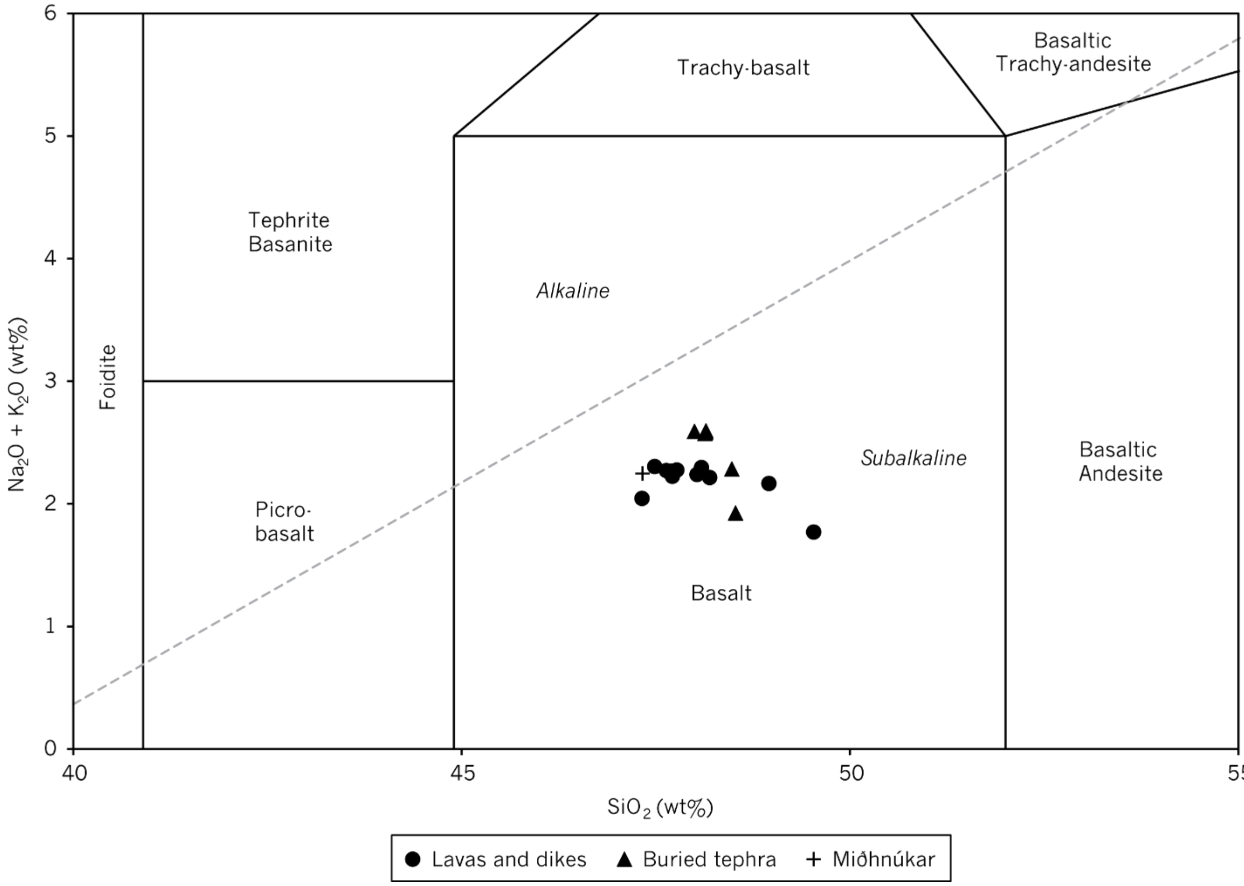

Figure 3.3. Fenner diagrams of MgO vs. the major oxides and chemical index of alteration (CIA). Circles represent lavas and dikes. Triangles represent buried tephra samples. The cross is the Miðhnúkar lava. Open symbols indicate samples with a high CIA samples likely to be affected by secondary alteration.

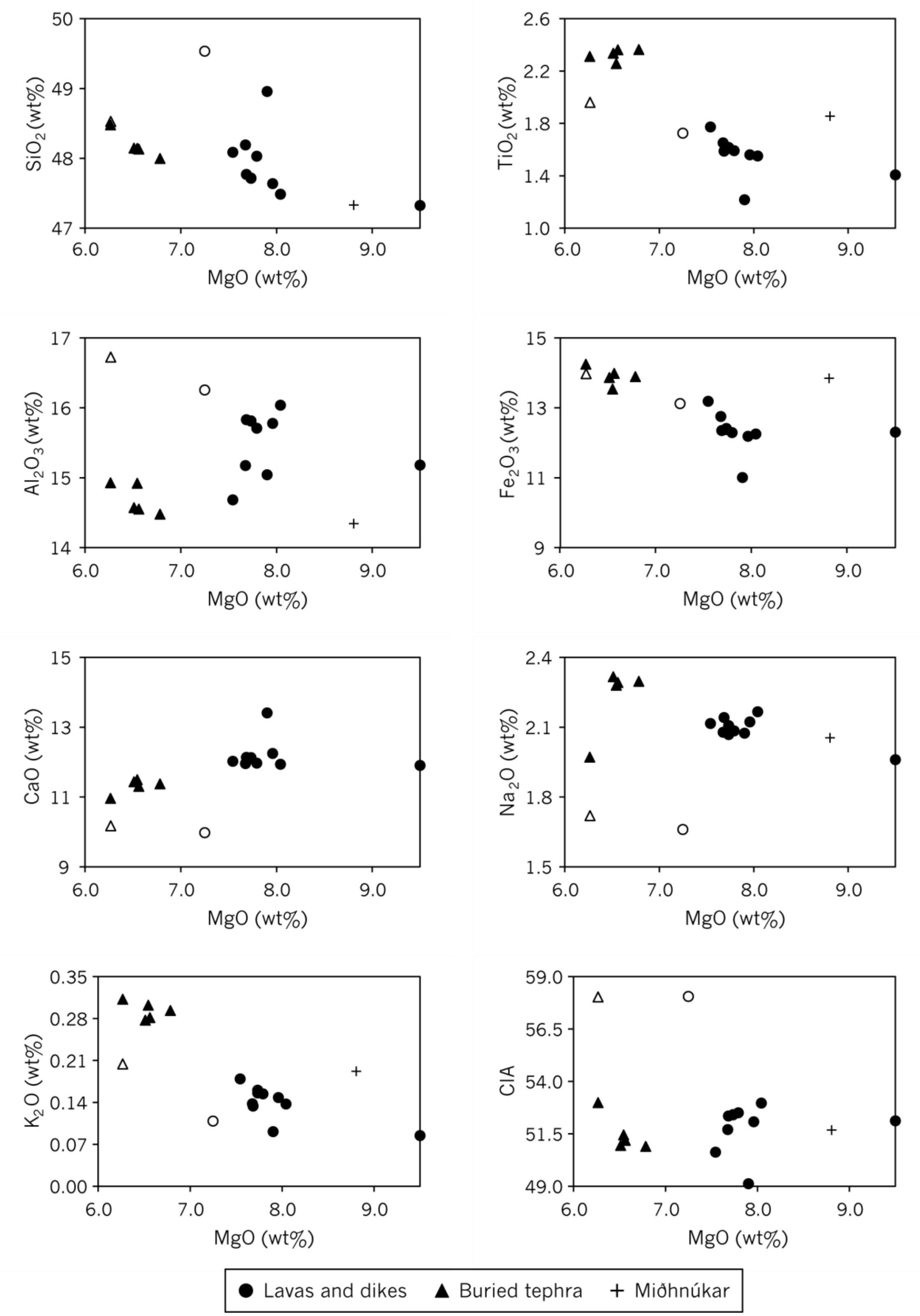

Figure 3.4. Plots of MgO vs. trace elements and CaO/Al_2O_3. Circles represent lavas and dikes while triangles represent buried tephra samples. The cross is the lava from Miðhnúkar. Open symbols indicate samples with a high CIA and likely to be affected by secondary alteration.

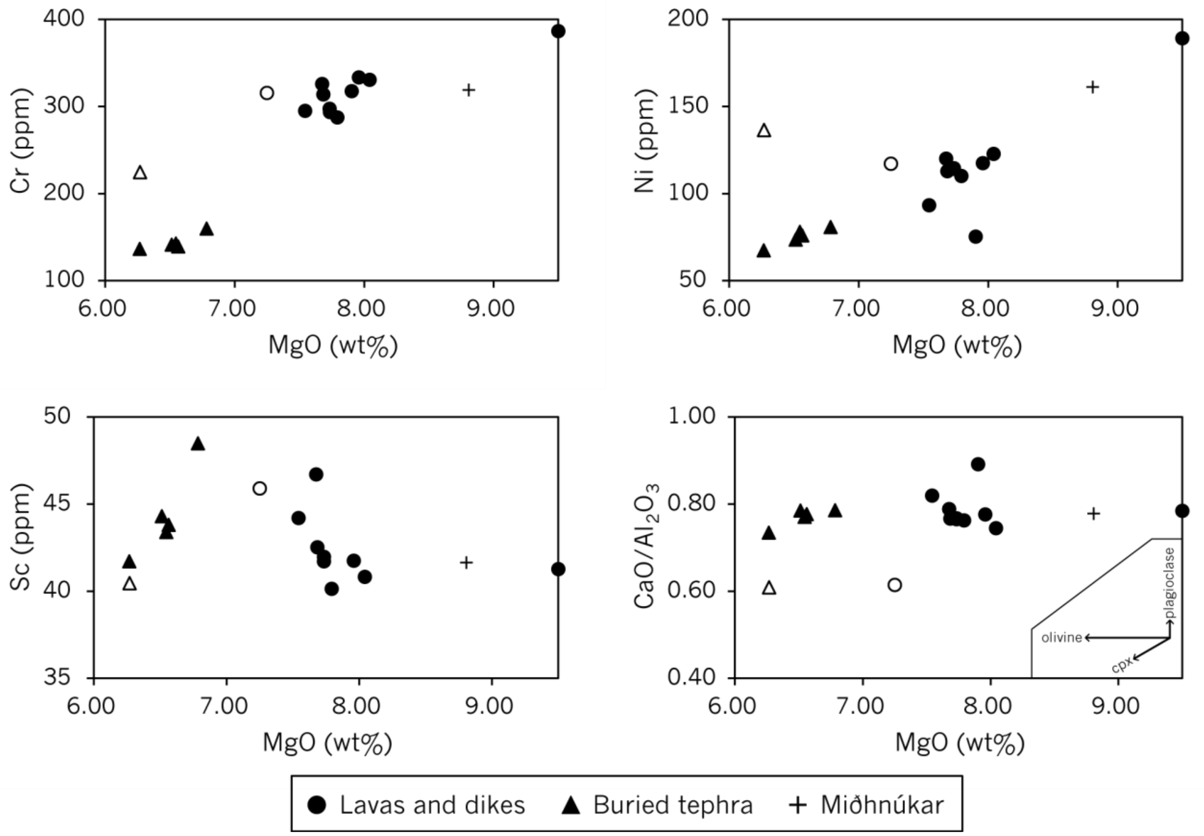

Figure 3.5. Primitive mantle normalized multielement diagram for the main sample suites and unique samples from Thríhnúkagígur. All samples are characterized by small positive Ba and U, and relatively large Nb and Ta anomalies. All samples have moderate to large negative Pb anomalies, except for the vent spatter (MC-612-03), which is thought to be a result of contamination. Most other trace elements display similar patterns across regardless of sample type, except for Sr which has a positive anomaly in relatively more depleted plugged conduit (TNG-14-18) and chilled margin of the dike (TNG-14-27e) and a negative anomaly in the more enriched buried tephra. Primitive mantle normalization values are from Sun and McDonough (1989).

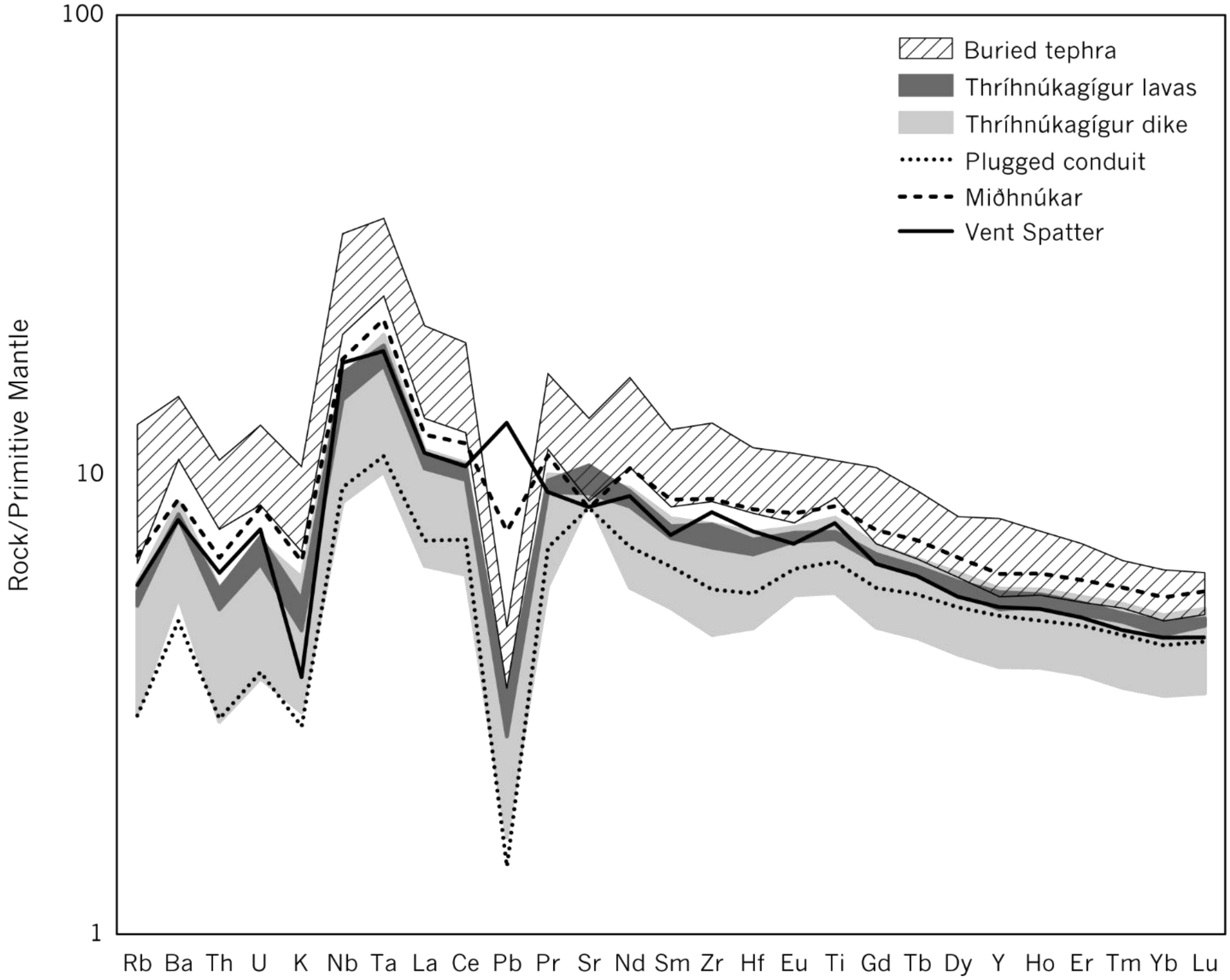

Figure 3.6. Chondrite normalized rare earth element (REE) spider diagram by rock type. All samples have a gently sloping negative trend with higher LREE values than HREE values. The chilled margin of the dike (TNG-14-27e) has a weak positive Eu anomaly. Chondrite normalization values are from Sun and McDonough (1989).

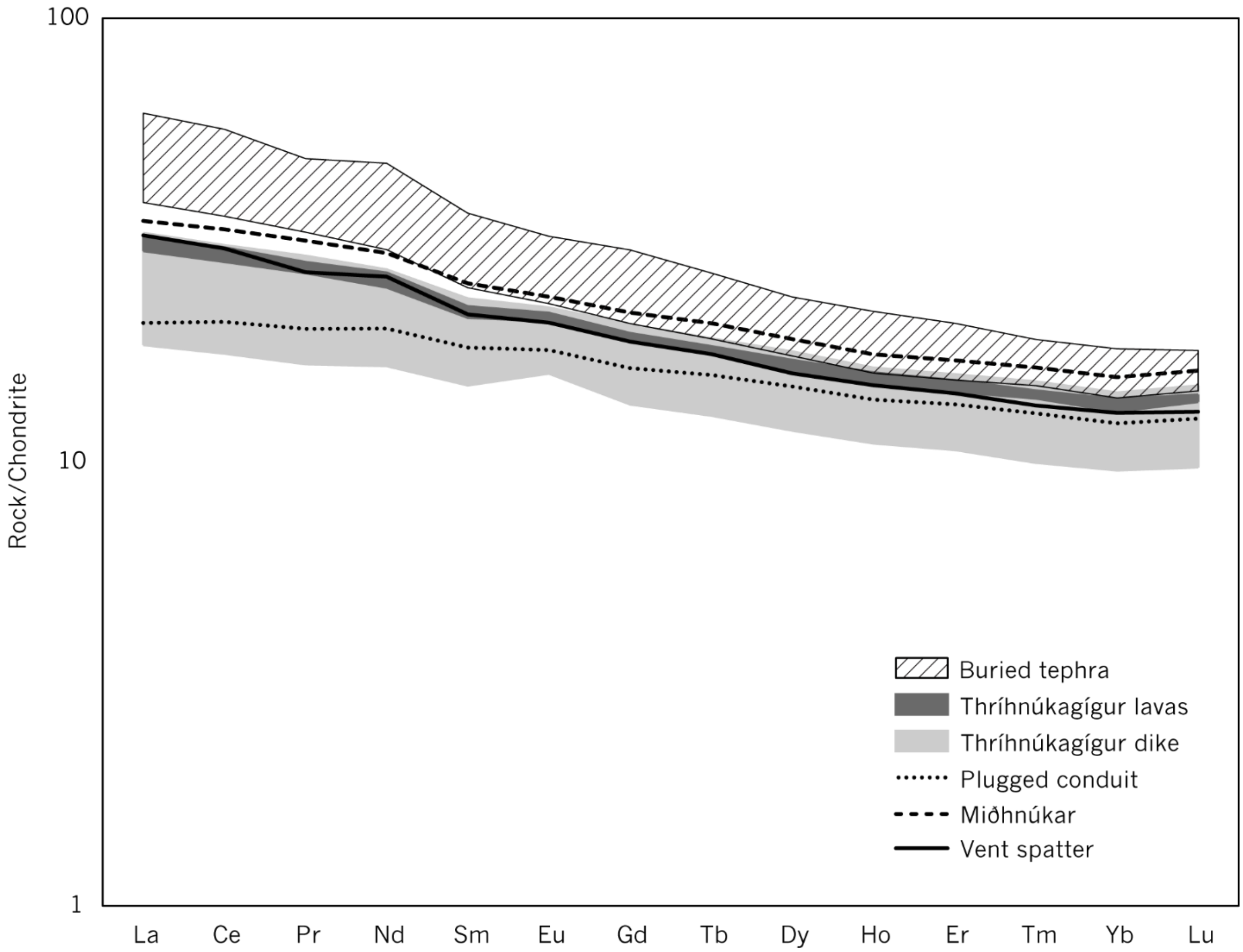

Figure 3.7. Plots of $^{206}Pb/^{204}Pb$ vs. $^{208}Pb/^{204}Pb$ (a) and $^{207}Pb/^{204}Pb$ (b). Circles represent lavas and dikes while triangles represent buried tephra samples. The cross is the lava from Miðhnúkar. Open symbols indicate samples with a high CIA. Error bars represent either the in run instrumental error or the standard reproducibility, whichever source of error is larger.

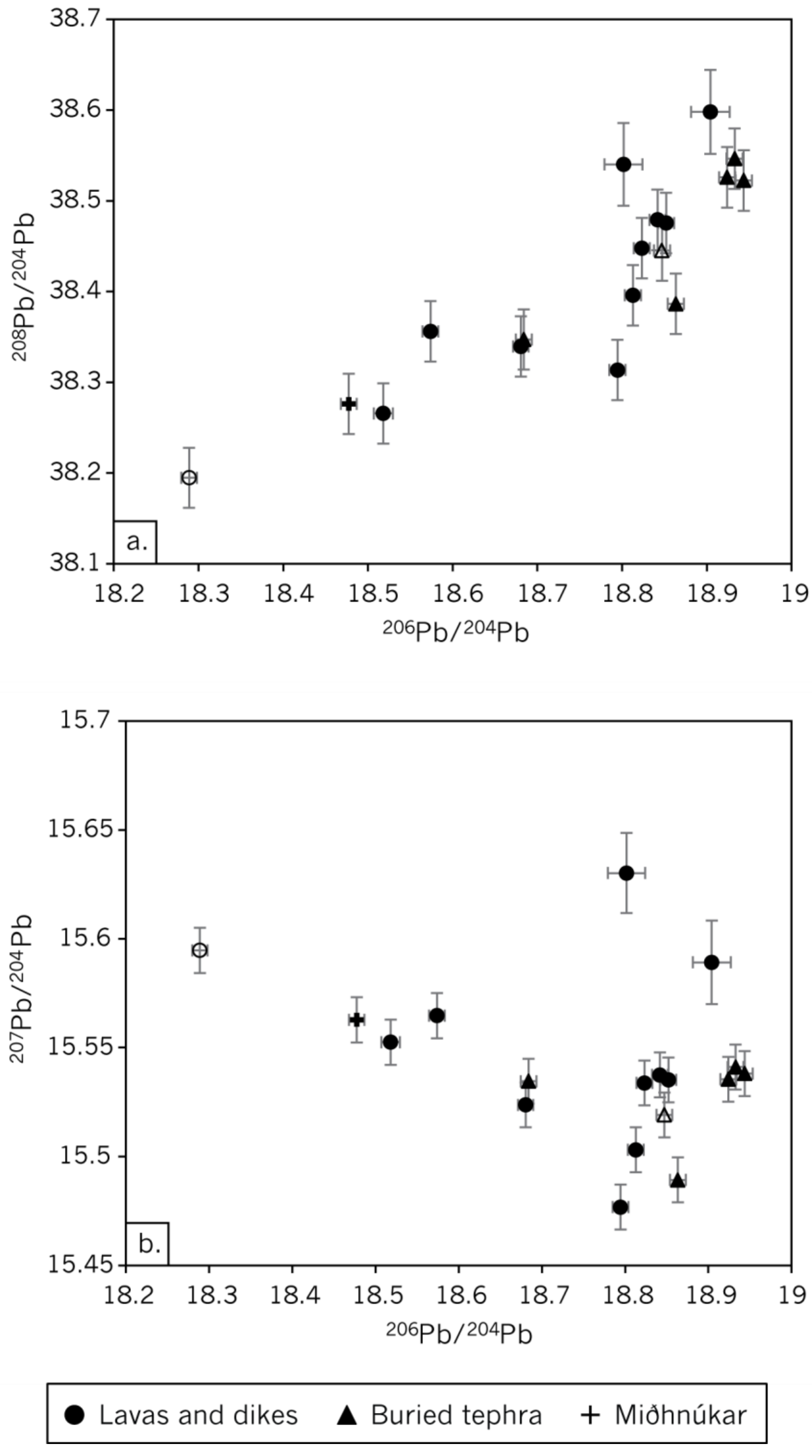

Figure 3.8. Plot of $^{87}Sr/^{86}Sr$ vs. $^{143}Nd/^{144}Nd$. The buried tephras have consistently lower $^{143}Nd/^{144}Nd$ ratios compared to the lavas and dikes across the same range of $^{87}Sr/^{86}Sr$ ratios. Three dike samples have the least radiogenic Sr isotope ratios at the same relative radiogenic Nd isotope ratio. Circles represent lavas and dikes while triangles represent buried tephra samples. The cross is the lava from Miðhnúkar. Open symbols indicate samples with a high CIA. Error bars represent either the in run instrumental error or the standard reproducibility, whichever source of error is larger.

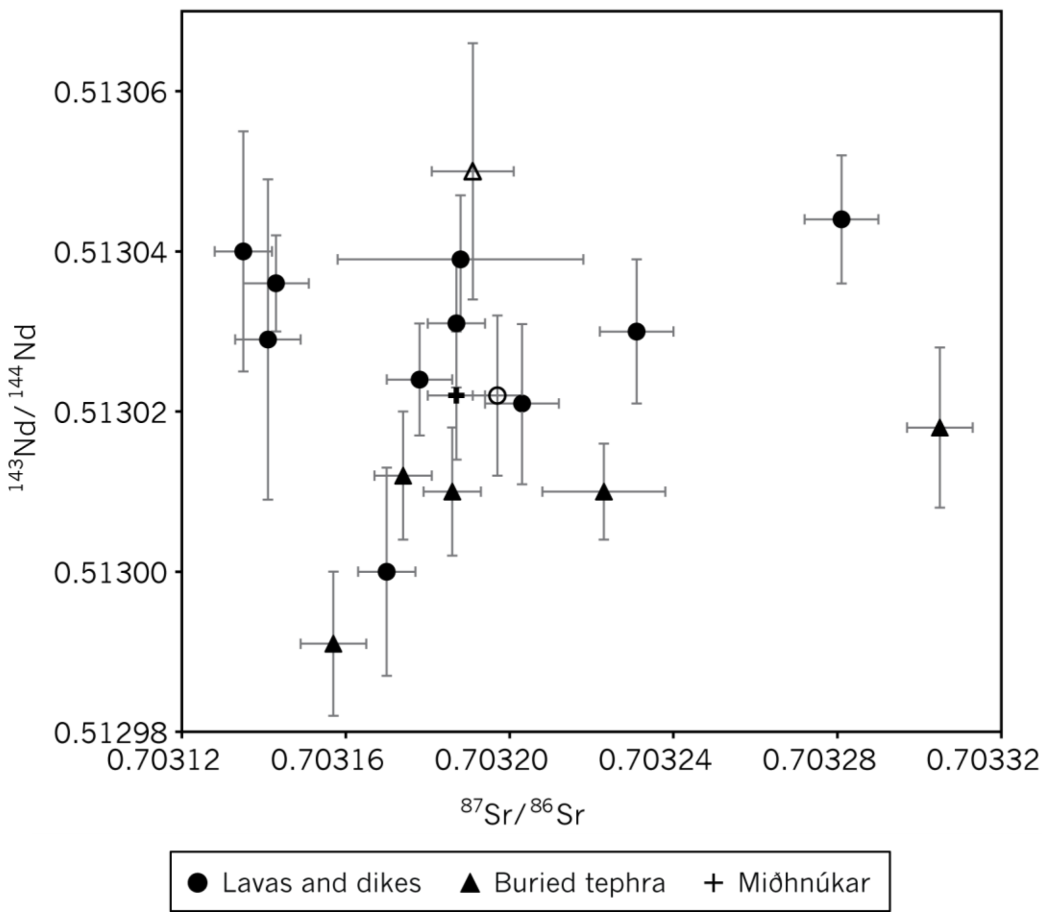

Figure 3.9. $(La/Yb)_N$ vs. Nb/Zr. Reykjanes Peninsula and the Western Volcanic Zone lavas in SW Iceland extend to similarly high Nb/Zr ratios as lavas in the Eastern Volcanic Zone, but at much lower $(La/Yb)_N$ ratios. Thríhnúkagígur lavas and dikes are consistent other lavas from SW Iceland while the buried tephra record some of the most enriched values in the region. Circles represent lavas and dikes while triangles represent buried tephra samples. The cross is the lava from Miðhnúkar. Open symbols indicate samples with a high CIA. Data for Vestmannaeyjar are from Furman et al. (1991), Kokfelt et al. (2006), and Peate et al. (2010); EVZ data are from Kokfelt et al. (2006), Peate et al. (2010), and Manning and Thirlwall (2014); WVZ data are from Kokfelt et al. (2006) and Koornneef et al. (2012); and data from the Reykjanes Peninsula are from Kokfelt et al. (2006), Peate et al. (2009), and Koornneef et al. (2012).

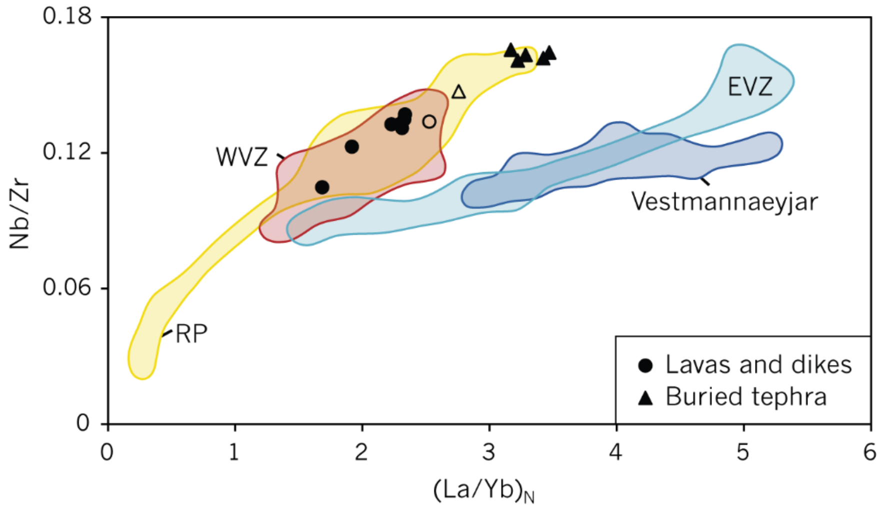

Figure 3.10. Plots of Nb vs. Nb/U (a) and Ce vs. Ce/Pb (b). Global ocean island basalts and mid-ocean ridge basalts yield Nb/U ratios of 47 ± 10 at all concentrations of Nb and Ce/Pb ratios of 25 ± 5 at all Ce concentrations (Hofmann et al., 1986). Dashed lines show these ranges. Lavas in SW Iceland on the Reykjanes Peninsula and in the WVZ yield much higher Nb/U and Ce/Pb than observed elsewhere, not just in Iceland, but globally. Circles represent lavas and dikes while triangles represent buried tephra samples. The cross is the lava from Miðhnúkar. Open symbols indicate samples with a high CIA. Data for Vestmannaeyjar are from Kokfelt et al. (2006) and Peate et al. (2010); EVZ data are from Sigmarsson et al. (1992), Kokfelt et al. (2006), Peate et al. (2010), and Manning and Thirlwall (2014); WVZ and RP data are from Kokfelt et al. (2006) and Koornneef et al. (2012).

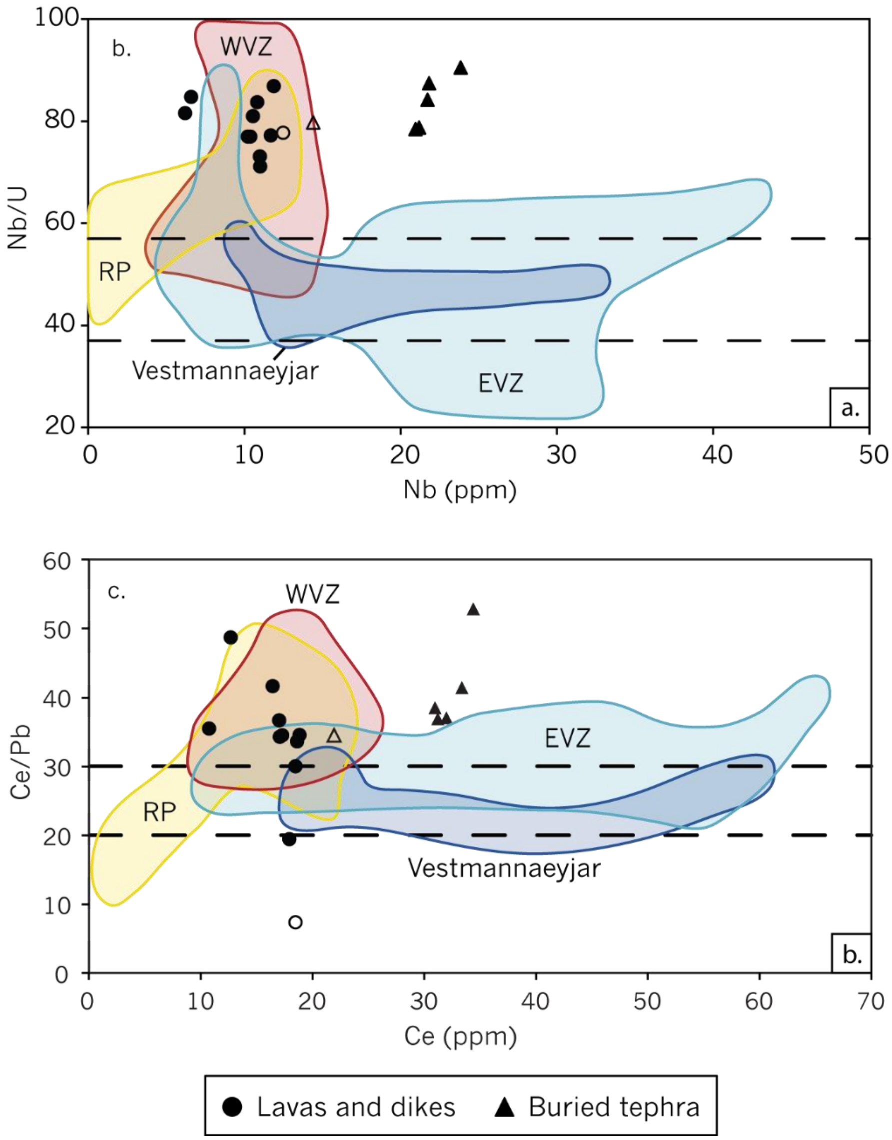

Figure 3.11. Plots of $^{206}Pb/^{204}Pb$ vs. $^{208}Pb/^{204}Pb$ with proposed mantle end members from Thirlwall et al. (2004) and Kitagawa et al. (2008). South Iceland lavas form an array primarily between an enriched and a depleted end member on both plots. Thríhnúkagígur samples are broadly consistent with composition observed on the Reykjanes Peninsula and Brennisteinsfjöll. They are pulled slightly off the NHRL (Hart, 1984) towards an EM1-like end member. Data for the southern Reykjanes Ridge (SRR) are from Thirlwall et al., 2004; Reykjanes, Krísuvík, and Brennisteinsfjöll data are from Thirlwall et al., 2004, Kokfelt et al., 2006, and Peate et al., 2009; Hekla and Katla data are from Park, 1990 and Furman et al., 1995; Vestmannaeyjar data are from Furman et al., 1991, Chauvel and Hémond, 2000, Kokfelt et al., 2006, and Peate et al., 2010.

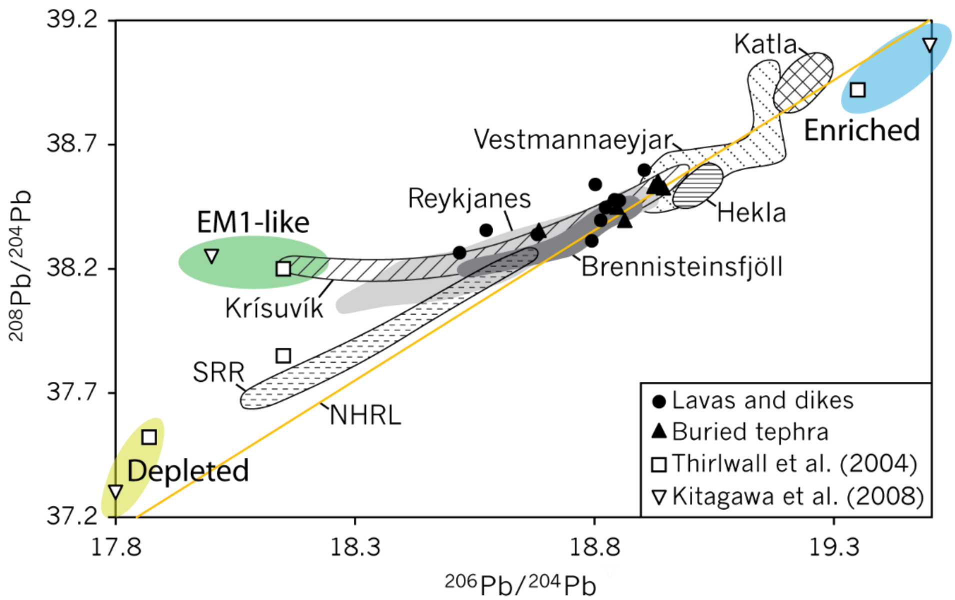

Figure 3.12. Nb/U plotted against $^{206}Pb/^{204}Pb$ (a), $^{208}Pb/^{204}Pb$ (b). Solid black triangles represent Thríhnúkagígur buried tephra. Solid black circles represent Thríhnúkagígur lavas and dikes. Grey circles represent other Reykjanes Peninsula lavas from Kokfelt et al. (2006).

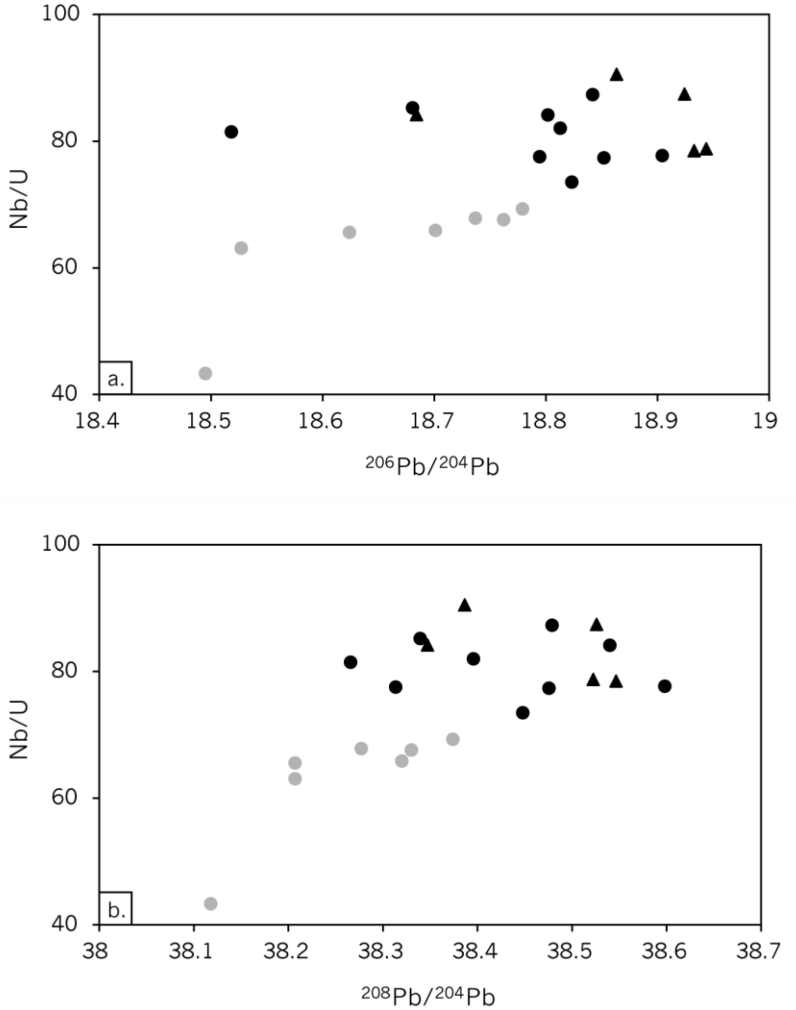

Figure 3.13. A plot of $^{87}Sr/^{86}Sr$ vs. $^{143}Nd/^{144}Nd$. Thríhnúkagígur samples are more consistent with the Reykjanes fissure swarm and Vestmannaeyjar than Brennisteinsfjöll and are influenced by an EM1-like component, or more likely, HAC. Sr-Nd isotopes, data for the southern Reykjanes Ridge (SRR) are from Thirlwall et al., 2004; Reykjanes, Krísuvík, and Brennisteinsfjöll data are from Thirlwall et al., 2004, Kokfelt et al., 2006, and Peate et al., 2009; Hekla data are from Park, 1990, Sigmarsson et al., 1992, and Furman et al., 1995; Katla data are from Park, 1990 and Furman et al., 1995; Vestmannaeyjar data are from Furman et al., 1991 and Kokfelt et al., 2006.

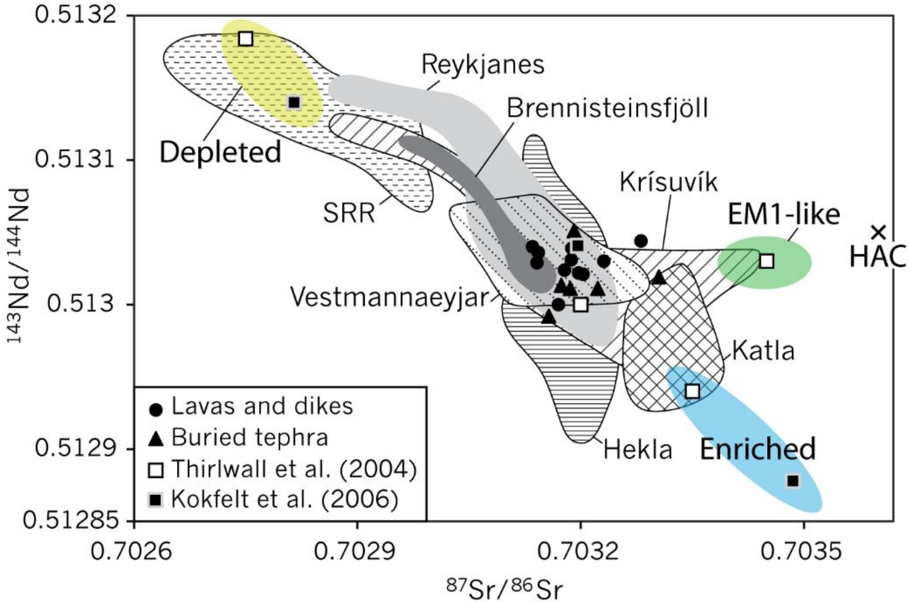

Figure 3.14. A plot of $^{206}Pb/^{204}Pb$ vs. $^{87}Sr/^{86}Sr$. Thríhnúkagígur samples are most consistent with the lavas with highly radiogenic Sr isotopes from the Reykjanes fissure swarm. Data for the southern Reykjanes Ridge (SRR) are from Thirlwall et al., 2004; Reykjanes, Krísuvík, and Brennisteinsfjöll data are from Thirlwall et al., 2004, Kokfelt et al., 2006, and Peate et al., 2009; Hekla data are from Park, 1990, Sigmarsson et al., 1992, and Furman et al., 1995; Katla data are from Park, 1990 and Furman et al., 1995; Vestmannaeyjar data are from Furman et al., 1991 and Kokfelt et al., 2006.

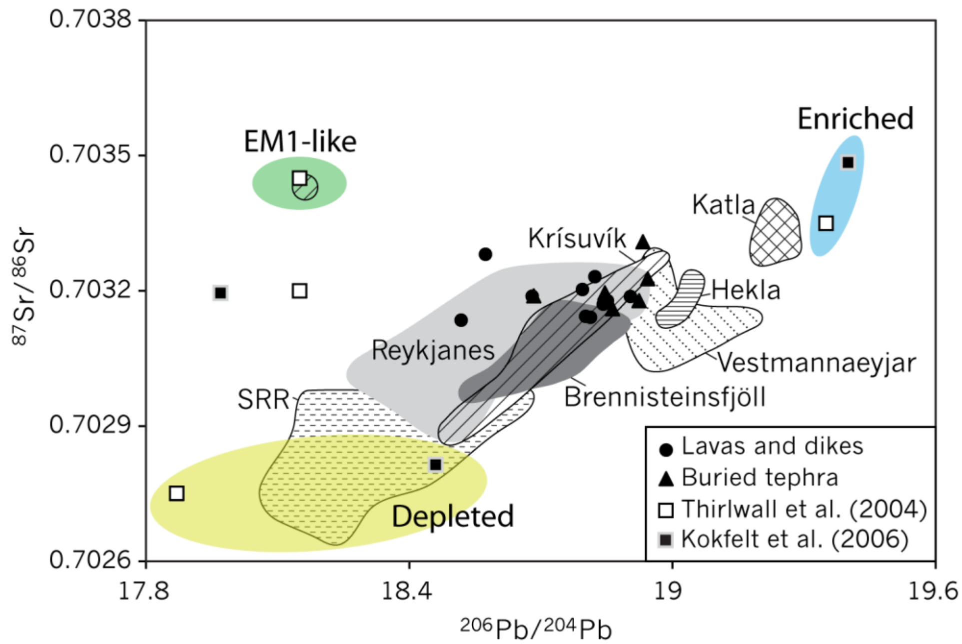

Figure 3.15. Sr-Nd isotope mixing model for Thríhnúkagígur lavas and dikes. First, the dike sample with the least radiogenic Sr isotope composition (TNG-14-24, purple circle) is mixed with a strongly radiogenic hydrothermally altered crustal end member from Gee et al., 1998 (blue cross). Then mixing occurs between various points along the first curve and the least radiogenic buried tephra sample, marked with a red triangle.

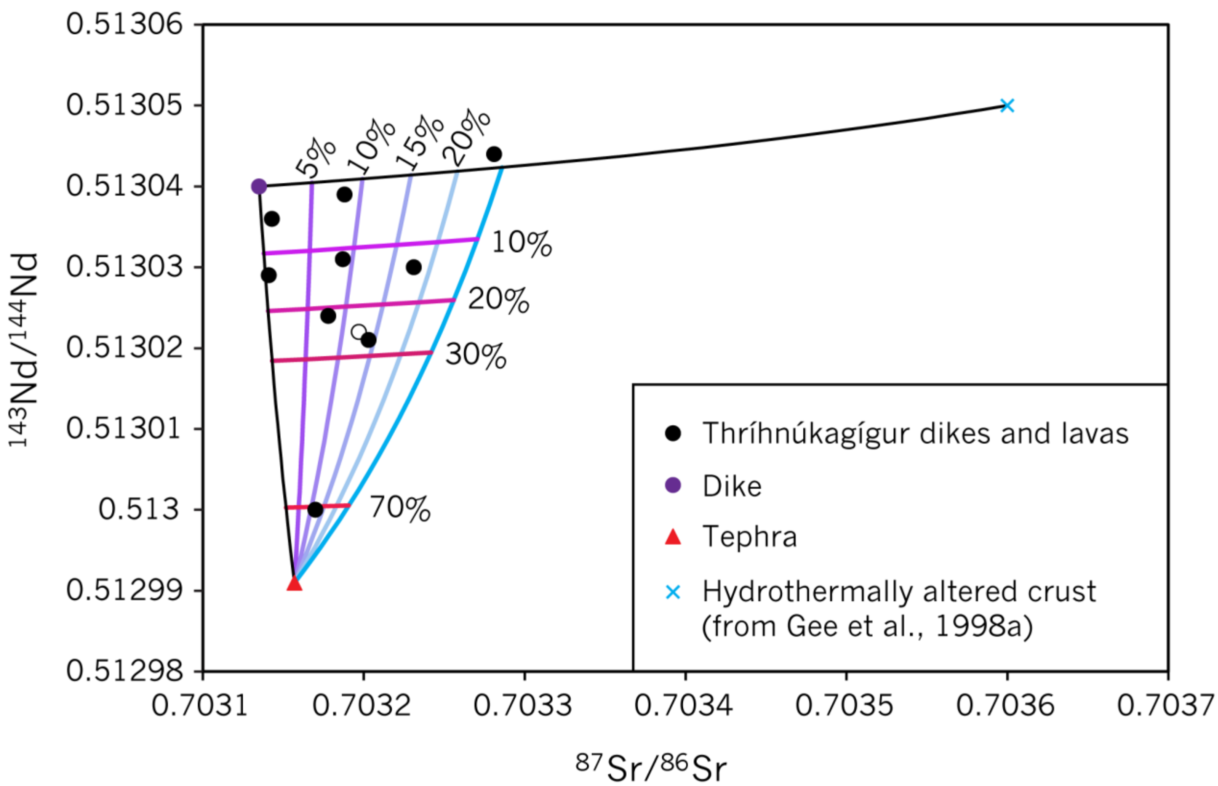

Figure 3.16. Incompatible trace element ratio mixing curve, Nb/Zr vs. La/Yb. The average buried tephra (red diamond) of the representative samples forms the enriched end member. The geochemistry of the intrusive part of the system is heterogeneous, so three possible end members are used (yellow diamonds): the plugged conduit (TNG-14-18), the chilled margin of the dike (TNG-14-27e), and isotopically most depleted dike sample (TNG-14-24) used as an end member in Figure 3.13. For the latter two primitive end members, green crosses on the mixing curves represent 20% buried tephra, blue crosses represent 10%, and red crosses represent 5%. Dikes and lavas representing possible mixtures of the buried tephra and original magma composition are blue and yellow circles.

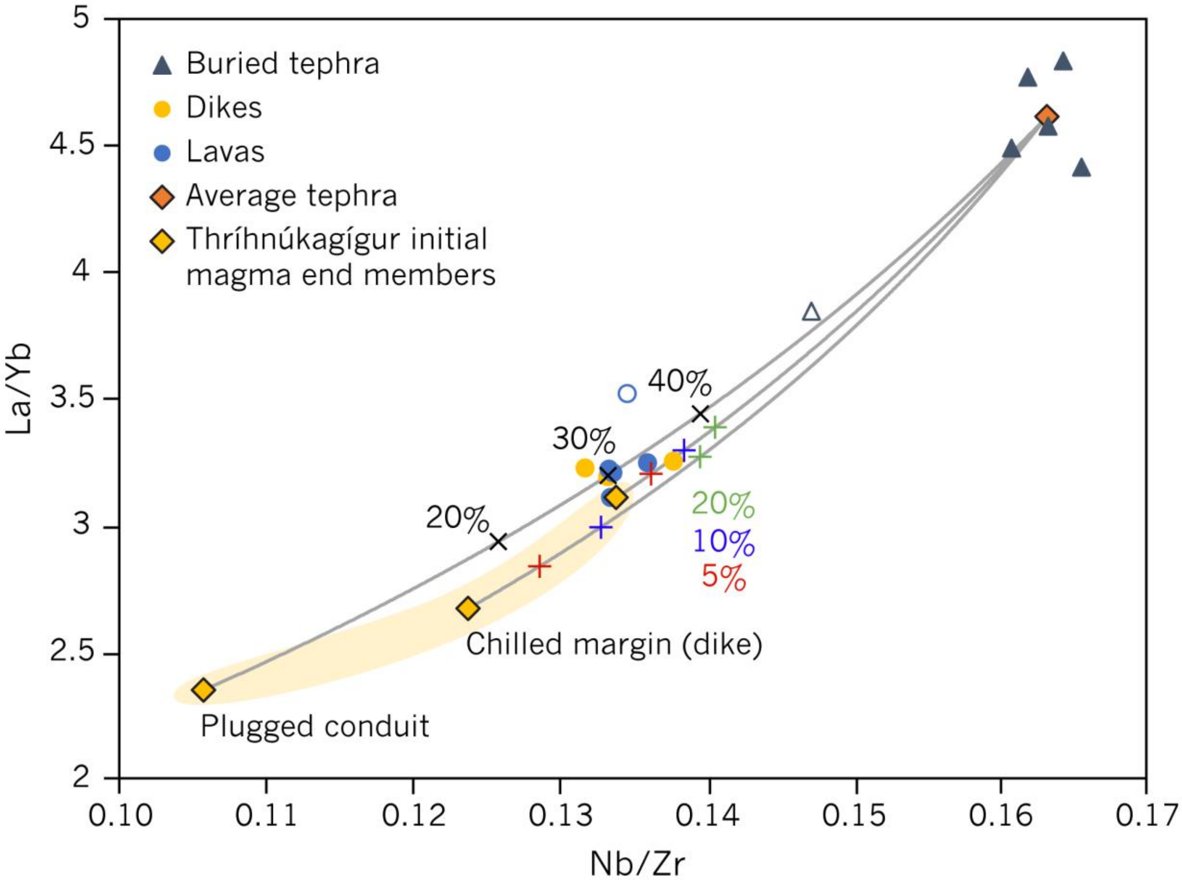

Figure 3.17. Cartoon of the magmatic plumbing system below Brennisteinsfjöll. The depth to the base of the crust is to scale, but the volcanic features, dikes, and sills are not to scale. Hydrothermally altered crust or hyaloclastite layers (HC) likely play a role in slowing magma ascent. Orange stippled zones represent sills or sill-like intrusions that have stalled at low density layers.

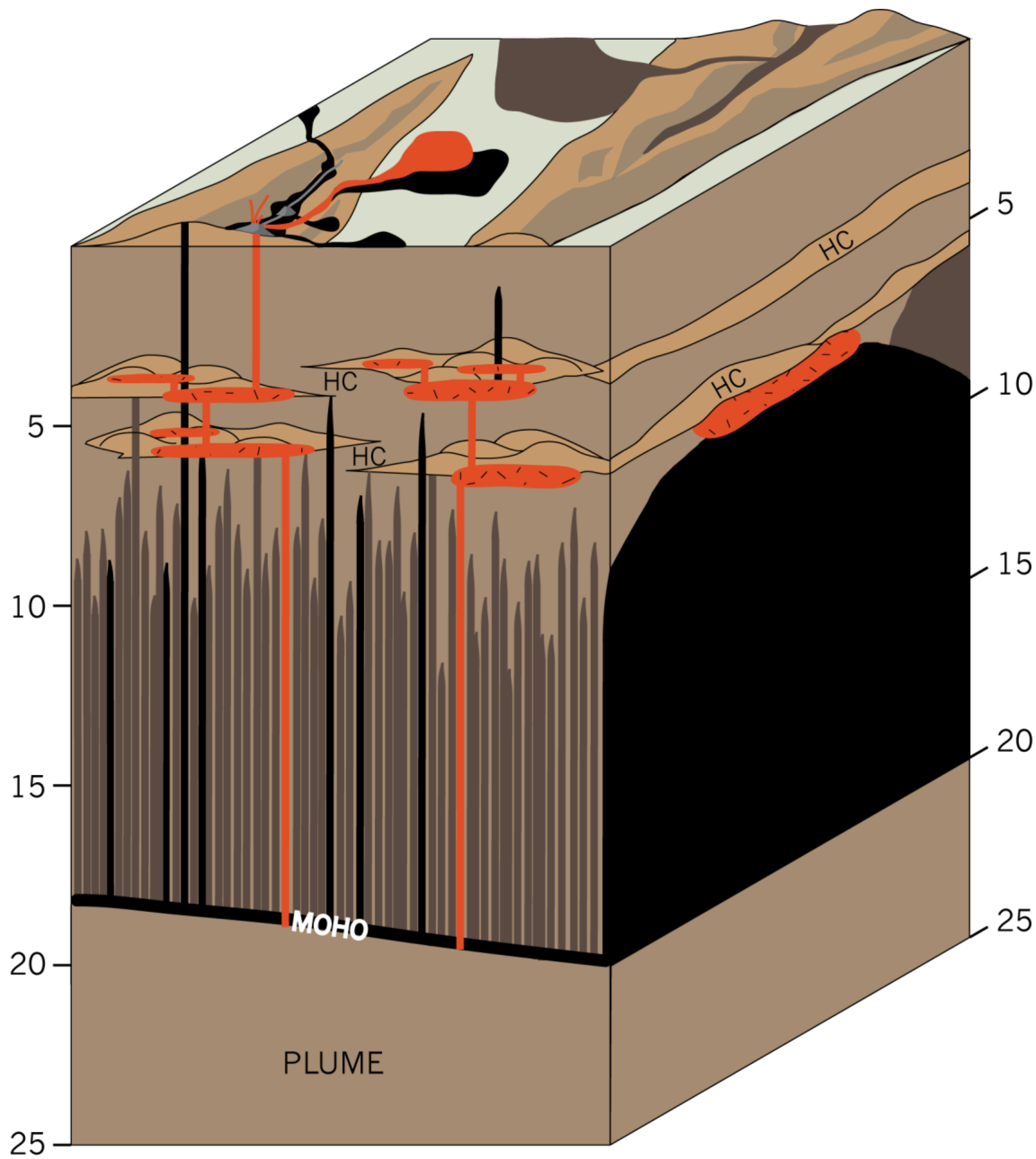

References

Bindeman I., Gurenko A., Sigmarsson O. and Chaussidon M. (2008) Oxygen isotope heterogeneity and disequilibria of olivine crystals in large volume Holocene basalts from Iceland: Evidence for magmatic digestion and erosion of Pleistocene hyaloclastites. *Geochim. Cosmochim. Acta* **72**, 4397–4420.

Bindeman I., Sigmarsson O. and Eiler J. M. (2006) Time constraints on the origin of large volume basalts derived from O-isotope and trace element mineral zoning and U-series disequilibria in the Laki and Grímsvötn volcanic system. *Earth Planet. Sci. Lett.* **245**, 245–259.

Chauvel C. and Hémond C. (2000) Melting of a complete section of recycled oceanic crust: Trace element and Pb isotopic evidence from Iceland. *Geochemistry, Geophys. Geosystems* **1**, n/a–n/a.

Clifton A. E., Sigmundsson F., Feigl K. L., Gunnar Guðmundsson and Árnadóttir T. (2002) Surface effects of faulting and deformation resulting from magma accumulation at the Hengill triple junction, SW Iceland, 1994-1998. *J. Volcanol. Geotherm. Res.* **115**, 233–255.

Condomines M., Muehlenbachs K., O'Nions R. K., Óskarsson N. and Oxburgh E. R. (1983) Helium, oxygen, strontium and neodynium isotopic relationships in Icelandic volcanics. *Earth Planet. Sci. Lett.* **66**, 125–136.

Elderfield H. and Greaves M. J. (1981) Strontium isotope geochemistry of Icelandic geothermal systems and implications for sea water chemistry. *Geochim. Cosmochim. Acta* **45**, 2201–2212.

Fronval T. and Jansen E. (1997) Eemian and Early Weichselian (140–60 ka) Paleoceanography and paleoclimate in the Nordic Seas with comparisons to Holocene conditions. *Paleoceanography* **12**, 443.

Furman T., Frey F. a. and Park K.-H. (1991) Chemical constraints on the petrogenesis of mildly alkaline lavas from Vestmannaeyjar, Iceland: the Eldfell (1973) and Surtsey (1963?1967) eruptions. *Contrib. to Mineral. Petrol.* **109**, 19–37.

Furman T., Frey F. A. and Park K.-H. (1995) The scale of source heterogeneity beneath the Eastern neovolcanic zone, Iceland. *J. Geol. Soc. London.* **152**, 997–1002.

Gee M. A. M., Taylor R. N., Thirlwall M. F. and Murton B. J. (2000) Axial magma reservoirs located by variation in lava chemistry along Iceland's mid-ocean ridge. *Geology* **28**, 699–702.

Gee M. A. M., Taylor R. N., Thirlwall M. F. and Murton B. J. (1998) Glacioisostacy controls chemical and isotopic characteristics of tholeiites from the Reykjanes Peninsula, SW Iceland. *Earth Planet. Sci. Lett.* **164**, 1–5.

Gee M. A. M., Thirlwall M. F., Taylor R. N., Lowry D. and Murton B. J. (1998) Crustal Processes: Major Controls on Reykjanes Peninsula Lava Chemistry, SW Iceland. *J. Petrol.* **39**, 819–839.

Hanan B. B. and Schilling J.-G. (1997) The dynamic evolution of the Iceland mantle plume: the lead isotope perspective. *Earth Planet. Sci. Lett.* **151**, 43–60.

Hart S. R. (1984) A large-scale isotope anomaly in the Southern Hemisphere mantle. *Nature* **309**, 753–757.

Higgins M. D. and Roberge J. (2007) Three magmatic components in the 1973 eruption of Eldfell volcano, Iceland: Evidence from plagioclase crystal size distribution (CSD) and geochemistry. *J. Volcanol. Geotherm. Res.* **161**, 247–260.

Hofmann A. W., Jochum K. P., Seufert M. and White W. M. (1986) Nb and Pb in oceanic basalts: new constraints on mantle evolution. *Earth Planet. Sci. Lett.* **79**, 33–45.

Jakobsson S. P., Jonsson J. and Shido F. (1978) Petrology of the Western Reykjanes, Peninsula. *J. Petrol.* **19**, 669–705.

Keiding J. K. and Sigmarsson O. (2012) Geothermobarometry of the 2010 Eyjafjallajökull eruption: New constraints on Icelandic magma plumbing systems. *J. Geophys. Res.* **117**, 1–15.

Kitagawa H., Kobayashi K., Makishima A. and Nakamura E. (2008) Multiple pulses of the mantle plume: Evidence from tertiary icelandic lavas. *J. Petrol.* **49**, 1365–1396.

Koerberle R., Hudak M. and Furman T. (2015) Crystal size distribution and textural analysis at Thríhnúkagígur volcano, Iceland. In *Geological Society of America Annual Meeting* p. 179.

Kokfelt T. F., Hoernle K., Hauff F., Fiebig J., Werner R. and Garbe-Schönberg D. (2006) Combined Trace Element and Pb-Nd-Sr-O Isotope Evidence for Recycled Oceanic Crust (Upper and Lower) in the Iceland Mantle Plume. *J. Petrol.* **47**, 1705–1749.

Koornneef J. M., Stracke A., Bourdon B., Meier M. A., Jochum K. P., Stoll B. and Grönvold K. (2012) Melting of a Two-component Source beneath Iceland. *J. Petrol.* **53**, 127–157.

Le Bas M. J. and Le Maitre R. W. (1986) A chemical classification of volcanic rocks based on the total alkali-silica diagram. *J. Petrol.* **27**, 745–750.

LaFemina P. C., Dixon T. H., Malservisi R., Árnadóttir T., Sturkell E., Sigmundsson F. and Einarsson P. (2005) Geodetic GPS measurements in south Iceland: Strain accumulation and partitioning in a propagating ridge system. *J. Geophys. Res.* **110**, B11405.

Manning C. J. and Thirlwall M. F. (2014) Isotopic evidence for interaction between Öræfajökull mantle and the Eastern Rift Zone, Iceland. *Contrib. to Mineral. Petrol.* **167**, 959.

Marks N., Zierenberg R. A. and Schiffman P. (2015) Strontium and oxygen isotopic profiles through 3 km of hydrothermally altered oceanic crust in the Reykjanes Geothermal System, Iceland. *Chem. Geol.* **412**, 34–47.

Michalczewska K., Hreinsdóttir S., Árnadóttir T., Hjartardóttir Á. R., Ágústsdóttir T., Gudmundsson M. T., Geirsson H., Sigmundsson F. and Gudmundsson G. B. (2012) Inflation and deflation episdoes in the Krísuvík volcanic system. In *American Geophysical Union Fall Meeting*

Nesbitt H. W. and Young G. M. (1982) Early Proterozoic climates and plate motion inferred from major element chemistry of lutites. *Nature* **299**, 715–717.

Park K.-H. (1990) Sr, Nd, and Pb isotope studies of ocean island basalts: constraints on their origin and evolution. Columbia University.

Peate D. W., Baker J. A., Jakobsson S. P., Waight T. E., Kent A. J. R., Grassineau N. V. and Skovgaard A. C. (2009) Historic magmatism on the Reykjanes Peninsula, Iceland: a snap-shot of melt generation at a ridge segment. *Contrib. to Mineral. Petrol.* **157**, 359–382.

Peate D. W., Breddam K., Baker J. A., Kurz M. D., Barker A. K., Prestvik T., Grassineau N. V. and Skovgaard A. C. (2010) Compositional Characteristics and Spatial Distribution of Enriched Icelandic Mantle Components. *J. Petrol.* **51**, 1447–1475.

Pedersen R. and Sigmundsson F. (2004) InSAR based sill model links spatially offset areas of deformation and seismicity for the 1994 unrest episode at Eyjafjallajökull volcano, Iceland. **31**, 5–9.

Pedersen R. and Sigmundsson F. (2006) Temporal development of the 1999 intrusive episode in the Eyjafjallajökull volcano, Iceland, derived from InSAR images. *Bull. Volcanol.* **68**, 377–393.

Raffone N., Ottolini L., Tonarini S., Gianelli G. and Fridleifsson G. Ó. (2008) A SIMS study of lithium, boron and chlorine in basalts from Reykjanes (southwestern Iceland). *Microchim. Acta* **161**, 307–312.

Rudge J. F., Maclennan J. and Stracke A. (2013) The geochemical consequences of mixing melts from a heterogeneous mantle. *Geochim. Cosmochim. Acta* **114**, 112–143.

Shorttle O., Maclennan J. and Piotrowski A. M. (2013) Geochemical provincialism in the Iceland plume. *Geochim. Cosmochim. Acta* **122**, 363–397.

Sigmarsson O. (1996) Short magma chamber residence time at an Icelandic volcano inferred from U-series disequilibria. *Nature* **382**, 440–442.

Sigmarsson O., Condomines M. and Fourcade S. (1992) A detailed Th, Sr and O isotope study of Hekla: differentiation processes in an Icelandic volcano. *Contrib. to Mineral. Petrol.* **112**, 20–34.

Sigmarsson O., Condomines M., Grönvold K. and Thordarson T. (1991) Extreme magma homogeneity in the 1783-1784 Lakagigar eruption: Origin of a large volume of evolved basalt in Iceland. *Geophys. Res. Lett.* **18**, 2229–2232.

Sigmarsson O., Vlastelic I., Andreasen R., Bindeman I., Devidal J.-L., Moune S., Keiding J. K., Larsen G., Höskuldsson A. and Thordarson T. (2011) Remobilization of silicic intrusion by mafic magmas during the 2010 Eyjafjallajökull eruption. *Solid Earth* **2**, 271–281.

Sigmundsson F., Hreinsdóttir S., Hooper A., Árnadóttir T., Pedersen R., Roberts M. J., Óskarsson N., Auriac A., Decriem J., Einarsson P., Geirsson H., Hensch M., Ofeigsson B. G., Sturkell E., Sveinbjörnsson H. and Feigl K. L. (2010) Intrusion triggering of the 2010 Eyjafjallajökull explosive eruption. *Nature* **468**, 426–30.

Skovgaard A. C., Storey M., Baker J. A., Blusztajn J. and Hart S. R. (2001) Osmium-oxygen isotopic evidence for a recycled and strongly depleted component in the Iceland mantle plume. *Earth Planet. Sci. Lett.* **194**, 259–275.

Stracke A., Zindler A., Salters V. J. M., McKenzie D., Blichert-Toft J., Albarède F. and Grönvold K. (2003) Theistareykir revisited. *Geochemistry, Geophys. Geosystems* **4**.

Sturkell E. and Sigmundsson F. (2003) Recent unrest and magma movements at Eyjafjallajökull and Katla volcanoes, Iceland. *J. Geophys. Res.* **108**.

Sun S. -s. and McDonough W. F. (1989) Chemical and isotopic systematics of oceanic basalts: implications for mantle composition and processes. *Geol. Soc. London, Spec. Publ.* **42**, 313–345.

Taisne B., Tait S. and Jaupart C. (2011) Conditions for the arrest of a vertical propagating dyke. *Bull. Volcanol.* **73**, 191–204.

Tarasewicz J., Brandsdóttir B., White R. S. and Hensch M. (2012) Using microearthquakes to track repeated magma intrusions beneath the Eyjafjallajökull stratovolcano, Iceland. *J. Geophys. Res.* **117**.

Tarasewicz J., White R. S., Brandsd B. and Schoonman C. M. (2014) Seismogenic magma intrusion before the 2010 eruption of Eyjafjallajökull volcano, Iceland. *Geophys. J. Int.* **198**, 906–921.

Tarasewicz J., White R. S., Woods A. W., Brandsdóttir B. and Gudmundsson M. T. (2012) Magma mobilization by downward-propagating decompression of the Eyjafjallajökull volcanic plumbing system. *Geophys. J. Int.* **39**.

Thirlwall M. F., Gee M. A. M., Taylor R. N. and Murton B. J. (2004) Mantle components in Iceland and adjacent ridges investigated using double-spike Pb isotope ratios. *Geochim. Cosmochim. Acta* **68**, 361–386.

Todt W., Cliff R. A., Hanser A. and Hofmann A. W. (1993) Recalibration of NBS lead standards using a 202Pb-205Pb double spike. *Terra Abstr.* **5**, 396.

Appendix

Isotope geochemistry procedures

A.1 Acid digestion

Approximately 200 mg of each sample were weighed and placed in Teflon vials. After adding 1 ml of HNO_3 and 2 ml of HF, the samples were capped and left on a hotplate for 5 days. Samples were dried down and 1 ml of HNO_3 was added to each vial and dried once more to remove any traces of HF. Between 2-4 ml of HCl were added to the samples, capped to facilitate dissolution, and once again dried down on the hotplate. Samples were dissolved in 1 ml of 0.7N HBr, then loaded into 2 ml centrifuge tubes. The solutions were run for 3 minutes at a rate of 8400 rpm in the centrifuge.

A.1.1 Pb separation

To prepare the Pb columns, fresh DOWEX 200-400 mesh resin was added to each columns and rinsed twice with 1 ml of 7N HCl to clean the resin. This was followed by two 1 ml rinses of triple distilled water (referred to as “3 sub” as the third distillation is under sub-boiling conditions). Another 1 ml of 7N HCl was added to the columns. Subsequently, a final 1 ml of 3 sub water was added. After cleaning, the columns were conditioned with 1 ml of 0.7N HBr was added to them. The acid collected from column washing was disposed and the sample vials were loaded beneath the columns.

Samples were loaded carefully so as to avoid loading any of the residuum in the centrifuge tubes. The columns were eluted with 1 ml of 0.7N HBr three times and once more with 0.75 ml. Following a 0.3 ml elution of 3N HCl, the eluate was collected for Sr and Nd and moved to a hot plate to dry down.

New sample vials were placed below the columns for Pb collection. Two 0.75 ml elutions of 7N HCl were collected and these were placed on the hot plate to dry.

A.1.2 Sr and REE separation

The Sr columns with [NAME] resin were cleaned and conditioned with 2 sets of 2.5 ml of 2.5N HCl. Samples dissolved in 2.5N HCl were loaded in the columns and subsequently rinsed three times with approximately 1/3 ml of 2.5N HCl. Either 12 or 16 ml of 2.5N HCl were added to the columns, depending on the amount of resin in the column. The waste was disposed and Sr collection vials were placed below the columns. Samples were eluted with 5 ml of 2.5N HCl and the eluate was collected Sr.

Either 2 or 3 ml of 6.6N HCl were added to each column based on the volume of resin. The eluate was disposed. Rare earth element vials were placed below the columns. Columns were eluted with 6 ml of 6.6N HCl for REEs and Nd separation. Both the Sr and REE eluates were placed on the hot plate to dry.

A.1.3 Nd separation

Acid in the pre-conditioned columns was drained. Meanwhile, 1 ml of 0.26N HCl was added to the dried REE sample. The bottom of the vial was gentle scratched and stirred and with a pipette tip to facilitate dissolution. The samples were added to the columns and subsequently rinsed with 1 ml of 0.26N HCl. Depending on the volume of resin, 10-12 ml of 0.26N HCl was eluted and disposed. The Nd vials were placed under the columns and 5 ml of 0.26N HCl were eluted and collected for Nd. Samples were placed on the hot plate to dry.

A.2 Filament preparation

For Pb, a 99.999% Re ribbon was used for the filaments while 99.98% Re was used for Sr and Nd. A single ribbon is welded onto a two-pronged sample holder for Pb and Sr. For Nd analysis, two ribbons are welded onto a four-pronged sample holder. One ribbon is used to host the sample while the other is oriented perpendicular and acts as another ionization source behind the sample. Once welded to the sample holders, the Re filaments were degassed and surface contamination was removed by running a 4.0 A current through the filament.

A.2.1 Pb loading and analysis

Samples for Pb analysis were dissolved in 1 μl of H_3PO_4 and loaded onto the filament between two layers of 1 μl tetraethyl orthosilicate (TEOS). During loading, filaments had currents of 0.8-0.9 A. Once the filaments were dry, the current was increased very briefly, 1-2 seconds, to 2.2 A. This procedure was also followed for the Pb standards (NIST SRM 981). This standard was always analyzed at the beginning of a batch of analyses and after every 3-4 samples. Samples were gradually heated to 1500 mA or ~900°C from 1000 mA at a rate of 100 mA/min. The current was thereafter increased 30 mA/min towards a target of 1300°C. Ten blocks of 10 cycles were measured for each sample once a stable signal was achieved.